A MODEL OF GREENLAND ICE SHEET DEGLACIATION CONSTRAINED BY OBSERVATIONS OF RELATIVE SEA LEVEL AND ICE EXTENT

Benoit S. Lecavalier[1,*], Glenn A. Milne[1,2], Matthew J.R. Simpson[3], Leanne Wake[4], Philippe Huybrechts[5], Lev Tarasov[6], Kristian K. Kjeldsen[7], Svend Funder[7], Antony J. Long[8], Sarah Woodroffe[8], Arthur S. Dyke[9], Nicolaj K. Larsen[10]

[1]*Department of Physics, University of Ottawa, Canada*
[2]*Department of Earth Sciences, University of Ottawa, Canada*
[3]*Norwegian Mapping Authority, Hønefoss, Norway*
[4]*Department of Geography, University of Northumbria, UK*
[5]*Vrije Universiteit Brussel, Belgium*
[6]*Department of Physics and Physical Oceanography, Memorial University, Canada*
[7]*Centre for GeoGenetics, Natural History Museum of Denmark, University of Copenhagen, Denmark*
[8]*Department of Geography, Durham University, UK*
[9]*Geological survey of Canada, NRCan, Canada and Department of Geography, Memorial University, Canada*
[10]*Department of Geoscience, Aarhus University, Denmark*
[*]*Now at Department of Physics and Physical Oceanography, Memorial University, Canada*

ABSTRACT

An ice sheet model was constrained to reconstruct the evolution of the Greenland Ice Sheet (GrIS) from the Last Glacial Maximum (LGM) to present to improve our understanding of its response to climate change. The study involved applying a glaciological model in series with a glacial isostatic adjustment and relative sea-level (RSL) model. The model reconstruction builds upon the work of Simpson et al. (2009) through four main extensions: (1) a larger constraint database consisting of RSL and ice extent data; model improvements to the (2) climate and (3) sea-level forcing components; (4) accounting for uncertainties in non-Greenland ice. The research was conducted primarily to address data-model misfits and to quantify inherent model uncertainties with the Earth structure and non-Greenland ice. Our new model (termed Huy3) fits the majority of observations and is characterised by a number of defining features. During the LGM, the ice sheet had an excess of 4.7 m ice-equivalent sea-level (IESL), which reached a maximum volume of 5.1 m IESL at 16.5 cal. ka BP. Modelled retreat of ice from the continental shelf progressed at different rates and timings in different sectors. Southwest and Southeast Greenland began to retreat from the continental shelf by ~16 to 14 cal. ka BP, thus responding in part to the Bølling-Allerød warm event (c. 14.5 cal. ka BP); subsequently ice at the southern tip of Greenland readvanced during the Younger Dryas cold event. In northern Greenland the ice retreated rapidly from the continental shelf upon the climatic recovery out of the Younger Dryas to present-day conditions. Upon entering the Holocene (11.7 cal. ka BP), the ice sheet soon became land-based. During the Holocene Thermal Maximum (HTM; 9-5 cal. ka BP), air temperatures across Greenland were marginally higher than those at present and the GrIS margin retreated inland of its present-day southwest position by 40 to 60 km at 4 cal. ka BP which produced a deficit volume of 0.16 m IESL relative to present. In response to the HTM warmth, our optimal model reconstruction lost mass at a maximum centennial rate of c. 103.4 Gt/yr. Our results suggest that remaining data-model discrepancies are affiliated with missing physics and sub-grid processes of the glaciological model, uncertainties in the climate forcing, lateral Earth structure, and non-Greenland ice (particularly the North American component). Finally, applying the Huy3 Greenland reconstruction with our optimal Earth model we generate present-day uplift rates across

Greenland due to past changes in the ocean and ice loads with explicit error bars due to uncertainties in the Earth structure. Present-day uplift rates due to past changes are spatially variable and range from 3.5 to -7 mm/a (including Earth model uncertainty).

1. INTRODUCTION

Between 26.5 and 19 thousand years before present (ka BP) global ice volume reached and maintained a maximum value resulting in global mean sea-level being 120-135 m below present (Clark and Mix, 2002; Lambeck et al., 2002; Milne et al., 2002; Clark et al., 2009; Austerman et al., 2013). During this period, known as the Last Glacial Maximum (LGM), there was large-scale glaciation across North America and Eurasia as well as more extensive ice in Greenland and Antarctica. The subsequent deglaciation and transition to a warmer interglacial climate saw the disappearance of the North American and Eurasian ice complexes, glaciers and ice caps shrank and withered away, and the mass of the Antarctic and Greenland ice sheets was significantly reduced. This change in the distribution of ice has left its mark on the landscape. Resultant features such as recessional moraines provide a direct means of reconstructing ice extent (e.g. Dyke and Prest, 1987). The transfer of water to oceans that accompanied these changes lead to a global-scale visco-elastic response of the solid Earth (e.g. Peltier and Andrews, 1976; Clark et al., 1978). Vertical land motion in previously glaciated areas resulted in raised marine deposits and landforms which provide valuable indirect information on changes in ice extent (e.g. Lambeck et al., 1998). Information from ice core records has also been used to constrain past ice thickness changes (Vinther et al., 2009). In this study, we apply a range of direct and indirect observations of ice extent and relative sea-level (RSL) to reconstruct the Greenland ice sheet (GrIS) during its most recent deglaciation.

The rapid change in global RSL and climate following the LGM had dramatic consequences for the evolution of the GrIS. Geological observations suggest that during the LGM the GrIS extended across large portions of the continental shelf and, in some areas, extended as far as the shelf break (e.g. Larsen et al., 2010; O'Cofaigh et al., 2012). This LGM maximum for the GrIS has been affiliated with an increase in volume of 2-3 m ice equivalent sea level (IESL) relative to present (Clark and Mix, 2002). In this study the term IESL refers to barystatic sea level, which is defined as the global mean sea-level change associated with the change of mass in the ocean (Gregory et al., 2013), additionally we account for a changing ocean area since the LGM (It is important to note, however, that this definition of IESL does not account for the increase in ocean basin volume associated with the retreat of marine-based ice. It is used here only to provide an additional measure of ice volume). During the subsequent deglaciation, the GrIS retreated initially through the calving of its marine-based ice as sea levels rose (Funder and Hansen, 1996; Kuijpers et al., 2007). By approximately 10 cal. ka BP, the GrIS was mainly land-based with the exception of some outlet glaciers (e.g. Funder et al., 2011a), after which time, retreat slowed and was dominated by surface melt. During the Holocene Thermal Maximum (HTM), between about 9 and 5 cal. ka BP, air temperatures across Greenland were warmer than present (Kaufman et al., 2004). It has been suggested that, in some areas, the GrIS retreated inland of its present-day margin in response to the HTM. It attained a post-LGM ice volume minimum around 4 cal. ka BP (Simpson et al., 2009). During the subsequent Neoglacial readvance (Kelly, 1980), all direct geomorphological evidence pertaining to the minimum configuration was overridden. Thus, the ice sheet's minimum configuration can only be inferred from RSL and ice-core records.

The motivation of this research is to more accurately understand the response of the GrIS to past climate change to better predict its future. For example, better constraining the response of the ice sheet to the HTM (a part analogue for future regional climate) is one clear application of using the past behaviour

of the ice sheet to assess and inform how it will respond in the future. The necessity to understand the current state of the GrIS is becoming increasingly evident. The GrIS is in dynamic and thermodynamic disequilibrium (on millennial and longer time-scales). This must be accounted for to accurately predict its future behaviour. Furthermore, future projection of GrIS mass loss for a given climate scenario relies on accurate estimates of contemporary mass loss. In this regard, satellite altimetry, interferometry, and gravimetry data sets have been applied to estimate the mass balance of the GrIS (Shepherd et al., 2012; Wouters et al., 2013); the results indicate that the GrIS lost mass at an accelerated rate with a total loss of 142 ± 49 Gt/yr between 1992 to 2011. However, prior to extracting mass loss using these data sets, it is necessary to correct them for the present-day vertical motion of the solid Earth due to past load changes. The glacial isostatic adjustment (GIA) model presented here, including uncertainties in the ice chronology and Earth structure, can be used directly for this purpose.

Several distinct approaches have previously been used to reconstruct the most recent GrIS deglaciation (Huybrechts, 2002; Tarasov and Peltier 2002; Fleming and Lambeck, 2004; Peltier, 2004; Simpson et al., 2009), each having advantages and disadvantages. The disadvantages include a lack of glaciological self-consistency (Peltier, 2004) to the use of a small set of observational constraints (Huybrechts, 2002). The current study builds upon the work of Simpson et al. (2009) (henceforth referenced as the Simpson study). They employed a three-dimensional ice sheet model forced by prescribed climatic conditions (e.g. Huybrechts, 2002). Output from the glaciological model was constrained to ice extent observations and RSL observations.

In this study, we initially adopt the Simpson model reconstruction of GrIS evolution (termed Huy2) and then improve it. The Huy2 reconstruction was achieved by simultaneously tuning/calibrating a 3-D thermomechanical ice sheet model in series with a GIA model of sea-level change. The ice sheet model was tuned through its ensemble parameters to generate hundreds of GrIS evolution histories, while the GIA model of RSL change was calibrated to yield a probability distribution based on data-model fits with respect to model parameters. As in the Simpson study, this procedure is herein referred to as simply calibrating the model. Our new reconstruction adopts this methodological approach but with four extensions. Firstly, we employ additional RSL and ice extent constraints, which are detailed in Section 2. Key additions are an up-to-date Greenland-wide marine limit data base (K. Kjeldsen and S. Funder, personal communication) and ice-core derived thinning curves (from GRIP, NGRIP, Dye-3, and Camp Century), which constrain elevation changes of the ice surface for the period 8 cal. ka BP to present (Vinther et al., 2009; Lecavalier et al., 2013). We also employ two improvements in the ice model: these are (1) a better parameterization of the positive degree day (PDD) algorithm for computing surface mass balance changes (Wake et al., 2014) and (2) consideration of spatial variability in the sea-level forcing to better match the observed marine retreat chronology. Finally we assess the extent to which RSL changes around Greenland are due to uncertainties in the deglacial history of the North American ice complex (NAIC; Tarasov et al., 2012). This study involves sensitivity analyses to investigate the level of non-uniqueness in the model calibration and to more accurately and precisely determine the optimal solution.

The article structure is as follows: Section 2 covers the pertinent datasets; Section 3 provides an overview of the models; Section 4 presents the modelling results and sequentially introduces the main extensions of this study resulting in the Huy3 model; finally Section 5 discusses the main features of the Huy3 model and remaining data-model misfits.

2. DATA

In this study we consider a range of field observations to constrain key model parameters. There are four sets of constraints: (1) past ice extent; (2) past changes in RSL; (3) ice-core derived thinning; (4)

the present-day configuration of the GrIS. As background to Sections 4 and 5, we review aspects of these observational constraints in the following sub-sections. The locations of the ice-core sites and sea-level data are shown in Figure 1a and the locations mentioned in the text are labeled in Figure 1b. The source references of the sea-level data are provided in Table 1. Henceforth, all dates given are listed in thousand calibrated years before present (ka BP) unless stated otherwise.

2.1 ICE EXTENT DURING DEGLACIATION

Geological and geomorphological field evidence constrains the past lateral and vertical extent of the GrIS; here we focus only on constraints used to infer margin positions since the LGM (Funder, 1989; Funder and Hansen, 1996; Alley et al., 2010; Funder et al., 2011a Funder et al., 2011b). During the LGM, Northwest Greenland ice was dynamically connected to the Innuitian ice sheet on Ellesmere Island. Marine-based ice in Nares Strait was fed by ice streams from both ice sheets and did not recede until ~12.5 ka BP (Blake, 1999, England, 1999). It was not until 11.2 ka BP that ice streams sustaining marine-based ice in the Strait retreated to their respective fjord mouths leading to a saddle collapse by ~10 ka BP (Kelly and Bennike, 1992; Zreda et al., 1999). In contrast, North Greenland had ice extending far onto the mid-outer continental shelf where it was buttressed against stationary multi-year sea ice (Möller et al., 2010; Jakobsson et al., 2013). Ice started to retreat between 16 to 10.3 ka BP before the final breakup of marine-based ice in this region by 10.1 ka BP (Larsen et al., 2010). Moraines on the Northeast Greenland continental shelf (Evans et al., 2009; Winkelmann et al., 2010) are interpreted as a minimum LGM extent with a plausible earliest retreat at 10 ka BP (Landvik, 1994; Hjort, 1997; Wilken and Mienert, 2006; Evans et al., 2009; Winkelmann et al., 2010). The marine sedimentary record near Kejser Franz Joseph Fjord on the East Greenland coast suggests glaciation of the continental shelf; a mid-shelf moraine defines a plausible LGM extent for the region (Evans et al., 2002) while mass-wasting deposits from submarine channels suggest grounded ice reaching the outer shelf (O'Cofaigh et al., 2004). Ice retreat here commenced after ~16.5 ka BP with the mid-shelf free of grounded ice by 13 ka BP. The inner shelf was most likely free of ice by ~8.5 ka BP (Evans et al., 2002; O'Cofaigh et al., 2004).

Ice extent in Scoresby Sund during the LGM reached Kap Brewster (Håkansson et al., 2007b; Håkansson et al., 2009). Marine cores off Scoresby Sund identify a maximum in ice-rafted debris deposition on the continental slope between 22 and 14 ka BP, which coincides with the retreat of ice from its LGM extent (Stein et al., 1996; Funder et al., 1998). By 12 to 10 ka BP, the outer fjord basins were ice-free (Funder et al., 1998). The South East margin of the GrIS reached the shelf edge at LGM as indicated by terminal moraines (Sommerhoff 1981; Andrews, 2008; Dowdeswell et al., 2010). The ice margin at Kangerlussuaq is inferred to have reached the shelf edge by 21 ka BP and began to retreat shortly after 17 ka BP (Andrews et al., 1997; Andrews et al., 1998; Jennings et al., 2006; Andrews, 2008). During the LGM, ice south of Helheim Glacier reached the shelf break and maximum values of coarse-grained, ice-rafted debris occurred during the period between 19 and 15 ka BP, which coincides with rapid ice retreat from the shelf after 16 ka BP (Nam et al., 1995; Kuijpers et al., 2003; Long et al., 2008); the present coastline was reached by the start of the Holocene (Roberts et al., 2008). Southern Greenland has a narrow shelf and ice reached the shelf break during the LGM; the initial retreat occurred at 15 ka BP, with surface exposure dates and RSL data suggesting that the ice-margin reached its present position by 10 ka BP (Bennike et al., 2002; Sparrenbom et al., 2006a,b; Larsen et al., 2011; Woodroffe et al., 2013). In West Greenland, sub-marine moraine-belts have suggested an LGM margin near the shelf break (Robert et al, 2009). Although the age of these moraines is not resolved (Funder et al, 2011a), evidence from cross-shelf troughs suggest that ice streams during the LGM reached the shelf edge and break (O'Cofaigh et al., 2012; Dowdeswell et al., 2013). Ice streams that extended out onto the shelf persisted into the early Holocene but had receded by 11.6 to 10.2 ka BP causing ice free conditions north of and in

Disko Bugt (Ingolfsson et al., 1990; Long and Roberts, 2003; Lloyd et al., 2005; Kelley et al., 2013; Lane et al., 2013).

The observational constraints indicate the initial retreat of the GrIS from its maximum extent varies in space and time. This variability likely reflects a variety of controlling processes and boundary conditions, such as rising sea-level, ocean and air temperatures, shelf bathymetry, sea-ice extent. The use of different proxies which have different sensitivities to margin position is also a factor to be considered when estimating post-LGM margin retreat. In general, however, marine-based portions of the ice sheet retreated from the shelf during the period 17 to 11.5 ka BP. The Younger Dryas cold event (YD; 12.8 to 11.7 ka BP (Steffensen et al., 2008)) caused a modest re-advance (or still-stand) of the ice margin in the Scoresby Sund region (Hall et al., 2010; O'Cofaigh et al., 2013) but no signal has been detected in many others (Kuijpers et al., 2003; Jennings et al., 2006; Sparrenbom et al., 2006b). Following the YD, air temperatures over the interior of the GrIS rose abruptly by as much as 10 degrees Celsius (Steffensen et al., 2008; Walker et al., 2009). That warming coincided with the establishment of a predominantly land based ice sheet (Funder and Hansen 1996; Bennike and Björck, 2002; Jennings et al., 2006; Sparrenbom et al., 2006b; Hall et al., 2008; Long et al., 2008a; Wagner et al., 2010; Larsen et al., 2010). During the Early Holocene the GrIS continued to retreat, driven by surface melt and calving of fjord glaciers. From 11 to 8 ka BP, large land-areas were uncovered by the retreating ice sheet in West Greenland (Funder and Hansen, 1996; Funder et al., 2004; Weidick and Bennike, 2007; Long et al., 2006).

Threshold lake data has been used to date the onset of ice free conditions, which can represent the timing at which the present-day margin is reached, the minimum configuration of the ice sheet, as well as periods of Holocene readvance (Briner et al., 2010, 2013; Larsen et al., 2011, 2013). The timing of the minimum GrIS configuration during the HTM is also inferred using C^{14}-dates of reworked material in moraines (Bennike and Weidick, 2001; Weidick et al., 2004; Weidick and Bennike, 2007; Levy et al., 2012). A wide range of proxies with differing sensitivities record a cooling trend across Greenland after approximately 5 to 3 ka BP which led to spatially variable regrowth of the ice sheet in most areas of the west and southwest culminating in a maximum extent during the Little Ice Age (0.7 to 0.1 ka BP)) as suggested by 'historical' moraines, assumed to have formed during the 1700s or at the end of the 1800s (Seidenkrantz et al., 2008; Jakobsen et al., 2008; Klug et al., 2009; Long et al., 2009; Nørgaard-Pedersen and Mikkelsen, 2009; Kelly and Lowell, 2009; Ren et al., 2009; Bennike et al., 2010; Schmidt et al., 2010; Kobashi et al., 2011; Weidick et al., 2012).

2.2 RELATIVE SEA LEVEL AND THE MARINE LIMIT

For this modelling study we are interested in millennial scale sea-level changes on the order of tens of meters. In Greenland, past sea levels have been reconstructed using a variety of indicators: isolation basins, raised beaches and deltas, marine shells, drift wood, whale bones, and lower elevational limits of perched boulders. Figure 1a illustrates the locations of the RSL observations used in this study and Table 1 lists the related source references.

The sea-level observations with the highest precision are those from isolation basins (Long et al., 2011). Isolation basin studies yield 122 relevant data points for this study (e.g. Long et al., 2011; Bennike et al., 2011; Woodroffe et al., 2013). In comparison, the Simpson study incorporated only 73 isolation basin sea-level index points. The limited number and uneven spatial distribution of these data requires the use of additional less precise sea-level proxies. The remaining sea-level proxies applied (360 data points) consist of marine shells (molluscs), drift wood, and whale bones that provide a limiting constraint on RSL. The temporal and height measurement uncertainty associated with these data points can be large

given the precision of present-day measurement techniques and apparatus (over ±1 ka and ±1 m, respectively). The marine limit (ML) for a given location defines an upper limit of RSL which constrains the timing and magnitude of the isostatic response due to the unloading of ice (Weidick 1972; Ingolffson et al., 1990; Funder and Hansen 1996; Rasch, 2000). The ML is often defined by the lower limit of perched boulders above wave-washed bedrock. Lakes that lack a marine phase have also been used to define the ML in some locations (e.g. Long and Roberts, 2003; Woodroffe et al., 2013). A total of 629 ML observations have been compiled covering the whole of Greenland (Figure S1) with characteristic dome features of high ML values (Weidick, 1976; Funder, 1989; Funder and Hansen, 1996; K. Kjeldsen and S. Funder, personal communication). These data are valuable in regions where other RSL observations are lacking, particularly in northwest and southeast Greenland, as illustrated in Figure 1a.

2.3 HOLOCENE THINNING CURVES

Vinther et al. (2009) applied a novel procedure to determine ice surface elevation curves at four GrIS ice-core locations (GRIP, NGRIP, DYE-3 and Camp Century; see Fig. 1a). These data-constrained curves depict a Holocene thinning history that is considerably more rapid and of greater amplitude than that indicated from numerical ice models. Recently, this analysis was revisited by Lecavalier et al. (2013) who concluded that the ice-core derived thinning curves have larger uncertainties than previously thought, and that prior to 8 ka BP the thinning curves cannot be defined due to the influence of the Innuitian Ice Sheet. However, regardless of these limitations, we include these constraints (see Section 4.5) given that they provide the only information available on past ice thickness changes in the interior of the ice sheet.

3. MODEL DESCRIPTION

The key model components and set-up applied in this study are shown in Figure 2. The calibration is initialized with a 3-D thermomechanical ice sheet model which freely simulates the evolution of the GrIS and is compared to lateral extent data and the present-day ice sheet geometry. The ice model output is then amalgamated to a global ice chronology to act as a primary input to the GIA model. In conjunction with a global ice chronology, a global Earth model is prescribed for the GIA model to produce sea-level and vertical land motion predictions. A sweep of a dozen key model parameters samples the range of model predictions which are compared to observations. Finally a statistical analysis yields optimal model parameters, those which minimize the misfit between model predictions and observations. The thermomechanical ice sheet model and GIA model operate independently in series and so are not coupled.

3.1 ICE SHEET MODEL

The glaciological model simulates the evolution of the GrIS in response to changes in past climate and sea-level over the last two glacial cycles. The model is described in detail in Huybrechts and de Wolde (1999) and Huybrechts (2002) and so only a brief overview of the most relevant aspects relating to ice dynamics, isostasy and mass balance are provided here. The model consists of 31 vertical layers and has a lateral resolution of 20 by 20 km which is represented by 11,703 lateral grid cells for the region. The ice dynamics are modelled using the shallow ice approximation (Hutter, 1983). Gravitationally-driven non-linear viscous flow represented using Glen's flow law governs internal deformation (Glen, 1955) while a parameterisation of basal sliding defines the flow over bedrock. Longitudinal stresses are ignored and grounding-line dynamics are not modelled but are expressed as parametric equations within the sea-level forcing component of the model. These parametric equations are tuned to fit geological and geomorphological evidence (see Section 4.2.3). This marine ice

parameterisation predicts to first-order inferences of northern hemispheric large-scale ice margin changes (Zweck and Huybrechts, 2003, 2005).

The isostatic component of the ice model differs to that employed in the GIA model of RSL change; it is based on a more simplistic elastic lithosphere overlying a relaxed asthenosphere with a single decay time of 3 ka. The mass balance of the ice model is defined as incoming precipitation minus meltwater runoff and calving. Due to the millennial timescale of the analysis, the surface runoff is calculated using a PDD algorithm (e.g. Braithwaite, 1995). The surface air temperatures are derived from the GRIP $\delta^{18}O$ record which is applied to generate a temperature profile across Greenland. Subsequently, the temperature profile is applied to generate a Gaussian distribution for monthly temperatures (see Section 4.2.2). The melt rate is correlated to the predicted degree-day total via the degree-day factor (DDF), and the amount of runoff, refreezing and water retention is calculated using the adjusted runoff model of Janssens and Huybrechts (2000). The ice sheet model is run from the Last Interglaciation (Eemian; 123 ka BP) at which time we adopt the reduced extent (compared to present) modelled in Huybrechts (2002). The glaciological model generates the Greenland component required for the subsequent GIA and RSL computations.

3.2 GLACIAL ISOSTATIC ADJUSTMENT AND RELATIVE SEA LEVEL MODEL

Our GIA model computes Earth deformation, gravity and sea-level changes resulting from the interaction between ice sheets and the solid Earth (e.g. Farrell and Clark 1976; Milne and Mitrovica 1998; Mitrovica and Milne 2003, Kendall et al., 2005). The model uses a global ice model and an Earth model as primary inputs. The background global ice loading chronology used is ICE-5G (Peltier, 2004). The ICE-5G chronology is revised by removing the original Greenland component (variant of GrB; Tarasov and Peltier, 2002; Peltier, 2004) and replacing it with our own reconstructions as noted in the previous section. As demonstrated in previous studies, RSL changes in Greenland are significantly influenced by the deglaciation of North America (Fleming and Lambeck, 2004; Simpson et al. 2009). To assess this sensitivity, we replace the North American component of ICE-5G by a high-variance sub-set of a data-calibrated distribution of glaciological reconstructions (Tarasov et al., 2012).

The Earth model adopted is typical in GIA modelling studies (Peltier, 1974), with a spherically symmetric geometry and Maxwell visco-elastic rheology. The elastic and density structure is given by the seismic Preliminary Reference Earth Model (PREM; Dziewonski and Anderson, 1981) with a depth resolution of 10-25 km; the viscous structure is more crudely defined into three shells - lithosphere, upper mantle, and lower mantle – given the uncertainty in this structure and the limited depth resolving power of RSL observations (Mitrovica and Peltier, 1991). The lithosphere was assigned a relatively high viscosity to simulate an elastic outer shell with a thickness that was varied (LT) when seeking an optimal model fit to the RSL data. The upper-lower mantle boundary was defined at a depth of 670 km and the viscosity in these two regions was also varied (UMV and LMV, respectively) to optimise model fits to the RSL data (e.g. Milne et al., 2001). The GIA model output includes the influence of ocean loading due to sea-level changes by solving the sea-level equation as presented in Mitrovica and Milne (2003) using the Kendall et al. (2005) algorithm. Furthermore, the model includes GIA-induced perturbations in Earth rotation due to a shift in the Earth's rotational inertia tensor based on the revised theory in Mitrovica et al. (2005). The model was run using a spherical harmonic truncation of degree and order 256, which corresponds to a surface spatial resolution of ~75 km in the Greenland region. A total of 243 Earth viscosity models were considered in seeking an optimal data-model fit for each ice model reconstruction. The results of the Earth model calibration exercise are given in section 4.4.

4. MODELLING RESULTS

4.1 INTRODUCTION

Since we build upon the Huy2 model of the Simpson study (Figure 3), we begin by comparing predictions from this model to our new constraint database in order to identify key weaknesses. We present in Figure 4 the sea-level predictions produced from our GIA model using the Huy2 reconstruction joined to ICE-5G with the Earth model identified as providing optimal fits to the RSL data base considered in the Simpson study. This Earth model consists of a 120 km lithosphere (LT120), upper mantle viscosity of 0.5×10^{21} Pas (UMV0.5), and lower mantle viscosity of 1×10^{21} Pas (LMV1). The optimal Earth model was determined by minimizing the data-model misfit using a χ^2 statistic. The Huy2 model is biased towards fitting data on the west Greenland coast due to the high number and precision of RSL data found there. Furthermore the χ^2 results suggested a different optimal Earth structure for the West and East coasts (LT120, UMV0.5, LMV1 and LT120, UMV0.3, LMV50 respectively). The existence and influence of lateral Earth structure was attributed as one of the major unknowns and model weaknesses which could have profound consequences on the accuracy of the ice chronology. Marine-based ice retreated from its maximum LGM shelf extent more or less simultaneously in all regions in the Huy2 model (Fig. 3); however geological observations suggest an asynchronous retreat on the East and West coast. As suggested in the Simpson study, the improvements in data-model fits by adopting different viscosity parameters for the east coast might also be achieved by revising the ice chronology such that there is asynchronous retreat on the east and west coasts. This is an issue we explore below (see Section 4.2.3).

The Huy2 RSL predictions are shown in comparison to another widely used Greenland reconstruction – the ICE-5G variant of the GrB model (Tarasov and Peltier, 2002; Peltier, 2004) – in Figure 4. The GrB model is the Greenland component in the global ICE-5G reconstruction (Peltier, 2004). The RSL predictions for this model were generated using the Earth model it was developed with, the "viscosity model 2" or VM2, which comprises an elastic and density structure defined by PREM (Dziewonski and Anderson, 1981) and a viscosity profile with an average upper mantle viscosity of $\sim 0.5 \times 10^{21}$ Pas and lower mantle of $\sim 2 \times 10^{21}$ Pas (See Fig 1 from Peltier, 2004). The GrB model predictions are shown for comparison in Figure 4 by the grey curve. Compared to the Huy2 results, the GrB model exhibits larger data-model discrepancies. This is most likely because less field data were available when it was developed and uncertainty in Earth viscosity structure was not considered.

We begin by focusing on the Huy2 RSL predictions denoted by the black curves in Figure 4. Data-model discrepancies will be discussed for all of Greenland, starting in west Greenland and working anti-clockwise. Around Disko Bugt, many isolation basin studies have demonstrated that after a rapid early Holocene fall, RSL fell below present by 5-4 ka BP to reach a lowstand at ~2 ka BP before rising to present (Long et al., 1999, 2003, 2006). Generally, the West Greenland Huy2 RSL predictions reproduce the RSL observations well with the exception of a few minor misfits in the rate of RSL fall and/or lowstand at Kangerluarsuk (1), Pakitsoq (3), Upernivik (4), Orpisook (5), Qeqertarsiatsuaq (7), Sisimiut(8), and Sondre (9). For example, the Huy2 prediction for Sisimiut suggests a RSL fall that is too gradual with a Late Holocene lowstand that does not sufficiently capture the data.

In the Nuuk region, the Huy2 model fails to produce the shape and amplitude required to fit the RSL limiting dates and index points. Continuing southwards along the southwest coast there is a

transition away from the characteristic type of RSL curve found in the west (e.g. Disko Bugt) starting at Paamiut (Fig. 4b) where sea-level was at an elevation equivalent to that at present, between 10-9 ka BP and remained below present thereafter. In southern Greenland, sea levels reached present at 10-8 ka BP and attained a lowstand sometime during the Mid Holocene. The Huy2 model does not capture well the ML, when present-day sea-level is first reached nor the lowstand amplitude at a number of locations in this region, specifically Paamiut (13), Qaqortoq (14), Tasiusaq (15), and Nanortalik (16) (Fig. 4b). The sea-level index points are seldom reached by the model predictions. The Simpson study noted the poor model fits in this region as they cannot be explained by model parameter uncertainties in the Earth structure. A similar result was obtained by Fleming and Lambeck (2004) with their GREEN1 Greenland model.

There are few RSL data from southeast Greenland and for those that exist (Ammassalik (17)), the timing of retreat from the shelf (12 ka BP) is too late compared to the geological evidence (Jennings et al., 2006; Andrews, 2008; Long et al., 2008). Additionally, the Huy2 model predicts relatively high RSL values and a rate of sea-level fall that is too late (site 17. Amm; Figure 4c). Similar misfits are evident in the East and Northeast where the model over-predicts the limiting dates (Fig. 4c). As mentioned above, the ice model was not revised in the Simpson study; instead a different viscosity structure was invoked to better fit the observations along the east coast. The alternate (East coast) viscosity structure produces an excellent fit to observations in the Scoreby Sund area; however, discrepancies are still evident at Wollaston (23) and Germania (24) where the initial timing of sea-level fall fails to capture the data (dashed black curves in Fig. 4c). In Northeast Greenland the Huy2 RSL predictions do fit the observations with the east coast Earth model from Hvalros Ø (26) to Ingelbord Halvø (31) (Fig. 4d), however, we note that these sites consist mainly of limiting dates and so the observational constraints are not precise.

In North Greenland the RSL observations are largely comprised of limiting dates. However, predictions based on the Huy2 model do not capture the timing nor the magnitude of the initial RSL fall indicated by the data (Fig. 4e). The initial timing of RSL fall is insensitive to variations in the adopted Earth structure which suggests that the misfit is due to the regional deglacial history. The fact that the Huy2 model does not simulate the coalescence of the Greenland and Innuitian ice sheets leads to thinner ice and therefore a smaller RSL fall, which is also an important issue to explore.

The RSL observations more effectively constrain the ice margin retreat history while the ice-core derived thinning curves provide complementary constraints in the interior. Thinning curves for the Huy2 model consist of both ice thinning and vertical land motion (based on the regional-wide optimal viscosity model). As discussed in Section 4.5, these results suggest that the model misrepresents the chronology by over-responding to the HTM at the DYE-3 site and, conversely, not responding enough at Camp Century. At the more central NGRIP ice-core sites, the Huy2 model captures the inferred thinning within the observational uncertainty (Lecavalier et al., 2013), however the summit of the GrIS (GRIP) does not thin sufficiently at ~8 ka BP.

The discrepancies noted in this section are primary targets used to guide the calibration of an improved deglaciation model for Greenland.

4.2 HUY3 CALIBRATION

All the changes introduced below were sequentially incorporated into the original Huy2 model. Firstly, the LGM ice extent is evaluated and a sensitivity analysis is conducted to arrive at a revised LGM ice mask. Subsequently, the climate and sea-level forcings are discussed and a sensitivity analysis focusing on these model aspects is presented. We then investigate the impact of the North American ice

complex on near-field Greenland RSL predictions by consideration of a suite of ice histories for this region. Finally, using our constraint database and the results of the sensitivity analyses we select optimal model parameters, highlight key parameter trade-offs and model weaknesses. The present study involved a total of over 300,000 sets of model predictions which were compared to the constraint data base. The workflow which resulted in this ensemble of predictions is delineated in Figure S2.

4.2.1 LGM MASK

The Simpson study experimented with three different LGM ice extent scenarios; (1) the original Huy1 LGM extent as the minimum extent, (2) a maximum extent mask which extended to the shelf edge around the periphery of Greenland, and (3) a hybrid extent based on some field evidence and combined elements from (1) and (2). The LGM mask acts as a direct boundary condition in the glaciological model meaning that if the ice sheet experiences positive mass balance, it can only grow to the maximal LGM mask extent. Based on the literature of the time, it was determined that the hybrid LGM mask was most appropriate and it also produced the best fits to RSL observations.

As discussed in section 2.1, new geological evidence has made a compelling case to re-evaluate the Greenland LGM mask (e.g. O'Cofaigh et al., 2012; Dowdeswell et al., 2013). In Figure 5, the Huy2 hybrid LGM mask is plotted in red. Recently Funder et al. (2011a) reviewed the literature and proposed an LGM ice extent (henceforth called the Funder extent) shown in green which is regarded as a "minimum" extent. The Funder extent more or less coincides with the Huy2 hybrid LGM extent. The differences between these two reconstructions are generally found in East and Northeast Greenland where Funder et al. (2011a) propose an inner-mid shelf LGM extent as opposed to outer shelf in the Huy2 hybrid LGM mask (see section 2.1). The accuracy of the two extent scenarios can be tested by comparing model predictions and observations for the ML as this quantity is highly sensitive to the magnitude of ice unloading and therefore the LGM extent. Figure S3a shows the location of relevant ML observations used to test which of the two extent scenarios is more accurate in Northeast Greenland. The Huy2 RSL predictions produce MLs which are substantially too high (Figure S3b) even when parametric uncertainties in the sea-level forcing and the Earth's viscosity structure are considered. In contrast, the Funder LGM mask results in lower RSL values which fall within the ML data (Fig. S3b). We note that while there remain ML data-model discrepancies for the Funder LGM mask, the residuals are within parametric uncertainties (e.g. climate and sea-level forcing).

The Huy2 LGM mask was also revised in the West and Northwest of Greenland (compare blue and red contours in Fig. 5). Along the west coast, between approximately 67 and 75 degrees North, we extend the LGM mask out towards the shelf break in order to capture the constraints of O'Cofaigh et al. (2012) and Dowdeswell et al. (2013) (see Section 2.1). Since the data only constrain the margin position near the Disko and Uummannaq Troughs, with the former accommodating the Jakobshaven Isbræ outlet glacier (approx. 68 degrees North), we use ML data to test the accuracy of a more extensive LGM margin north of this location (Figure S3c and d).

In contrast to the results for the Northeast region, the Huy2 optimal LGM mask predicts ML values that are, in general, too low in the Northwest (even when considering parametric uncertainty) thus supporting the more extensive LGM margin scenario. We note that this revision is not inconsistent with the Funder LGM mask as it was intended to represent a minimum plausible scenario in regions that remain unconstrained by direct observations. In the far North, the LGM mask was also pushed father out. While there are no RSL data to support this revision, it was made to compensate for the lack of a dynamically connected Greenland and Innuitian ice sheet.

Numerous other LGM extent scenarios were investigated in addition to the final revised scenario (blue line in Fig. 5) to assess parametric trade-off between ice extent and sea-level forcing (Section 4.2.3) on the resulting RSL predictions (see Figure S2). Based on this sensitivity analysis and results described above, we adopt the blue contour line in Fig. 5 as the LGM mask for our new model since it is consistent with the majority of direct geological observations and optimises the fit to the RSL data.

4.2.2 TEMPERATURE FORCING

The temperature reconstruction based on the GRIP $\delta^{18}O$ record (Dansgaard et al., 1993) is used to generate a temperature profile across Greenland to force the ice model (as described in Simpson et al., 2009). The GRIP $\delta^{18}O$ record is converted to temperature using a conversion factor (Cuffey, 2000) and corrected for latitude and elevation changes across Greenland. However the conversion does not consider the influence of elevation changes on the sensitivity of this isotope to climate which can be non-negligible over periods of small temperature change (Huybrechts, 2002). This is one explanation for the lack of a clearly defined HTM in this temperature reconstruction compared to those reconstructed from other ice-cores and other archives in the northern hemisphere (Dansgaard et al., 1971; Koerner and Fisher, 1990; Cuffey et al., 1995; Dahl Jensen et al., 1998; Bennike and Weidick, 2001; Kaufman et al., 2004; Lecavalier et al., 2013). This is accounted for in the Simpson study by superimposing a parabolic function to incorporate a pronounced HTM in the temperature forcing. We adopt their revised GRIP temperature record but consider departures from it by scaling the HTM amplitude to investigate the sensitivity of the model to uncertainty in this forcing component and find the forcing that optimises the fit to observations. Figure 6 illustrates the GRIP temperature record and Huy2 and Huy3 HTM scaling from which a temperature profile is derived across Greenland. The amplitude of the HTM parabola in the revised GRIP record is adjusted to maximize the fit to the ice extent and RSL observations that suggest a response of the ice sheet to the HTM. Previous modelling studies have suggested that the southwest region responded most dramatically to the HTM (Tarasov and Peltier, 2002; Simpson et al., 2009). The imposed HTM causes a margin retreat inland of its present-day location and a subsequent re-growth which causes a change from RSL fall to rise in the southwest of Greenland during the late Holocene. RSL along the west and southwest coasts is well constrained during the Holocene suggesting that it might be possible to infer a minimum ice margin configuration. The results of this modelling exercise are presented in Section 5.1.2.

In addition to testing the sensitivity of the ice sheet to the form of the HTM, this study also makes changes to the calculation of melt potential using the PDD method, which is necessary to calculate surface runoff using the retuned runoff model of Janssens and Huybrechts (2000). The standard deviation of the Gaussian temperature distribution generated from the temperature record is traditionally held constant (4.2^{o}C)) in the PDD algorithm. Recently, weather station observations have been used to define a relationship between the standard deviation and temperature (Wake et al., 2014). This relationship was adopted in the glaciological model applied here. Notably, this modification allowed us to keep degree-day factors fixed for the duration of the model run, in contrast to the Huy2 study. Although there is a scientific basis for the reduction of degree-day factors (DDFs) from the Holocene until present due to declining incoming isolation (Hock, 2003), it is not possible to constrain this relationship at present. In Huy3, DDFs act uniformly across the ice sheet and are, respectively, for snow and ice, 3 and 8 mm/day/degree C (water equivalent) (Braithwaite, 1995; Janssens and Huybrechts, 2000; Hock, 2003). In the original Huy1 and Huy2 studies, the DDFs were tuned over the Holocene period and subsequently reset so that the model reproduced the present-day ice sheet geometry. A sensitivity analysis was conducted on the DDFs and it was determined that few permutations could simultaneously reproduce present-day ice volume and

compare relatively well against the constraint database. These developments had the effect of removing the need to apply tuning of DDFs to reproduce the present-day ice sheet geometry (Figure S4).

4.2.3 SEA LEVEL FORCING

As discussed in section 3.1, the interaction of sea level and marine-based ice is expressed by parametric equations which reproduce to first-order large-scale ice margin changes (Zweck and Huybrechts, 2003, 2005). These equations correlate sea level to the grounding line ice thickness through an empirical formulation that defines a maximum grounding depth beyond which the ice calves. The empirical relationship produces periods of ice advance over the shelf when barystatic sea level is low, enabling the expansion of the GrIS to its LGM position. Conversely, as sea level rises the ice sheet retreats landward. The position of the grounding line is parameterised as a function of barystatic sea level which is taken from the SPECMAP stack of marine oxygen-isotope values (Imbrie et al., 1984). In section 2.1, several geological records indicate a spatially and temporally varying retreat of marine-based ice across the shelf. Even though the spatial coverage of these data is low and the timing at which the retreat occurs is poorly constrained in many areas, there is enough information to demonstrate the limitation of this aspect of the Huy2 model, which results in a similar timing of retreat around the entire margin (minor variations in the timing of the marine retreat in the Huy2 model reflects ocean bathymetry).

In the Simpson study, three different sea-level forcings were applied that were based on parametric equations composed of linear and quadratic expressions (see their equations 3, 4 and 5). The three retreat scenarios are generalized to represent early, mid, and late cases (initial retreat by 16, 14, and 12 ka BP; respectively). The rate at which the ice retreats varies substantially; the late case produces an abrupt and rapid retreat while the early case yields a more gradual withdrawal from the shelf. The sea-level forcing clearly has a strong control on the resulting RSL predictions, affecting the amplitude and timing of the initial RSL fall. The Simpson study chose their late retreat equation since it optimised the fit to the highest quality data in the Disko Bugt area; however, it was clear that RSL data from the East and Northeast favoured an earlier retreat. RSL and other data suggest a range of different times for the onset of retreat around Greenland and these cannot be captured by applying a single sea-level forcing across the entire GrIS. Therefore, a spatially variable sea-level forcing was implemented for the development of Huy3 by allowing regional variation in the applied parametric equations to capture the timing of initial retreat and rate of retreat suggested by geological evidence, and to maximize the fit to the RSL data (Figure S5). Even though this approach is crude in the sense that the underlying physical processes that cause marine grounding line retreat are not modelled (Cornford et al., 2013), it presents the opportunity to match the growing field evidence and produce a more accurate deglaciation history. The forcing mechanism responsible for the observed retreat cannot be explicitly considered given the simple nature of the parameterisation.

In West Greenland, evidence from cross-shelf troughs suggests that the ice extended out to the shelf break during the LGM and initially retreated around ~14 ka BP to reach the present-day coastline by ~10 ka BP (O'Cofaigh et al., 2012). This chronology is in good agreement with an intermediate sea-level forcing scenario which also happens to achieve the strongest fit to the RSL observations, similar to the original Huy1 forcing. Southern Greenland also experiences a better fit to the RSL observations with this forcing, with an initial retreat ~16 ka BP and ice reaching the present-day coastline by 12 to 10 ka BP and present-day extent shortly thereafter (Bennike et al., 2002; Sparrenbom et al. 2006a,b; Larsen et al., 2011; Woodroffe et al., 2013). Margin retreat in Southeast Greenland is constrained by a small collection of

RSL observations at Ammassalik (south of the Helheim Glacier; Long et al., 2008) as well as ice-rafted debris, both of which suggest a rapid retreat shortly after 16 ka BP (Nam et al., 1995; Kuijpers et al., 2003). An intermediate sea-level forcing (black curve from Figure S5), similar to that adopted for West Greenland, best fits the geological record and RSL observations in this region. Observations from East Greenland suggest a rapid and relatively late retreat and so favour a sea-level forcing that lies between the original Huy1 "intermediate" and Huy2 "late" parameter values (Figure S5). This East Greenland sea-level parameterization results in the deglaciation of outer Scoresby Sund by 12 ka BP and all of it by 10 ka BP, exactly as suggested by Funder et al. (1998). Northeast Greenland marine-based ice initially retreated by 10 ka BP (Evans et al., 2009; Winkelmann et al., 2010) whereas in North Greenland the retreat started sometime during 16 to 10.3 ka BP (Larsen et al., 2010). Furthermore, the high ML observations in North Greenland suggest a late retreat which is best encapsulated by the lower bound sea-level forcing parametric equation found in Figure S5. The deglaciation of the Nares Strait is also captured best by a late forcing scenario.

The ability to apply regionally specific sea-level forcing parameterisations across Greenland to better match the field constraints has led to an important result: optimal fits to RSL data from both the East and West coasts can be achieved using a single viscosity model. That is, there is no need to invoke lateral variations in Earth viscosity structure to fit the RSL data as done in the Simpson study. We believe this is one of the more significant contributions of this study since the Huy3 chronology does not hide model weaknesses in poorly constrained lateral Earth structure. In certain regions of Greenland there is either a lack of data or relatively poor constraints making it difficult to discriminate between the different sea-level forcing parameterisations (see section 2.1). Also, it is important to note that, even given the broad range of parameters considered, the marine retreat does not occur before 16 ka BP or after 12 ka BP which simply reflects the fact that the input barystatic curve does not change sufficiently before or after this time interval.

In the following sections, the revised ice extent mask from section 4.2.1 is applied and the improvements in the climate (Section 4.2.2) and sea-level forcing are adopted with their optimal parameterizations. The resulting GrIS reconstruction defines the Huy3 model with the ice margin chronology shown in Figure 7.

4.3 NORTH AMERICAN ICE SHEET

As mentioned above, previous studies have demonstrated the influence of the NAIC on postglacial RSLs around Greenland (Fleming and Lambeck, 2004; Simpson et al., 2009). Therefore, to accurately reconstruct the evolution of the GrIS, it is necessary to consider the influence of this adjacent body of ice. By incorporating our GrIS reconstruction within the ICE-5G global model, the influence of the NAIC is implicitly considered. However, all ice model reconstructions have inherent uncertainty and to account for this we adopt a series of alternative NAIC models. Specifically, we consider a high variance subset of NAIC deglacial histories from a large-ensemble Bayesian calibration of a glaciologically self-consistent and dynamical ice sheet model (Tarasov et al., 2012). These models were constrained using a number of different data types, including ice extent, RSL histories and rates of present-day land uplift. The model calibration procedure applied by Tarasov et al. (2012) produces a probability distribution of NAIC deglaciation scenarios. We selected an 11 member high variance subset of the best-scoring reconstructions from this distribution to replace the NAIC component of the global ICE-5G reconstruction.

Figure 8 shows the differences between ICE-5G (Peltier, 2004) and the best-scoring nn9927 solution from Tarasov et al. (2012). It illustrates the proximity of the NAIC to the GrIS and its relevance

to Greenland near-field RSL. The two NAIC models shown in Figure 8 demonstrate clear differences in grid resolution, where ICE-5G suffers from significant discontinuities between grid cells resulting in glaciologically unphysical slopes. For example, at 16 ka BP the ICE-5G NAIC has neighbouring grid points with differences in ice thickness of 3000 metres. Additionally, the NAIC models exhibit very different ice volumes, thicknesses, and chronologies. At 16 ka BP, both models cover a comparable areal extent, however, their respective ice thicknesses differ in many places by over one kilometre with the ICE-5G component providing larger thickness estimates. At 12 ka BP, the best-fitting Tarasov et al. (2012) nn9927 model exhibits a larger ice volume and extent with the Cordilleran ice sheet remaining, which contrasts to the NAIC in ICE-5G. By 8 ka BP, the ICE-5G NAIC is all but gone while the nn9927 model has large ice caps scattered across eastern and northern Canada. Figure 8 clearly illustrates the resulting differences in chronology between a loading model (Peltier, 2004) and glaciologically self-consistent model (Tarasov et al., 2012). Figure 9 compares the non-Greenland RSL contribution from ICE-5G and nn9927 at 16 ka BP. The difference of these two NAIC RSL contributions around the periphery of Greenland is shown in Fig. 9c.

The uncertainty in Greenland near-field RSL due to the inherent uncertainties in NAIC reconstructions is shown in Figure S6 using a high variance subset of NAIC reconstructions from Tarasov et al. (2012) and ICE-5G. The uncertainty is spatially variable with the greatest amplitude in Northwest and South Greenland of up to 60 m and 15 m at 16 ka BP (Figure S6b and e), respectively. In comparison there are regions such as East Greenland where RSLs are relatively unaffected by the NAIC during deglaciation. Northwest Greenland RSL predictions are highly sensitive to changes in the Innuitian ice sheet while South Greenland is most sensitive to the Laurentide ice sheet. The North American Bayesian calibration yields a wide range of reconstructions which fit the observations. The envelope of uncertainty on Greenland RSL resulting from these NAIC reconstructions (Figure S6) should be considered when gauging the accuracy of our GrIS reconstruction based on fits to these data.

4.4 RSL PREDICTION

In this section, the revised ice model resulting from the previous sections (4.2.1-4.2.3; referred to as Huy3) is applied to generate RSL predictions with the Tarasov et al. (2012) best-fitting NAIC model (nn9927). We compute RSL for the Huy3 model using a suite of 243 Earth viscosity models. The data-model discrepancies are encapsulated within the χ^2 values shown in Figure 10. Using the RSL data described in Section 2.2, the minimum χ^2 values for Huy2 and Huy 3 are 708.3 and 377.4, respectively, indicating a statistically significant improvement in the data-model fits for the Huy3 model. The optimal Huy3 Earth model was found to have a 120 km lithosphere, an upper mantle viscosity of 0.5×10^{21} Pas and lower mantle viscosity of 2×10^{21} Pas. Our study investigated a broader range of viscosity models than the Simpson study; however the general pattern in the χ^2 results remains similar. As in Simpson et al. (2009), temporal uncertainty in the RSL observations were not considered when computing the χ^2 values. Incorporating dating uncertainty into the χ^2 analysis will most likely result in lower χ^2 values and a smaller variation in these values when changing model input parameter values. Inspection of Fig. 10 indicates that the model fits are more sensitive to changes in upper rather than lower mantle viscosity which is compatible with the spatial scale of the loading changes (Figure S7). There are a number of Earth models which produce comparable fits to the observations based on an F-test (nominal 95% confidence interval). We cannot discriminate between these Earth models; therefore they represent the uncertainty in Earth viscosity structure on the RSL predictions. It should be noted that the optimal Earth model found by the Simpson study falls within the nominal 95% confidence interval of the Huy3 χ^2 result (Table 2).

In Figure 11 we show predicted RSL patterns around Greenland for the optimal Huy3 model. Output from this model is compared to our RSL database in Figure 12. We show the envelope of predictions due to uncertainties in the NAIC deglacial history in Figure S6 and due to uncertainties in the Earth viscosity model as defined above (Fig. 12). The Huy3 predictions are shown with the Huy2 optimal East and West predictions in Fig. 12 (dotted and solid black lines, respectively). In the remainder of this sub-section we discuss the data-model fits with a focus on the Huy3 results and the implications of these results for the ice chronology. It is well known that constraining a regional GIA model is a non-unique inverse problem; therefore, we discuss parameter trade-offs and highlight, when possible, independent observational evidence that reduces the possible solution parameter space.

Starting in West Greenland and working anti-clockwise we discuss data-model discrepancies. The best-fitting Huy3 predictions produce an excellent fit to the western sites 1-6 (Fig. 12a & S6a); this is not surprising since the χ^2 results are heavily weighted to this region due to the high density of precise sea-level index point data. Compared to the Huy2 RSL predictions, the Huy3 model achieves a slightly better fit to the sea-level lowstand (e.g. compare results for site 4. Upe, in Fig. 4a, 12a & S6a) and rate of RSL fall (e.g. site 5. Orp, Fig. 12a), especially when taking into consideration the uncertainty in Earth structure (Fig. 12a) and non-Greenland ice (Fig. S6a). There remain two persistent data-model discrepancies at Kangerluarsuk (1) and Pakitsoq (3) where Mid-Holocene RSL observations are under predicted. Overall, the west Greenland Huy3 RSL predictions have much higher amplitude; however they remain consistent with the ML observations since the relevant sites became ice-free sometime between 12 to 9 ka BP (Funder et al., 2011a). At Sisimiut (8) and Søndre (9) the Huy3 predictions improve upon the Huy2 model in most respects: capturing the ML, rate of RSL fall and the Late Holocene lowstand. The western shelf and Disko Bugt were covered at the LGM and this area was probably the site of a Jakobshavn Isbrae precursor which extended out to the shelf edge (Funder and Hansen, 1996; Long and Roberts, 2003; Weidick and Bennike, 2007; O'Cofaigh et al., 2012; Dowdeswell et al., 2013). In contrast to the Huy2 reconstruction which adopts an inner shelf LGM extent, we found that a more extensive LGM extent improved the fit to the geomorphological observations while maintaining a high quality fit to RSL observations. Furthermore, the Huy2 model has a late deglaciation in West Greenland starting at 12 ka BP leaving the shelf ice free by 10 ka BP. Recent marine geological data (O'Cofaigh et al., 2012) have suggested an earlier deglaciation, which is explicitly incorporated into the Huy3 model. This consistency between multiple lines of evidence gives a high level of confidence in the accuracy of the Huy3 model in this region.

South of Disko Bugt in the Nuuk area (Sites 10-12), the Huy2 model fails to fit the RSL observations with its optimal Earth model. The Huy3 reconstruction remains consistent with its Earth model and produces an adequate fit to the observations, falling within the limiting dates and capturing a good number of the sea-level index points; however the predicted RSL amplitudes fall short of the ML observations (Fig12b, S6b). At present the southwest margin is the largest ice-free land area in Greenland where observational evidence of the Holocene retreat is well documented with recessional moraine systems and threshold lake data (e.g. Van Tatenhove et al., 1995; Larsen et al., 2013). In areas with little fjord-drainage such as the Kangerluussuaq area in West Greenland, the present ice-margin position may not have been attained until 6 ka BP (Van Tatenhove et al., 1996), whereas in other areas with a fjord setting the present-day margin was reached by 9 ka BP (Larsen et al., 2013). Results from both Huy2 and Huy3 broadly agree with the observations.

Southwest and South Greenland are areas of high quality data, but also where the largest Huy2 and Huy3 RSL data-model discrepancies exist (Figure 12b). Compared to the Huy2 model, the Huy3 RSL predictions achieve an improved fit to the observations at all four sites, Paamiut (13), Qaqortoq (14), Tasiusaq (15), and Nanortalik (16), especially when considering uncertainties in non-Greenland ice

(Figure S6b). The Huy3 RSL predictions capture the Middle to Late Holocene lowstand, reaching present-day values of sea-level between 10 to 8 ka BP. However, the MLs are not reached at any of the southern sites and the amplitude of rapid RSL fall from 12 to 10 ka BP is not captured at Paamiut, Tasiusaq and Nanortalik. Several sensitivity analyses were conducted in this region by varying the sea-level and climate forcing. The results indicated that a late retreat of marine-based ice would not sufficiently increase the amplitude of RSL change given that it produces a very rapid unloading of ice from the narrow continental shelf which limits the overall magnitude of unloading (Woodroffe et al., 2013). In addition, several parameters in the climate forcing were tuned to examine the impact of a Younger Dryas readvance. We inspected a spectrum of scenarios ranging from no readvance to a pronounced regrowth to the continental edge. This was found to influence the characteristic shape of the RSL prediction in terms of initial fall in RSL but the overall amplitude was left relatively unaffected. As shown by the grey envelop in Fig. S6b, the NAIC has a significant impact on South Greenland RSL and it has the potential to improve the fit to the Holocene sea-level index points, though it does not sufficiently increase predicted MLs by 12 ka BP. The very rapid RSL fall around 9 ka BP at these sites is also compatible with the influence of postglacial faulting which can produce displacements on the order of 10 metres (Steffen et al., 2014). This process is not simulated in the model applied here. Though a weak viscosity structure under South Greenland could account for some of the discrepancies, we chose to avoid considering models outside of the nominal 95% range of the χ^2 minimum given the lack of evidence to support the existence of low viscosities in this part of Greenland.

In the southeast, the Ammassalik (17) sea-level observations are predicted accurately with the Huy3 reconstruction within uncertainties of the Earth viscosity structure and NAIC (Figure 12c, S6c). Furthermore, we emphasise that this result is achieved using an Earth model which is consistent Greenland-wide. This dramatically improved fit for a single Earth model persists for the remaining eastern and northeastern sites, suggesting that the inferred eastern viscosity structure in the Simpson study was masking inaccuracies in the ice chronology. We note, however, that there are a few sites where the Huy2 model and its alternate (East) Earth structure produce a marginally better fit to the observations such as at Mesters Vig (20). The Huy3 predictions do not capture the upper RSL constraints, nor do they capture the fall in early Holocene RSL to reach present-day by ~7 to 6 ka BP. In East Greenland, the present-day margin was reached by approximately 8 to 7.5 ka BP (Funder, 1987) with the outer fjord ice free by 12 to 10 ka BP (Funder et al., 1998). This is represented well by the Huy3 chronology. North of Scoresby Sund, the Huy3 RSL predictions produce a better fit to observations compared to the Huy2 model, especially considering our consistent Earth structure. Some data-model discrepancies remain, however, even when taking uncertainties in Earth structure into account. At site 23 (Wollaston; Figure 12c) the ML is reached; however the timing and rate of RSL fall is inaccurate causing predicted RSL to fall above the upper limiting dates.

The Huy3 RSL predictions fit the majority of observations in Northeast Greenland within uncertainty of the Earth structure (Figure 12d). In contrast, North Greenland has a number of significant data-model misfits. The data is of low precision but they generally indicate a late and rapid fall in RSL (Figure 12e). Results for Northwest Greenland indicate a similar data-model discrepancy where the model fails to produce a sufficiently late RSL fall (Figure 12f). Neither the Huy2 nor Huy3 models satisfactorily fit the observations in these regions, even though both adopt a late sea-level forcing parameterisation. However, as previously stated, the model can only produce a retreat of marine-based ice as late as ~12 ka BP. Furthermore, the ice model applied to reconstruct the GrIS does not account for the dynamic connection to the Innuitian ice sheet, which would act to produce a thicker ice sheet in North and Northwest Greenland, and hence greater Holocene rebound and RSL fall.

4.5 ICE SHEET INTERIOR

A valuable boundary condition which has significant constraining power, particularly in the ice-sheet interior, is the topography of the present-day GrIS. Bamber et al. (2001) applied ice thickness data from ice-penetrating radar measurements to derive the present-day ice geometry with a volume of c. 7 m barystatic sea level. The present-day Huy3 comparison to the Bamber et al. (2001) present-day ice thickness is shown in Figure 13. The misfits shown in Figure 13a and their potential sources are discussed in greater detail in Section 5.2. With optimal ice and Earth models, present-day vertical land motion predictions are generated across Greenland (Fig. 13b; Figure S8). These can be applied with geodetic observations to interpret contemporary behaviour of the GrIS. Dome features of crustal uplift across North and East Greenland where rates are up to 3 mm/yr illustrate the viscous response of the Earth to a retreating and thinning ice margin. Moreover, a large area of subsidence in Southwest Greenland (minimum -6 mm/yr) highlights the significance of the neoglacial regrowth, combined with the on-going collapse of the Laurentide Ice Sheet forebulge.

Ice-core derived thinning curves at GRIP, NGRIP, Camp Century, and DYE-3 provide a further constraint on the GrIS interior (Lecavalier et al., 2013). The Huy3 thinning curve predictions (dashed black curve) are in Figure 14. The evolution of the surface elevation is generated using the Huy3 ice thickness chronology and model predictions for vertical land motion from the nominal 95% confidence interval from the χ^2 analysis (grey envelop; Figure 14). Given the uncertainty of the ice-core derived thinning curves, the model predictions generally remain within error. Compared to the Huy2 results, the primary improvement for those of Huy3 is the improved fit at Dye-3. The misfit at Camp Century is not resolved with either model, as the rapid thinning between 8 and 6 ka BP and the subsequent maximum response to the HTM are not captured. As noted above, thicker ice across northeast Greenland and rapid thinning after the disintegration of the Nares strait ice stream could account for the remaining discrepancy at the Camp Century thinning curve. Additionally, it is possible that we misrepresent the timing and magnitude of the HTM in North Greenland where it is poorly documented. A warmer HTM in this region could explain RSL data-model misfits. Furthermore, at the GRIP site the thinning curve is marginally under predicted at 8 ka BP, similar to the Huy2 prediction. This could be due to poorly constrained boundary conditions at the bedrock allowing for more rapid transport of ice and permitting the present-day summit to thin more quickly during the Holocene. Additionally, as suggested by the Camp Century thinning curve and misrepresented by Huy3 model, significant thinning in North Greenland could propagate to the interior of the ice sheet and thus produce enhanced thinning at the summit.

5. DISCUSSION

5.1 GREENLAND ICE SHEET EVOLUTION

5.1.1 ICE VOLUME AND MARINE RETREAT

The Huy3 model features a number of distinct large scale characteristics. Figures 15 and S9 illustrate the evolution of the ice volume and areal extent of the Huy3 deglaciation and Figure 16 shows ice thickness at the times 16, 12, 8 and 4 ka BP. The Huy3 model has a relatively large LGM volume (4.7 m excess IESL) and areal extent compared to previous estimates: 2-3 m (Clark and Mix, 2002), 1.9-3.5 m (Huybrechts, 2002), 4.1 m (Huy2). The general trend to a larger Greenland LGM volume is consistent with recent geological findings from the continental shelf (e.g. O'Cofaigh et al., 2012). As in Huy2, Huy3 reaches a maximum volume after the global LGM at 16.5 ka BP with 5.1 m excess IESL compared to 4.6

m for Huy2. The timing of this volume maximum is controlled by the relative pacing of accumulation and ablation (Cuffey and Clow, 1997). Following the maximum volume at 16.5 ka BP, the Huy3 model predicts a spatially variable retreat from the shelf; the southern half of Greenland underwent a slow gradual retreat from ~16 to 10 ka BP while in the north, retreat is rapid and late starting at ~12 ka BP. In comparison, the GREEN1 model begins to retreat from the shelf at 16.3 ka BP while the GrB and Huy2 models do so at 12 ka BP. By 10 ka BP the Nares Strait was ice free and, regardless of region, the Huy3 margin had retreated to the present-day coastline, as shown by the predicted deglaciation dates (Fig. S10) and supported by field observations (Funder et al., 2011a). By incorporating a spatially variable sea-level forcing, the Huy3 marine retreat history better encapsulates the regional variability reflected in the observations compared to previous studies.

5.1.2 LAND-BASED RETREAT AND REGROWTH

In response to the HTM, the margin of Huy3 in some areas retreated inland of the present-day margin (Figure 7). As in the Huy2 model, the Southwest margin responded most dramatically and had retreated behind the present-day margin by 8 to 6 ka BP, which is in agreement with deglaciation dates (Bennike, 2008; Levy et al., 2012; Larsen et al., 2013; Briner et al., 2013). In response to the HTM, the Huy3 model reconstruction lost mass at a maximum century-average rate of c. 103.4 Gt/yr at 7.8 ka BP when modelled temperatures across Greenland were peaking. While there are some discrepancies between Huy3 and observed deglaciation dates, these are mostly related to the model resolution (20x20km) which limits the accuracy of margin predictions. The minimum areal extent of Huy3 is reached between 5 to 3.5 ka BP with the greatest volume deficit of 0.16 m IESL occurring at 4 ka BP (Figure 16d and S10). While the Huy2 model produced a similar ice volume deficit at minimum extent (0.17 m), it had too great of a response to the HTM, particularly in the southwest as suggested by the DYE-3 thinning curve (Figure 14). In the Huy2 reconstruction, the southwest margin responded by receding 60 to 100 km past the present-day margin position; in comparison the Huy3 model produces a more modest retreat of 20 to 60 km. The Huy3 model exhibits more widespread thinning in the Southwest compared to Huy2 which compensates for the more modest margin response and results in similar IESL deficits in the two models. In comparison, the GrB model (Tarasov and Peltier, 2002) reached an extent minimum considerably earlier at 8 ka BP with a significant and widespread retreat behind the present margin by 60 to 160 km in the Southwest. In the GREEN1 model (Fleming and Lambeck, 2004) a retreat of 40 km in the southwest was imposed in order to fit RSL observations in this region. In general, the Huy3 model is more consistent with the observational evidence compared to other modelling studies. Based on the sensitivity tests performed in generating Huy3, we agree with the conclusions arrived at in previous studies, that a Neoglacial regrowth of the GrIS is required to fit RSL observations from West Greenland (Kelly, 1985; Tarasov and Peltier, 2002; Fleming and Lambeck, 2004; Simpson et al., 2009).

5.2 DATA-MODEL MISFIT

While the Huy3 GrIS reconstruction does account for a number of data-model misfits shown by the Huy2 model (Figures 12 and 14), there remain a number of outstanding data-model discrepancies (e.g. Figure 12e). Here we discuss these discrepancies in the context of parameter trade-off, model limitations and model uncertainty, which highlights avenues of future research.

The Earth model applied here is spherically symmetric and so cannot accurately account for heterogeneity in the Earth structure. This model limitation is undoubtedly a source of some data-model discrepancy due to the likely existence of lateral Earth structure beneath Greenland (e.g. Darbyshire et al., 2004; Yakovlev et al., 2011; Petrunin et al., 2013). In the Simpson study, the existence of lateral Earth

structure was proposed as one possible source of the data-model discrepancies with the Huy2 model. The Simpson study also proposed that RSL misfits given a single Earth structure along the East coast could have been due to the unrealistic limitation of a spatially uniform sea-level forcing resulting in synchronous marine retreat. Subsequent studies have supported this idea (e.g. Funder et al., 2011a) and so an important element of our work was the implementation of a regionally variable sea-level forcing to test this hypothesis further. Our results show that the West-East data-model residuals can be addressed with this model extension, thus providing further support for this hypothesis. However, this does not rule out the likely influence of lateral Earth structure in some areas of Greenland.

The non-Greenland ice with greatest influence on Greenland RSL is the NAIC. During deglaciation of the NAIC, the net effect on Greenland sea-levels was a fall due to the influence of gravitational changes acting to lower the ocean surface. By 8 ka BP, North American ice was mostly gone and thus the prevailing contribution to sea-level was vertical land motion related with subsidence of the peripheral forebulge causing a rise in RSL. Due to Northwest Greenland's proximity to Ellesmere Island and the Innuitian ice sheet, postglacial rebound due to deglaciation of this area dominates over the collapse of the Laurentide forebulge leading to a sea-level fall in this part of Greenland (see Fig. 9). As previously stated in the Simpson study, once the GrIS was predominantly land-based, the contribution to local RSL from changes in non-Greenland ice can be equal or opposite to changes driven by the GrIS. Thus RSL predictions around Greenland can be highly sensitive to the adopted NAIC model as illustrated in Figure S6 where we plot predictions for the ICE-5G North American component and a high variance subset of NAIC models from Tarasov et al. (2012). This figure illustrates that some previous model discrepancies can be accounted for given uncertainties in the NAIC reconstructions. However, this uncertainty does not account for the relatively large residuals in Northwest Greenland.

The Huy3 ice model is compared to the present-day ice sheet extent from Bamber et al. (2001). The differences are shown in Figure 13. Calculating the root mean square of the differences between the modelled and observed ice thicknesses gives a value of 214.1 m. This is comparable to the Huy2 value of 239.3 m. When comparing the Huy3 model to the present-day geometry, negligible discrepancies are noticed over the interior of the GrIS but large differences are evident at the margins. Fig. 13 indicates that the Huy3 model over predicts ice thickness at the margins. This is expected given the margin is not simulated at the right position everywhere. The margin has a steep horizontal gradient in thickness, small changes in extent quickly translate in large thickness changes (a 20 km mismatch in extent is approximately a 500 m thickness mismatch farther inland). The modelled position of the margin is almost entirely determined by the surface mass balance and less so by the flow law or basal sliding. Therefore, a small mismatch in ice extent introduces large discrepancies when comparing to present-day ice geometries. Additionally, this produces RSL data-misfits for misrepresenting the unloading of ice at the margin. Also, ice streams are not well resolved due to the grid spacing adopted and so the discharge of ice at the margins is under-estimated, which will also lead to an overestimate of ice thickness at the margins. These model limitations are common to a number of recent analyses (e.g. Tarasov et al., 2012; Whitehouse et al., 2012). Therefore, there is a need to improve the model resolution particularly in marginal areas with short wavelength, high amplitude topography. Also, given the importance of surface mass balance in governing margin position, there is a clear need to obtain regionally constrained temperatures to avoid the reliance on a single temperature record from the ice sheet interior. Climate reconstructions from marginal lakes show good potential in this regard (e.g. Axford et al., 2013). Furthermore, the climate forcing is the largest source of uncertainty on the modelled deglacial chronology. Exploring this uncertainty source more fully requires a much more extensive analysis than that carried out here (e.g. Tarasov et al., 2012).

Even though parameter variations in the treatment of ice flow, isostasy, marine calving and basal processes have a considerable impact on the resulting reconstruction, there remain data-model discrepancies not accounted for by parametric uncertainties, particularly in North and South Greenland. This suggests limitations in our adopted glaciological, RSL and GIA model. Some physical processes are not represented in our ice model. The grid spacing prevents a physical resolution of ice stream and outlet glacier dynamics (e.g. Saito et al., 2003). With regards to marine-based ice, the model lacks a proper ice calving law, and because it is not fully understood, our ice model applies a series of parametric equations to simulate grounding line migration. Finally, given that a full-stokes solution to simulate ice dynamics over the deglaciation is too computationally intensive (Gillet-Chaulet et al., 2012; Larour et al., 2012), a shallow ice approximation is used. Even though the approximation is less accurate at the margins where bedrock and surface slope are steep (Baral et al., 2001), it has been used many times to simulate the large-scale evolution of an ice sheet over deglaciation (e.g. Van de Wal., 1999; Huybrechts, 2002; Tarasov et al., 2012). Furthermore, there is no coupling between the glaciological model and GIA model of RSL change which can have a significant impact on extent changes of marine-based ice (Gomez et al., 2013). At present, these modelling challenges are a focus of current research. However, most of these recent advances are computationally demanding and therefore target shorter timescales (order 100 a) than those considered here (order 100 ka). The present study involved a total of over 300,000 sets of model predictions to sample only a component of the parametric phase-space and thus partly assess solution non-uniqueness (Figure S2).

6. CONCLUSIONS

1. A new deglacial model of the GrIS (Huy3) is presented. It incorporates several model developments and a larger constraint database and produces significantly better agreement to a number of sea-level, ice extent and elevation observations relative to previous reconstructions.

2. The Huy3 model exhibits an excess IESL of 4.7 m at the LGM and reaches a maximum volume of 5.1 m by 16.5 ka BP. These larger values are a product of revisions to the lateral extent of the LGM GrIS margin.

3. By implementing a spatially variable ocean forcing, we considered a variety of marine margin retreat scenarios that were consistent with the available constraint data. A best fit to the extent, elevation and RSL data was achieved with the following chronology: in Southwest and Southeast Greenland, initial retreat of the model occurs between 16 to 14 ka BP with some regions experiencing a readvance during the Younger Dryas period. In contrast, the northern half of Greenland experienced a rapid and late retreat at ~12 ka BP. The present-day coastline was reached across Greenland by ~10 ka BP. Implementation of this chronology negates the requirement to invoke a strong East-West gradient in mantle viscosity structure, which was a feature of the Simpson study.

4. The model response to the HTM is characterised by 40 to 60 km retreat inland of the present-day margin in Southwest Greenland, which corresponds to a deficit volume of 0.16 m IESL. In comparison to the Huy2 model, the optimal response was achieved using a decreased temperature forcing resulting in a reduced margin retreat but increased marginal thinning to produce a similar IESL deficit. Thus, the Huy3 model exhibits a greater sensitivity to temperature change. Finally, in response to the HTM, our optimal model reconstruction lost mass at a maximum centennial rate of c. 103.4 Gt/yr.

5. The isostatic response of the solid Earth to past changes in ice and ocean load is required to correct geodetic satellite observations to obtain present-day mass balance of the GrIS. Using the Huy3

reconstruction with its optimal Earth model, predictions for present-day uplift rates are generated for past changes in the ice sheet (Figure 13 and S8).

6. With regard to the influence of North American ice sheet on Greenland RSL, we expanded upon previous studies (Fleming and Lambeck, 2004; Simpson et al., 2009) by considering a number of model reconstructions for the NAIC. Our results show that this source of uncertainty is largest in North West, West, and South Greenland and can account for some of the data-model misfits in these areas.

7. The Huy3 model achieves an improved fit to the constraint database, particularly when considering a single Earth model. There remain significant discrepancies, however, particularly on the Southern tip of Greenland where one or more of the following might be the main factor(s): lateral Earth structure, non-Greenland ice, postglacial faulting. Discrepancies also exist in North Greenland where the magnitude of ice thinning is insufficient and most likely due the lack of buttressing from the Innuitian ice sheet in the model simulations and/or poorly constrained climatic conditions.

ACKNOWLEDGEMENTS

Support provided by the Natural Science and Engineering Research Council of Canada, the Canada Research Chairs program, the Canadian Foundation for Innovation and the University of Ottawa. We thank Shawn Marshall for discussions that contributed to the results presented in this paper.

REFERENCES

Alley, R. B., Andrews, J. T., Brigham-Grette, J., Clarke, G. K. C., Cuffey, K. M., Fitzpatrick, J. J., Funder, S., Marshall, S.J., Miller, G.H., Mitrovica, J.X., Muhs, D.R., Otto-Bliesner, B.L., Polyak, L., White, J.W.C., 2010. History of the Greenland Ice Sheet: paleoclimatic insights. Quaternary Science Reviews 29(15), 1728-1756.

Andrews, J., Thang, P., Smith, I.M., Preston, R., Cooper, T., Jennings, A.E., 1997. Spatial and temporal patterns of iceberg rafting (IRD) along the East Greenland margin, ca. 68N, over the last 14 cal. ka. Journal of Quaternary Science 12, 1–13.

Andrews, J.T., Cooper, T.A., Jennings, A.E., Stein, A.B., Erlenkeuser, H.,1998. Late Quaternary iceberg-rafted detritus events on the Denmark Strait-Southeast Greenland continental slope (c. 65N) related to North Atlantic Heinrich events? Marine Geology 149, 211–228.

Andrews, J.T., 2008. The role of the Iceland ice sheet in the north Atlantic during the late Quaternary: a review and evidence from Denmark Strait. Journal of Quaternary Science 23 (1), 3–20.

Austermann, J., Mitrovica, J. X., Latychev, K., & Milne, G. A. 2013. Barbados-based estimate of ice volume at Last Glacial Maximum affected by subducted plate. Nature Geoscience 6(7), 553-557.

Axford, Y., Losee, S., Briner, J. P., Francis, D., Langdon, P. and Walker, I., 2013. Holocene temperature history at the western Greenland Ice Sheet margin reconstructed from lake sediments. Quaternary Science Reviews 59, 87-100.

Bamber, J.L., Layberry, R.L., Gogineni, S., 2001. A new ice thickness and bed data set for the Greenland ice sheet 1. Measurement, data reduction, and errors. Journal of Geophysical Research – Atmospheres 106 (D24), 33773–33780.

Baral, D.R., Hutter, K., Greve, R., 2001. Asymptotic theories of large-scale motion, temperature, and moisture distribution in land-based polythermal ice sheets: a critical review and new developments. Applied Mechanics Reviews 54 (3), 215–256.

Bennike, O., 1995. Paleoecology of two lake basins from Disko, west Greenland. Journal of Quaternary Science 10 (2), 149–155.

Bennike, O., Weidick, A., 2001. Late Quaternary history around Nioghalvfjerdsfjorden and Jokelbugten, north-east Greenland. Boreas 30 (3), 205–227.

Bennike, O., 2002. Late Quaternary history of Washington Land, north Greenland. Boreas 31 (3), 260–272.

Bennike, O., Björck, S., 2002. Chronology of the last recession of the Greenland ice sheet. Journal of Quaternary Science 17 (3), 211–219.

Bennike, O., Björck, S., Lambeck, K., 2002. Estimates of south Greenland late-glacial ice limits from a new relative sea level curve. Earth and Planetary Science Letters 197 (3–4), 171–186.

Bennike, O., 2008. An early Holocene Greenland whale from Melville Bugt, Greenland. Quaternary Research 69 (1), 72–76.

Bennike, O., Anderson, N.J., McGowan, S., 2010. Holocene palaeoecology of southwest Greenland inferred from macrofossils in sediments of an oligosaline lake. Journal of Paleolimnology 43, 787–798.

Bennike, O., Wagner, B., Richter, A., 2011. Relative sea level changes during the Holocene in the Sisimiut area, south-western Greenland. Journal of Quaternary Science 26 (4), 353-361.

Bennike, O., Wagner, B., 2012. Deglaciation chronology, sea-level changes and environmental changes from Holocene lake sediments of Germania Havn Sø, Sabine Ø, northeast Greenland. Quaternary Research 78, 103-109.

Berglund, M.H., 2003. The architecture at three Saqqaq sites in the Nuuk Fjord, Greenland. Études/Inuit/Studies 27 (1-2), 329-346.

Björck, S., Wohlfarth, B., Bennike, O., Hjort, C., Persson, T. 1994. Revision of the early Holocene lake sediment based chronology and event stratigraphy on Hochstetter Forland, NE Greenland. Boreas 23(4), 513-523.

Bindschadler, R.A., 1984. Jakobshavn Glacier Drainage-Basin – a balance assessment. Journal of Geophysical Research – Oceans 89 (NC2), 2066–2072.

Blake, W., 1999. Glaciated landscapes along Smith Sund, Ellesmere Island, Canada and Greenland. Annals of Glaciology 28, 40–46.

Braithwaite, R.J., 1995. Positive degree-day factors for ablation on the Greenland ice-sheet studied by energy-balance modeling. Journal of Glaciology 41 (137), 153–160.

Briner, J.P., Stewart, H.A.M., Young, N.E., Philipps, W., Losee, S., 2010. Using proglacial-threshold lakes to constrain fluctuations of the Jakobshavn Isbrae ice margin, western Greenland, during the Holocene. Quaternary Science Reviews 29, 3861-3874.

Briner, J. P., Kaufman, D. S., Bennike, O., & Kosnik, M. A. 2014. Amino acid ratios in reworked marine bivalve shells constrain Greenland Ice Sheet history during the Holocene. Geology 42(1), 75-78.

Christiansen, H. H., Bennike, O., Böcher, J., Elberling, B., Humlum, O., & Jakobsen, B. H. 2002. Holocene environmental reconstruction from deltaic deposits in northeast Greenland. Journal of Quaternary Science 17(2), 145-160.

Clark, J. A., Farrell, W. E., Peltier, W. R., 1978. Global changes in postglacial sea level: a numerical calculation. Quaternary Research, 9(3), 265-287.

Clark, P.U., Mix, A.C., 2002. Ice sheets and sea level of the Last Glacial Maximum. Quaternary Science Reviews 21 (1–3), 1–7.

Cornford, S.L., Martin, D.F., Graves, D.T., Ranken, D.F., Le Brocq, A.M., Gladstone, R.M., Payne, A.J., Ng, E.G., Lipscomb, W.H., 2013. Adaptive mesh, finite volume modeling of marine ice sheets. Journal of Computational Physics 232, 529-549.

Cuffey, K.M., Clow, G.D., Alley, R.B., Stuiver, M., Waddington, E.D., Saltus, R.W., 1995. Large arctic temperature-change at the Wisconsin-Holocene glacial transition. Science 270 (5235), 455–458.

Cuffey, K.M., Clow, G.D., 1997. Temperature, accumulation, and ice sheet elevation in central Greenland through the last deglacial transition. Journal of Geophysical Research – Oceans 102 (C12), 26383–26396.

Cuffey, K.M., 2000. Methodology for use of isotopic climate forcings in ice sheet models. Geophysical Research Letters 27 (19), 3065–3068.

Dahl-Jensen, D., Mosegaard, K., Gundestrup, N., Clow, G.D., Johnsen, S.J., Hansen, A.W., Balling, N., 1998. Past temperatures directly from the Greenland ice sheet. Science 282 (5387), 268–271.

Dahl-Jensen, D. and NEEM community members, 2013. Eemian interglacial reconstructed from a Greenland folded ice core. Nature 493, 489-494.

Dansgaard, W., Johnsen, S.J., Clausen, H.B., Langway Jr., C.C., 1971. Climatic record revealed by the Camp Century ice core. In: Turekian, K.K. (Ed.), The Late Cenozoic Glacial Ages. Yale University Press, New Haven, CT, pp. 37–56.

Dansgaard, W., Johnsen, S.J., Clausen, H.B., Dahl Jensen, D., Gundestrup, N.S., Hammer, C.U., Hvidberg, C.S., Steffensen, J.P., Sveinbjornsdottir, A.E., Jouzel, J., Bond, G., 1993. Evidence for general instability of past climate from a 250-Kyr ice-core record. Nature 364 (6434), 218–220.

Dowdeswell, J.A., Evans, J., O'Cofaigh, C., 2010. Submarine landforms and shallow acoustic stratigraphy of a 400 km-long fjord-shelf-slope transect, Kangerlussuaq margin, East Greenland. Quaternary Science Reviews 29, 3359–3369.

Dowdeswell, J. A., Hogan, K. A., Ó Cofaigh, C., Fugelli, E. M. G., Evans, J., Noormets, R. 2013. Late Quaternary ice flow in a West Greenland fjord and cross-shelf trough system: submarine landforms from Rink Isbrae to Uummannaq shelf and slope. Quaternary Science Reviews.

Dyke, A.S., Prest, V.K., 1987. Late Wisconsinan and Holocene Retreat of the Laurentide Ice Sheet. Scale 1:5,000,000. Map 1702A. In: Geological Survey of Canada, Ottawa, Ontario, Canada.

Dziewonski, A.M., Anderson, D.L., 1981. Preliminary reference Earth model. Physics of the Earth and Planetary Interiors 25 (4), 297–356.

England, J., 1985. The late Quaternary history of Hall Land, northwest Greenland. Canadian Journal of Earth Sciences 22(10), 1394-1408.

England, J., 1999. Coalescent Greenland and Innuitian ice during the Last Glacial Maximum: revising the Quaternary of the Canadian High Arctic. Quaternary Science Reviews 18 (3), 421–456.

Evans, J., Dowdeswell, J. A., Grobe, H., Niessen, F., Stein, R., Hubberten, H. W., Whittington, R. 2002. Late Quaternary sedimentation in Kejser Franz Joseph Fjord and the continental margin of east Greenland. Geological Society, London, Special Publications, 203, 149-179.

Evans, J., O´Cofaigh, C.A., Dowdeswell, J.A., Wadhams, P., 2009. Marine geophysical evidence for former expansion and flow of the Greenland Ice Sheet across the north-east Greenland continental shelf. Journal of Quaternary Science 24, 279–293.

Farrell, W.E., Clark, J.A., 1976. Postglacial sea-level. Geophysical Journal of the Royal Astronomical Society 46 (3), 647–667.

Fisher, D.A., Koerner, R.M., Reeh, N., 1995. Holocene climatic records from Agassiz Ice Caps, Ellesmere Island, NWT, Canada. The Holocene 5(1), 19-24.

Fleming, K., Lambeck, K., 2004. Constraints on the Greenland ice sheet since the Last Glacial Maximum from sea-level observations and glacial-rebound models. Quaternary Science Reviews 23 (9–10), 1053–1077.

Fredh, D., 2008. Holocene Relative Sea-level Changes in the Tasiusaq Area, Southern Greenland, with Focus on the Ta4 Basin. Examensarbeten i geologivid Lunds universitet, (221).

Fredskild, B., 1972. Palynological evidence for Holocene climatic changes in Greenland. In Vasari, Y., Hyvarinen, H., and Hicks, S. (eds.), Climatic Changes in Arctic Areas During the Last Ten Thousand Years, Acta Universitatis Ouluensis Series. A., No. 3, Geol. No. 1: 277-305.

Fredskild, B., 1983. The Holocene vegetational development of the Godthåbsfjord area, West Greenland. Meddelelser om Grønland Geoscience 10, 28.

Fredskild, B., 1985. The Holocene vegetational development of Tugtuligssuaq and Qeqertat, Northwest Greenland. Meddelelser om Grønland Geoscience 14, 20.

Funder, S., 1987. Quaternary Geology and Landforms of the Coast of Jameson Land, East Greenland. In: Geological Survey of Greenland, Copenhagen (map sheet).

Funder, S., Abrahamsen, N., 1988. Palynology in a polar desert, eastern north Greenland. Boreas 17 (2), 195–207.

Funder, S., 1989. Quaternary geology of the ice-free areas and adjacent shelves of Greenland. In: Fulton, R.J. (Ed.), Quaternary Geology of Canada and Greenland. Geological Survey of Canada, pp. 741–792.

Funder, S. 1990. Late Quaternary stratigraphy and glaciology in the Thule area, Northwest Greenland (22). Kommissionen for Videnskabelige Undersøgelser i Grønland.

Funder, S., Hansen, L., 1996. The Greenland ice sheet – a model for its culmination and decay during and after the Last Glacial Maximum. Bulletin of the Geological Society of Denmark 42, 137–152.

Funder, S., Hjort, C., Landvik, J.Y., Nam, S.I., Reeh, N., Stein, R., 1998. History of a stable ice margin east Greenland during the Middle and Upper Pleistocene. Quaternary Science Reviews 17 (1–3), 77–123.

Funder, S., Jennings, A., Kelly, M., 2004. Middle and Late Quaternary glacial limits in Greenland. In: Ehlers, J., Gibbard, P. (Eds.), Quaternary Glaciations. Extent and Chronology II. Elsevier, Amsterdam, pp. 425–430.

Funder, S., Kjeldsen, K.K., Kjær, K.H., O'Cofaigh, C., 2011a. The Greenland ice sheet during the past 300,000 years: A review. In: Ehlers, J., Gibbard, P.L., Hughes, P.D. (Eds.), Quaternary Glaciations. Extent and Chronology. Elsevier, Amsterdam, Developments in Quaternary Science 15, 699-713.

Funder, S., Goosse, Hugues, Jepsen, H., Kaas, E., Kjær, K.H., Korsgaard, N.J., Larsen, N.K., Linderson, H., Lyså, A., Möller, P., Olsen, J., Willerslev, E., 2011b. A 10,000-year record of Arctic Ocean sea-ice variability – view from the beach. Science 333 (6043), 747-750.

Gillet-Chaulet, F., Gagliardini, O., Seddik, H., Nodet, M., Durand, G., Ritz, C., Zwinger, T., Greve, R., Vaughan. D.G., 2012. Greenland Ice Sheet contribution to sea-level rise from a new-generation ice-sheet model. The Cryosphere 6, 1561-1576.

Glen, J.W., 1955. The creep of polycrystalline ice. Proceedings of the Royal Society of London Series A, 228 (1175), 519-538.

Gomez, N., Pollard, D., Mitrovica, J. X., 2013. A 3-D coupled ice sheet–sea level model applied to Antarctica through the last 40 ky. Earth and Planetary Science Letters, 384, 88-99.

Grachev, A. M., Severinghaus, J. P. 2005. A revised +10±4 C magnitude of the abrupt change in Greenland temperature at the Younger Dryas termination using published GISP2 gas isotope data and air thermal diffusion constants.Quaternary Science Reviews 24(5), 513-519.

Gregory, J. M., White, N. J., Church, J. A., Bierkens, M. F. P., Box, J. E., van den Broeke, M. R., Cogley, J.G., Fettweis, X., Hanna, E., Huybrechts, P., Konikow, L.F., Leclercq, P.W., Marzeion, B., Oerlemans, J., Tamisiea, M.E., Wada, Y., Wake, L.M., van de Wal, R.S.W., 2013. Twentieth-century global-mean sea-level rise: is the whole greater than the sum of the parts? Journal of Climate 26, 4476-4499.

Håkansson, L., Briner, J., Alexanderson, H., Aldahan, A., Possnert, G., 2007b. Be-10 ages from central east Greenland constrain the extent of the Greenland ice sheet during the Last Glacial Maximum. Quaternary Science Reviews 26 (19–21), 2316–2321.

Håkansson, L., Alexanderson, H., Hjort, C., Möller, P., Briner, J.P., Aldahan, A., Possnert, G., 2009. Late Pleistocene glacial history of Jameson Land, central East Greenland, derived from cosmogenic 10Be and 26Al exposure dating. Boreas 38, 244–260.

Hall, B., Baroni, C., Denton, G., Kelly, M.A., Lowell, T., 2008. Relative sea-level change, Kjove Land, Scoresby Sund, East Greenland: implications for seasonality in Younger Dryas time. Quaternary Science Reviews 27, 2283–2291.

Hall, B., Baroni, C., Denton, G., 2010. Relative sea-level changes, Schuchert Dal, East Greenland, with implications for ice extent in late-glacial and Holocene times. Quaternary Science Reviews 29, 3370–3378.

Hjort, C., Funder, S., 1974. The subfossil occurrence of Mytilus edulis L. in central East Greenland. Boreas. 3 (1), 23-33.

Hjort, C., 1979. Glaciation in northern East Greenland during the late Weichselian and Early Flandrian. Boreas. 8 (3), 281-296.

Hjort, C., 1981. A glacial chronology for northern East Greenland. Boreas, 10 (3), 259-274.

Hjort, C., 1997. Glaciation, climate history, changing marine levels and the evolution of the northeast Water Polynya. Journal of Marine Systems 10 (1–4), 23–33.

Hock, R., 2003. Temperature index melt modelling in mountain areas. Journal of Hydrology, 282 (1), 104-115.

Holland, D.M., Thomas, R.H., de Young, B., Ribergaard, M.H., Lyberth. B., 2008. Acceleration of Jakobshavn Isbrae triggered by warm subsurface ocean waters. Nature Geoscience, 1 (10), 659-664.

Hutter, K., 1983. Theoretical Glaciology: Material Science of Ice and the Mechanics of Glaciers and Ice Sheets. Kluwer Academic, Norwell, Massachusetts.

Huybrechts, P., 1996. Basal temperature conditions of the Greenland ice sheet during the glacial cycles. Annals of Glaciology 23, 226–236.

Huybrechts, P., de Wolde, J., 1999. The dynamic response of the Greenland and Antarctic ice sheets to multiple-century climatic warming. Journal of Climate 12 (8), 2169–2188.

Huybrechts, P., 2002. Sea-level changes at the LGM from ice-dynamic reconstructions of the Greenland and Antarctic ice sheets during the glacial cycles. Quaternary Science Reviews 21 (1–3), 203–231.

Ingolfsson, O., Frich, P., Funder, S., Humlum, O., 1990. Paleoclimatic implications of an early Holocene glacier advance on Disko-Island, west Greenland. Boreas 19 (4), 297–311.

Imbrie, J.Z., Hays, J.D., Martinson, D.G., MacIntyre, A., Mix, A.C., Morley, J.J., Pisias, N.G., Prell, W.L., Shackleton, N.J., 1984. The orbital theory of Pleistocene climate: support from a revised chronology of the marine d18O record. In: Berger, A., Imbrie, J.Z., Hays, J.D., Kukla, G., Saltzman, B. (Eds.). Milankovitch and Climate. D. Reidel, Dordrecht, pp. 269–305.

Jakobsen, B.H., Fredskild, B., Pedersen, J.B.T., 2008. Holocene changes in climate and vegetation in the Ammassalik area, East Greenland, recorded in lake sediments and soil profiles. Danish Journal of Geography 108, 21–50.

Jakobsson, M., Andreassen, K., Bjarnadóttir, L. R., Dove, D., Dowdeswell, J. A., England, J. H., Funder, S., Hogan, K., Ingolfsson, O., Jennings, A., Larsen, N.K., Kichne, N., Landvik, J.Y., Mayer, L.,

Mikkelsen, N., Möller, P., Niessen, F., Nilsson, J., O'Regan, M., Polyak, L., Nørgaard-Pedersen, N., Stein, R., 2013. Arctic Ocean glacial history.Quaternary Science Reviews 92, 40-67..

Janssens, I., Huybrechts, P., 2000. The treatment of meltwater retention in mass balance parameterizations of the Greenland ice sheet. Annals of Glaciology 31, 133–140.

Jennings, A.E., Hald, M., Smith, M., Andrews, J.T., 2006. Freshwater forcing from the Greenland ice sheet during the Younger Dryas: evidence from southeastern Greenland shelf cores. Quaternary Science Reviews 25 (3–4), 282–298.

Johnsen, S.J., Clausen, H.B., Dansgaard, W., Gundestrup, N.S.,Hansson, M., Jonsson, P., Steffensen, J.P., Jouzel, J., Stauffer, B., 1992. A 'deep' ice core from East Greenland. Meddelelser om Grønland. Geoscience 29, 1-22.

Kaufman, D.S., Ager, T.A., Anderson, N.J., Anderson, P.M., Andrews, J.T., Bartlein, P.J., Brubaker, L.B., Coats, L.L., Cwynar, L.C., Duvall, M.L., Dyke, A.S., Edwards, M.E., Eisner, W.R., Gajewski, K., Geirsdottir, A., Hu, F.S., Jennings, A.E., Kaplan, M.R., Kerwin, M.N., Lozhkin, A.V., MacDonald, G.M., Miller, G.H., Mock, C.J., Oswald, W.W., Otto-Bliesner, B.L., Porinchu, D.F., Ruhland, K., Smol, J.P., Steig, E.J., Wolfe, B.B., 2004. Holocene thermal maximum in the western Arctic (0–180 degrees W). Quaternary Science Reviews 23 (5–6), 529–560.

Kelly, M., 1980. The status of the neoglacial in western Greenland. Rapport Grønlands Geologiske Undersøgelse 96, 24.

Kelly, M., Bennike, O., 1992. Quaternary geology of western and central North Greenland. Rapport Grønlands Geologiske Undersøgelse 153, 34.

Kelly, M., Funder, S., Houmark-Nielsen, M., Knudsen, K.L., Kronborg, C., Landvik, J.Y., Sorby, L., 1999. Quaternary glacial and marine environmental history of north-west Greenland: a review and reappraisal. Quaternary Science Reviews 18, 373–392.

Kelly, M.A., Lowell, T.V., 2009. Fluctuations of local glaciers in Greenland during latest Pleistocene and Holocene time. Quaternary Science Reviews 28, 2088–2106.

Kelley, S.E., Briner, J.P., Young, N.E., 2013. Rapid ice retreat in Disko Bugt supported by ^{10}Be dating of the last recession of the western Greenland ice sheet. Quaternary Science Reviews 82, 13-22.

Kendall, R.A., Mitroviva, J.X., Milne, G.A., 2005. On post-glacial sea level: II. Numerical formulation and comparative results on spherically symmetric models. Geophysical Journal International 161 (3), 679–706.

Khan, S.A., Wahr, J., Leuliette, E., van Dam, T., Larson, K.M., Francis, O., 2008. Geodetic measurements of postglacial adjustments in Greenland. Journal of Geophysical Research – Solid Earth 113, B02402.

Klug, M., Bennike, O., Wagner, B., 2009. Repeated short-term bioproductivity changes in a coastal lake on Store Koldewey, northeast Greenland: an indicator of varying sea-ice coverage? Holocene 19, 653–663.

Kobashi, T., Kawamura, K., Severinghaus, J.P., Barnola, J.-M., Nakaegawa, T., Vinther, B.M., Johnsen, S.J., Box, J.E., 2011. High variability of Greenland surface temperature over the past 4000 years estimated from trapped air in an ice core, Geophysical Research Letters, 38 (21).

Koerner, R.M., Fisher, D.A., 1990. A record of Holocene summer climate from a Canadian High-Arctic Ice Core. Nature 343 (6259), 630–631.

Kuijpers, A., Troelstra, S.R., Prins, M.A., Linthout, K., Akhmetzhanov, A., Bouryak, S., Bachmann, M.F., Lassen, S., Rasmussen, S., Jensen, J.B., 2003. Late Quaternary sedimentary processes and ocean circulation changes at the southeast Greenland margin. Marine Geology 195 (1–4), 109–129.

Kuijpers, A., Dalhoff, F., Brandt, M.P., Hümbs, P., Schot, T., Zotova, A., 2007. Giant iceberg plow marks at more than 1 km water depth offshore West Greenland. Marine Geology 246, 60–64.

Lambeck, K., Smither, C., Johnston, P. 1998. Sea-level change, glacial rebound and mantle viscosity for northern Europe. Geophysical Journal International, 134 (1), 102-144.

Lambeck, K., Yokoyama, Y., Purcell, T. 2002. Into and out of the Last Glacial Maximum: sea-level change during Oxygen Isotope Stages 3 and 2.Quaternary Science Reviews 21(1), 343-360.

Landvik, J.Y., 1994. The last glaciation of Germania-land and adjacent areas, northeast Greenland. Journal of Quaternary Science 9 (1), 81–92.

Landvik, J. Y., Weidick, A., Hansen, A. 2001. The glacial history of the Hans Tausen Iskappe and the last glaciation of Peary Land, North Greenland. Meddelelser om Grønland Geoscience 39, 27-44.

Lane, T. P., Roberts, D. H., Rea, B. R., Ó Cofaigh, C., Vieli, A., Rodés, A. 2013. Controls upon the Last Glacial Maximum deglaciation of the northern Uummannaq Ice Stream System, West Greenland. Quaternary Science Reviews.

Larour, E., Seroussi, H., Morlighem, M., Rignot, E. 2012. Continental scale, high order, high spatial resolution, ice sheet modeling using the Ice Sheet System Model (ISSM). Journal of Geophysical Research: Earth Surface (2003–2012), 117(F1).

Larsen, N.K., Kjær, K.H., Funder, S., Möller, P., van der Meer, J., Schomacker, A., Linge, H., Darby, D., 2010. Extensive ice shelf glaciation in northern Greenland during the Last Glacial Maximum. Quaternary Science Reviews 29, 3399–3414.

Larsen, N. K., Kjær, K. H., Olsen, J., Funder, S., Kjeldsen, K. K., Nørgaard-Pedersen, N. 2011. Restricted impact of Holocene climate variations on the southern Greenland Ice Sheet. Quaternary Science Reviews 30(21), 3171-3180.

Larsen, N. K., Funder, S., Kjær, K. H., Kjeldsen, K. K., Knudsen, M. F., Linge, H., 2013. Rapid early Holocene ice retreat in West Greenland. Quaternary Science Reviews. In Press.

Lecavalier, B. S., Milne, G. A., Vinther, B. M., Fisher, D. A., Dyke, A. S., Simpson, M. J., 2013. Revised estimates of Greenland ice sheet thinning histories based on ice-core records. Quaternary Science Reviews, 63, 73-82.

Letré guilly, A., Reeh, N., Huybrechts, P.,1991. The Greenland ice-sheet through the Last Glacial interglacial cycle. Global and Planetary Change 90 (4), 385–394.

Levy, L. B., Kelly, M. A., Howley, J. A., Virginia, R. A., 2012. Age of the Ørkendalen moraines, Kangerlussuaq, Greenland: Constraints on the extent of the southwestern margin of the Greenland Ice Sheet during the Holocene: Quaternary Science Reviews 52,1-5.

Lloyd, J.M., Park, L.A., Kuijpers, B., Moros, M., 2005. Early Holocene palaeoceanography and deglacial chronology of Disko Bugt, west Greenland. Quaternary Science Reviews 24 (14–15), 1741–1755.

Long, A.J., Roberts, D.H., Wright, M.R., 1999. Isolation basin stratigraphy and Holocene relative sea-level change on Arveprinsen Ejland, Disko Bugt, west Greenland. Journal of Quaternary Science 14 (4), 323–345.

Long, A.J., Roberts, D.H., 2002. A revised chronology for the 'Fjord Stade' moraine in Disko Bugt, west Greenland. Journal of Quaternary Science 17 (5–6), 561–579.

Long, A.J., Roberts, D.H., 2003. LateWeichselian deglacial history of Disko Bugt, west Greenland, and the dynamics of the Jakobshavns Isbrae ice stream. Boreas 32 (1), 208–226.

Long, A.J., Roberts, D.H., Rasch, M., 2003. New observations on the relative sea level and deglacial history of Greenland from Innaarsuit, Disko Bug. Quaternary Research 60 (2), 162–171.

Long, A.J., Roberts, D.H., Dawson, S., 2006. Early Holocene history of the west Greenland ice sheet and the GH-8.2 event. Quaternary Science Reviews 25 (9–10), 904–922.

Long, A.J., Roberts, D.H., Simpson, M.J.R., Dawson, S., Milne, G.A., Huybrechts, P., 2008a. Late Weichselian relative sea-level changes and ice sheet history in southeast Greenland. Earth and Planetary Science Letters 272 (1–2), 8–18.

Long, A., Woodroffe, S., Dawson, S., Roberts, D.H., Bryant, C., 2008b. Late Holocene relative sea level rise and the Neoglacial history of the Greenland ice sheet. Journal of Quaternary Science 24, 345-359.

Long, A.J., Woodroffe, S.A., Roberts, D.H., Dawson, S., 2011. Isolation basins, sea-level changes and the Holocene history of the Greenland ice sheet. Quaternary Science Reviews 30 (27-28), 3748-3768.

Milne, G. A., Davis, J. L., Mitrovica, J. X., Scherneck, H. G., Johansson, J. M., Vermeer, M., Koivula, H., 2001. Space-geodetic constraints on glacial isostatic adjustment in Fennoscandia. Science, 291 (5512), 2381-2385.

Milne, G. A., Mitrovica, J.X., 1998. Postglacial sea-level change on a rotating Earth. Geophysical Journal International, 133(1), 1-19.

Milne, G. A., Mitrovica, J. X., & Schrag, D. P. 2002. Estimating past continental ice volume from sea-level data. Quaternary Science Reviews 21(1), 361-376.

Mitrovica, J.X. & W.R. Peltier, 1991. A complete formalism for the inversion of post-glacial rebound data: resolving power analysis. Geophysical Journal International 104, 267-288.

Mitrovica, J.X., Milne, G.A., 2003. On post-glacial sea level: I. General theory. Geophysical Journal International 154 (2), 253–267.

Mitrovica, J.X., Wahr, J., Matsuyama, I., Paulson, A., 2005. The rotational stability of an ice-age earth. Geophysical Journal International, 161 (2), 491-506.

Möller, P., Larsen, N.K., Kjær, K., Funder, S., Schomacker, A., Linge, H., 2010. Early to middle Holocene valley glaciations on northernmost Greenland. Quaternary Science Reviews 29, 3379–3398.

Nam, S.I., Stein, R., Grobe, H., Hubberten, H., 1995. Late Quaternary glacial interglacial changes in sediment composition at the east Greenland continental margin and their paleoceanographic implications. Marine Geology 122 (3), 243–262.

Nghiem, S.V., Hall, D.K., Mote, T.L., Tedesco, M., Albert, M.R., Keegan, K., Shuman, C.A., DiGirolamo, N.E., Neumann, G., 2012. The extreme melt across the Greenland ice sheet in 2012. Geophysical Research Letters 39, L20502.

Nørgaard-Pedersen, N., Mikkelsen, N., 2009. 8000 year marine record of climate variability and fjord dynamics from Southern Greenland. Marine Geology 264, 177–189.

O'Cofaigh, C., Dowdeswell, J.A., Evans, J., Kenyon, N.H., Taylor, J., Mienert, A., Wilken, M., 2004. Timing and significance of glacially influenced mass-wasting in the submarine channels of the Greenland Basin. Marine Geology 207 (1–4), 39–54.

O'Cofaigh, C., Dowdeswell, J.A., Jennings, A.E., Hogan, K.A., Kilfeather, A., Hiemstra, J.F., Noormets, R., Evans, J., McCarthy, D.J., Andrews, J.T., Lloyd, J.M., Moros, M., 2012. An extensive and dynamic ice sheet on the west Greenland shelf during the last glacial cycle. Geology 41 (2), 219-222.

Pedersen, J. B. T., Kroon, A., Jakobsen, B. H., 2011. Holocene sea-level reconstruction in the Young Sound region, Northeast Greenland. Journal of Quaternary Science 26 (2), 219-226.

Peltier,W.R., 1974. The impulse response of a Maxwell Earth. Reviews of Geophysics and Space Physics 12, 649–669.

Peltier, W.R., 2004. Global glacial isostasy and the surface of the ice-age earth: the ICE-5G (VM2) model and grace. Annual Review of Earth and Planetary Sciences 32, 111–149.

Peltier, W.R., Andrews, J.T., 1976. Glacial-Isostatic Adjustment—I. The Forward Problem. Geophysical Journal of the Royal Astronomical Society 46 (3), 605-646.

Petrunin, A. G., Rogozhina, I., Vaughan, A. P. M., Kukkonen, I. T., Kaban, M. K., Koulakov, I., & Thomas, M. (2013). Heat flux variations beneath central Greenland's ice due to anomalously thin lithosphere. Nature Geoscience, 6(9), 746-750.

Ren, J., Jiang, H., Seidenkrantz, M.S., Kuijpers, A., 2009. A diatom-based reconstruction of Early Holocene hydrographic and climatic change in a southwest Greenland fjord. Marine Micropaleontology 70, 166–176.

Rignot, E., Mouginot, J., 2012. Ice flow in Greenland for the International Polar Year 2008-2009. Geophysical Research Letters 39, L11501.

Roberts, D. H., Long, A. J., Schnabel, C., Davies, B. J., Xu, S., Simpson, M. J., Huybrechts, P., 2009. Ice sheet extent and early deglacial history of the southwestern sector of the Greenland Ice Sheet. Quaternary Science Reviews 28 (25), 2760-2773.

Saito, F., Abe-Ouchi, A., Blatter, H., 2003. Effects of first-order stress gradients in an ice sheet evaluated by a three-dimensional thermomechanical coupled model. Annals of Glaciology 37, 166–172.

Schmidt, S., Wagner, B., Heiri, O., Klug, M., Bennike, O., Melles, M., 2010. Chironomids as indicators of the Holocene climatic and environmental history of two lakes in Northeast Greenland. Boreas 40, 116-130.

Seidenkrantz, M.-S., Roncaglia, L., Fischel, A., Heilmann-Clausen, C., Kuijpers, A., Moros, M., 2008. Variable North Atlantic climate seesaw patterns documented by a late Holocene marine record from Disko Bugt, West Greenland. Marine Micropaleontology 68, 66–83.

Shepherd, A., Ivins, E.R., Geruo, A., Barletta, V.R., Bentley, M.J., Bettadpur, S., Briggs, K.H., Bromwich, D.H., Forsberg, R., Galin, N., Horwath, M., Jacobs, S., Joughin,I., King, M.A., Lenaerts, J.T.M., Li, J., Ligtenberg, S.R.M., Luckman, A., Luthcke, S.B., McMillan, M., Meister, R., Milne, G.A., Mouginot, J., Muir, A., Nicolas, J.P., Paden, J., Payne, A.J., Pritchard, H., Rignot, E., Rott, H., Sørensen, L.S., Scambos, T.A., Scheuchl, B., Schrama, E.J.O., Smith, B., Sundal, A.V., van Angelen, J.H., van de Berg, W.J., van den Broeke, M.R., Vaughan, D.G., Velicogna, I., Wahr, J., Whitehouse, P.L., Wingham, D.J., Yi, D., Young, D., Zwally H.J., 2012. A reconciled estimate of ice-sheet mass balance. Science 338 (6111), 1183-1189

Simpson, M.J.R., Milne, G.A., Huybrechts, P., Long, A.J., 2009. Calibrating a glaciological model of the Greenland ice sheet from the Last Glacial Maximum to present-day using field observations of relative sea level and ice extent. Quaternary Science Reviews 28, 1631–1657.

Simpson, M.J.R., Wake, L., Milne, G.A., Huybrechts, P., 2011. The influence of decadal to millennial-scale ice mass changes on present-day vertical land motion in Greenland: Implications for the interpretation of GPS observations. Journal of Geophysical Research 116, B02406.

Sommerhoff, G., 1981. Geomorphologische Prozesse in der Labrador – und Imingersee. Ein Beitrag zur submarinen Geomorphologie einer subpolaren Meeresregion. Polarforschung 51, 175–191.

Sparrenbom, C.J., 2006. Constraining the Southern Part of the Greenland Ice Sheet since the Last Glacial Maximum from Relative Sea-Level Changes, Cosmogenic Dates and Glacial-Isostatic Adjustment Models. Ph.D. thesis. Centre for Geo- Biosphere Science, Lund University.

Sparrenbom, C.J., Bennike, O., Björck, S., Lambeck, K., 2006a. Relative sea-level changes since 15 000 cal. yr BP in the Nanortalik area, southern Greenland. Journal of Quaternary Science 21 (1), 29–48.

Sparrenbom, C.J., Bennike, O., Björck, S., Lambeck, K., 2006b. Holocene relative sealevel changes in the Qaqortoq area, southern Greenland. Boreas 35 (2), 171–187.

Steffen, R., Wu, P., Steffen, H., Eaton, D. W., 2014. The effect of earth rheology and ice-sheet size on fault slip and magnitude of postglacial earthquakes. Earth and Planetary Science Letters, 388, 71-80.

Steffensen, J.P., Andersen, K.K., Bigler, M., Clausen, H.B., Dahl-Jensen, D., Fischer, H., Goto-Azuma, K., Hansson, M., Johnsen, S.J., Jouzel, J., Masson-Delmotte, V., Popp, T., Rasmussen, S.O., Rothlisberger, R., Ruth, U., Stauffer, B., Siggaard-Andersen, M-L., Sveinbjornsdottir, A.E., Svensson, A.,

White, J.W.C., 2008. High-resolution Greenland ice core data show abrupt climate change happens in few years. Science 321, 680–684.

Stein, R., Nam, S., Grobe, H., Hubberten, H., 1996. Late Quaternary glacial history and short-termice-rafted debris fluctuations along the east Greenland Continental Margin. In: Andrews, et al., (Ed.), Late Quaternary Paleoceanography of the North Atlantic Margins, Geological Society Special Publication, 111, 135–151.

Tarasov, L., Peltier, W.R., 2002. Greenland glacial history and local geodynamic consequences. Geophysical Journal International 150 (1), 198–229.

Tarasov, L., Dyke, A.S., Neal, R.M., Peltier, W.R., 2012. A data-calibrated distribution of deglacial chronologies for the North American ice complex from glaciological modeling. Earth and Planetary Science Letters 315-316, 30-40.

Ten Brink, N.W., Weidick, A., 1974. Greenland ice sheet history since the last glaciation. Quaternary Research 4, 429–440.

Trautman, M.A., Willis, E.H., 1963. Isotopes, Inc., radiocarbon measurements III. Radiocarbon 5, 62–79.

Van deWal, R.S.W.,1999. The importance of thermodynamics for modeling the volume of the Greenland ice sheet. Journal of Geophysical Research 104, 3887-3898.

Van den Berg, J., van de Wal, R.S.W., Oerlemans, J., 2006. Effects of spatial discretization in ice-sheet modelling using the shallow-ice approximation. Journal of Glaciology 52, 89–98.

Van Tatenhove, F.G.M., van der Meer, J.J.M., Huybrechts, P., 1995. Glacial–geological geomorphological research in west Greenland used to test an ice-sheet. Quaternary Research 44 (3), 317–327.

Van Tatenhove, F.G.M., van der Meer, J.J.M., Koster, E.A., 1996. Implications for deglaciation chronology from new AMS age determinations in central west Greenland. Quaternary Research 45 (3), 245–253.

Van Tatenhove, F. G., van der Meer, J. J., and Koster, E. A., 1996. Implications for deglaciation chronology from new AMS age determinations in central West Greenland. Quaternary Research, 45(3), 245-253.

Vinther, B.M., Buchardt, S.L., Clausen, H.B., Dahl-Jensen,D., Johnsen, S.J., Fisher, D.A., Koerner, R.M., Raynaud, D., Lipenkov, V., Andersen, K.K., Blunier, T., Rasmussen, S.O., Steffensen, J.P., Svensson, A.M., 2009. Holocene thinning of the Greenland ice sheet. Nature 461, 385–388.

Wagner, B., Bennike, O., Cremer, H., Klug, M., 2010. Late Quaternary history of the Kap Mackenzie area, northeast Greenland. Boreas 39, 492–504.

Wake , L. M., Marshall, S. J., 2014, (Submitted). Revision of the Positive Degree Day (PDD) methodology for application throughout the cryosphere. Journal of Glaciology.

Walker, M., Johnsen, S., Rasmussen, S.O., Popp, T., Steffensen, J-P., Gibbard, P., Hoek, W., Lowe, J., Andrews, J., Björck, S., Cwynar, L.C., Hughen, K., Kershaw, P., Kromer, B., Litt, T., Lowe, D.J.,

Nakagawa, T., Newnham, R., Schwander, J., 2009. Formal definition and dating of the GSSP (Global Stratotype Section and Point) for the base of the Holocene using the Greenland NGRIP ice core, and selected auxiliary records. Journal of Quaternary Science 24, 3–17.

Washburn, A.L., Stuiver, M., 1962. Radiocarbon-dated post-glacial deleveling in northeast Greenland and its implications. Arctic 15, 66–73.

Weidick, A., 1972. Holocene shore-lines and glacial stages in Greenland – an attempt at correlation. Rapport Grønlands Geologiske Undersøgelse 41, 1–39.

Weidick, A., 1976. Glaciation and the Quaternary of Greenland. In: Escher, A., Watt, W.S. (Eds.), Geology of Greenland. Geological Survey of Greenland, Copenhagen, pp. 405–458.

Weidick, A., Oerter, H., Reeh, N., Thomsen, H.H., Thorning, L.S., 1990. The recession of the Inland Ice margin during the Holocene climatic optimum in the Jakobshavn Isfjord area of West Greenland. Palaeogeography, Palaeoclimatology, Palaeoecology 82, 389–399.

Weidick, A., Kelly, M., Bennike, O., 2004. Late Quaternary development of the southern sector of the Greenland ice sheet, with particular reference to the Qassimiut lobe. Boreas 33 (4), 284–299.

Weidick, A., Bennike, O., 2007. Quaternary glaciation history and glaciology of Jakobshavn Isbrae and the Disko Bugt region, west Greenland: a review. Geological Survey of Denmark and Greenland Bulletin 14.

Weidick, A., Bennike, O., Citterio, M., Nørgaard-Pedersen, N., 2012. Neoglacial and historical glacier changes around Kangersuneq fjord in southern West Greenland. Geological Survey of Denmark and Greenland 27, 68.

Wilken, M., Mienert, J., 2006. Submarine glacigenic debris flows, deep-sea channels and past ice-stream behaviour of the east Greenland continental margin. Quaternary Science Reviews 25 (7–8), 784–810.

Winkelmann, D., Jokat, W., Jensen, L., Schenke, H-W., 2010. Submarine end moraines on the continental shelf off NE Greenland—implications for Lateglacial dynamics. Quaternary Science Review 29, 1069–1077.

Whitehouse, P.L., Bentley, M.J., Le Brocq, A.M., 2012. A deglacial model for Antarctica: geological constraints and glaciological modelling as a basis for a new model of Antarctic glacial isostatic adjustment. Quaternary Science Reviews 32, 1-24.

Woodroffe, S.A., Long, A.J., Lecavalier, B.L., Milne, G.A., 2013. Using relative sea-level data to constrain the deglacial and Holocene history of southern Greenland. Quaternary Science Reviews.

Wouters, B., Bamber, J. L., van den Broeke, M. R., Lenaerts, J. T. M., & Sasgen, I. 2013. Limits in detecting acceleration of ice sheet mass loss due to climate variability. Nature Geoscience 6(8), 613-616.

Yokoyama, Y., Lambeck, K., De Dekker, P., Johnston, P., Fifield, L.K., 2000. Timing of the Last Glacial Maximum from observed sea-level minima. Nature 406 (6797), 713–716.

Zreda, M., England, J., Phillips, F., Elmore, D., Sharma, P., 1999. Unblocking of the Nares Strait by Greenland and Ellesmere ice-sheet retreat 10,000 years ago. Nature 398 (6723), 139–142.

Zweck, C., Huybrechts, P., 2003. Modeling the marine extent of northern Hemisphere ice sheets during the last glacial cycle. Annals of Glaciology 37,173–180.

Zweck, C., Huybrechts, P., 2005. Northern hemisphere ice sheet modeling of the last glacial cycle and glaciological sensitivity. Journal of Geophysical Research 110, D07103.

Region	Site	Site name	Source reference
West	1	Kangerluarsuk (Kan)	Bennike, 1995; Long et al., 2011
	2	Arveprinsen (Arv)	Long et al., 1999
	3	Pakitsoq (Paq)	Long et al., 2006
	4	Upernivik (Upe)	Long et al., 2006
	5	Orpisook (Orp)	Long and Roberts, 2002
	6	Innaarsuit (Inn)	Long et al., 2003
	7	Qeqertarsiatsuaq (Qeq)	Long and Roberts, 2003
Southwest	8	Sisimiut (Sis)	Long et al., 2008; Bennike et al., 2011
	9	Sondre (Son)	Weidick, 1972; Ten Brink, 1974; van Tatenhove and van der Meer, 1996
	10	Godmouth (Gom)	Weidick, 1976; Fredskild, 1983; Berglund, 2003
	11	Nuuk (Nuu)	Fredskild, 1983
	12	Godhead (Goh)	Fredskild, 1972; Weidick, 1976; Fredskild, 1983; McGovern et al., 1996
	13	Paamiut (Paa)	Woodroffe et al., 2013
South	14	Qaqortoq (Qaq)	Sparrenbom et al., 2006b
	15	Tasiusaq (Tas)	Fredh, 2008
	16	Nanortalik (Nan)	Bennike et al., 2002; Sparrenbom et al., 2006a
Southeast	17	Ammassalik (Amm)	Long et al., 2008
East	18	Scoresby Sund (Sco)	Funder and Hansen, 1996
	19	Schuchert (Sch)	Hall et al., 2010
	20	Mesters Vig (Mes)	Washburn and Stuiver, 1962; Trautman and Willis, 1963
	21	Hudson (Hud)	Hjort and Funder, 1974; Hjort, 1979; Hjort, 1981
	22	Young Sound (You)	Pedersen et al., 2011
	23	Wollaston (Wol)	Hjort, 1979; Christiansen et al., 2002
	24	Germania (Ger)	Bennike and Wagner; 2012
	25	Hochstetter (Hoc)	Björck et al., 1994
Northeast	26	Hvalroso (Hva)	Landvik, 1994
	27	Blaso (Bla)	Bennike and Weidick, 2001
	28	Hovgaard (Hov)	Bennike and Weidick, 2001
	29	Holm Land (Hol)	Funder et al., 2011b
	30	Kronprins (Kro)	Hjort, 1997; Funder et al., 2011b
	31	Ingebord Halvo (Hal)	Funder et al., 2011b
North	32	Herlufsholm (Her)	Funder et al., 2011b
	33	Jorgen (Jor)	Funder and Abrahamsen, 1988
	34	Ole Chiewitz (Ole)	Funder et al., 2011b
	35	Constable (Con)	Funder et al., 2011b
	36	JPKoch (Koc)	Kelly and Bennike, 1992; Landvik et al., 2001

Northwest	37	Nyboe (Nyb)	England, 1985; Kelly and Bennike, 1992
	38	HallEast (Hae)	England, 1985; Kelly and Bennike, 1992
	39	HallWest (Haw)	England, 1985; Kelly and Bennike, 1992
	40	Lafayette (Laf)	Bennike, 2002
	41	Humboldt (Hum)	Bennike, 2002
	42	Qeqertat (Qeq)	Fredskild, 1985
	43	Saunders (Sau)	Funder, 1990
	44	Thule (Thu)	Funder, 1990; Kelly et al., 1999

Table 1: The RSL observations applied in this study and their source references. The locations of these observations are marked in Fig. 1.

LT (km)	UMV (10^{21} Pas)	LMV(10^{21} Pas)
120	0.5	1
120	**0.5**	**2**
120	0.5	3
120	0.5	5
120	0.5	8
120	0.5	10

Table 2: The sub-set of Earth structures considered in this study that are within the nominal 95% confidence interval of the χ^2 minimum, where LT, UMV and LMV are the lithospheric thickness, upper and lower mantle viscosity, respectively. Values in bold face represent the optimal parameters.

Figure 1 – (a) The locations and names of RSL and ice-core data sites discussed and applied in this study. The circles indicate the location of sea-level index point data while triangles refer to sea-level limiting data. A list of RSL data site locations and the corresponding source literature used to compile the data base used in this study is found in Table 1. (b) The locations of places mentioned in the text.

Figure 2: A flow diagram describing the modelling methodology of this study. Firstly, a glaciological model simulates the evolution of the GrIS (Huybrechts and de Wolde, 1999; Huybrechts, 2002). The Greenland ice model is then combined with a background global ice model lacking a Greenland component (ICE-5G - GrB; Peltier, 2004). A sensitivity analysis on the global ice model was also conducted by swapping the ICE-5G North American ice complex with a high variance set from Tarasov et al. (2012). The global ice and Earth model were adopted in the GIA model to produce predictions of RSL which are compared to observations. Optimal Earth model parameters were determined using a χ^2 analysis and an F-test.

Figure 3: The chronology of lateral ice extent for the Huy2 model (16 ka BP – pink; 14 ka BP – dark blue; 12 ka BP – light blue; 10 ka BP – yellow; 9 ka BP – orange; 6 ka BP – red; 4 ka BP – green; present-day – black).

Figure 4: RSL predictions for the Huy2 and GrB ice models with their respective optimal Earth model(s). The Huy2 model predictions are generated using its two optimal Earth models - the black curves denote the optimal viscosity structure obtained using the entire regional RSL data set (120 km lithosphere, upper mantle viscosity of 0.5×10^{21}Pas, and lower mantle viscosity of 10^{21} Pas) and the dashed black curves represent the alternate viscosity structure obtained by considering data from the East coast only (120 km lithosphere, upper mantle viscosity of 0.3×10^{21}Pas, and lower mantle viscosity of 50×10^{21} Pas). In contrast, the Greenland ice model of ICE5G (variant of GrB; Tarasov and Peltier, 2002) is applied with the VM2 Earth model to produce RSL predictions (grey curves). Sea-level index points are shown as

crosses with both time and height error bars. Lower limiting dates are denoted by grey upward pointing triangles, while upper limiting dates are shown by white downward pointing triangles with both time and height error bars. The black horizontal line highlights present-day sea-level. The grey dashed horizontal line represents the marine limit which marks the highest point reached by sea-level during ice-free conditions at each location. Data locations are shown in Fig. 1a.

Figure 5: The three LGM ice mask extents which are discussed in this study: the original Huy2 LGM extent (red), the Funder extent (green) (Funder et al., 2011a), and the revised Huy3 LGM ice mask (blue).

Figure 6: The GRIP temperature record prescribed in the model is represented by the black curve alongside the Huy2 revised HTM temperature forcing (upper bound of dark grey envelop). The Huy3 model HTM was parameterized within the grey envelop with an optimal imposed HTM scaling shown in light grey. The following climatic events are annotated: Bølling-Allerød (BA), Younger Dryas (YD), and Holocene Thermal Maximum (HTM).

Figure 7: The chronology of lateral ice extent for the Huy3 model (16 ka BP – pink; 14 ka BP – dark blue; 12 ka BP – light blue; 10 ka BP – yellow; 9 ka BP – orange; 6 ka BP – red; 4 ka BP – green; present-day – black).

Figure 8: The left panes show the glaciologically self-consistent Tarasov et al. (2012) optimal NAIC model while the right panes show the ICE-5G NAIC component (Peltier, 2004). The two panes at the top, middle and bottom represent the 16, 12, and 8 ka BP time slices, respectively. In all panes, the Greenland component shown is the Huy3 model. There are clearly significant differences in the grid resolution, ice volume, thickness, and chronology between the two reconstructions.

Figure 9: A spatial plot of RSL predictions for non-Greenland ice at 16 ka BP from the (a) ICE-5G reconstruction and (b) ICE-5G with the NAIC component from the optimal Tarasov et al. (2012) reconstruction. (c) Results in (a) minus those in (b) illustrate the propagating impact on Greenland RSL predictions considering uncertainties in the NAIC. The optimum viscosity model for the Huy3 model was used (see Fig. 10).

Figure 10: The χ^2 results for the Huy3 model with each frame showing results for a fixed value of lithospheric thickness (120 km (top), 96 km (middle), 71 km (bottom)). The optimal fit was achieved with a lithospheric thickness of 120 km, upper mantle viscosity of 0.5×10^{21} Pas and lower mantle viscosity of 2×10^{21} Pas. A subset of best-fitting models (nominal 95% confidence interval) is listed in Table 2.

Figure 11: Spatial plots of RSL predictions (in meters) from the Huy3 reconstruction using the optimal Earth model for the time slices: (a) 16 ka BP, (b) 12 ka BP, (c) 8 ka BP, and (d) 4 ka BP.

Figure 12: RSL predictions generated by the Huy2 reconstruction with the optimal Earth model (black curves) and alternate eastern Earth model (dashed black curves). The Huy3 RSL predictions were generated using the optimal Earth model (LT120, UMV0.5, LMV2; see Figure 11) and are shown by the dark grey curves with the light grey envelop representing the range in RSL predicted using Earth viscosity structures within the nominal 95% confidence interval of the χ^2 analysis (Table 2). Sea-level index points are shown as crosses with both time and height error bars. Lower limiting dates are denoted by grey upward pointing triangles, while upper limiting dates are shown by white downward pointing triangles with both time and height error bars. The black horizontal line highlights present day sea-level. The grey dashed horizontal line represents the marine limit which marks the highest point reached by sea-level during ice-free conditions at each locality.

Figure 13: (a) Present-day observed (Bamber et al., 2001) minus modelled (Huy3) ice thickness in metres. (b) Present-day uplift rates as predicted by the Huy3 reconstruction and its optimal Earth model. The Earth structure uncertainty (upper and lower bound) on present-day uplift rates was generated using the nominal 95% confidence interval of the χ^2 analysis and is shown in Figure S8.

Figure 14: The ice-core derived thinning curves (darker coloured bands) along with the estimated 1-σ uncertainty (lighter coloured bands) compared to the Huy3 model predictions (dashed black curves) at GRIP, NGRIP, DYE-3, and Camp Century. The predictions consist of ice thinning at each core site along with vertical land motion due to glacial isostatic adjustment using the optimal Earth model (LT120, UMV0.5, LMV2). The subset of optimum Earth models that partner the Huy3 ice model (Table 2) were also used but make very little difference to the model curves (grey band). Results for the Huy2 ice model and its partnering Earth model (LT120, UMV0.5, LMV1) are shown by the solid black curves.

Figure 15: The Huy3 model predictions (blue curves) for ice sheet volume (top) and areal extent (bottom) compared to the Huy2 predictions (black curves).

Figure 16: Huy3 ice thickness for the time slices: (a) 16 ka BP, (b) 12 ka BP, (c) 8 ka BP, and (d) 4 ka BP.

SUPPLEMENTARY MATERIAL

Figure S1: A map showing the location of individual ML observations that supplement the RSL observations shown in Fig. 1a; these observations are particularly useful where RSL data is sparse.

Figure S2: Schematic diagram that delineates the modelling workflow of this study, which involved varying a number of key parameters and exploring uncertainties in boundary conditions. The LGM ice extent was varied in poorly constrained regions to explore alternate extent scenarios which resulted in 16 substantially different LGM extents. The 16 LGM extent scenarios were combined with 10 spatially uniform SLF parametric equations from the continuous spectrum shown in Figure S6. The resulting 160 Greenland reconstructions were individually amalgamated within the 11 alternate global ice model scenarios described in Section 4.3 (ICE-5G with the high variance subset from Tarasov et al., 2012 and the original ICE-5G NAIC component). A subset of 27 viscosity models was sampled from the full set of 243 to evaluate RSL variability with respect to this model input. The sensitivity analysis depicted in the left-hand-side of the diagram yielded in a collection of 47,520 sets of model predictions. Comparison of these to the observations described in Section 2 permitted the inference of spatial variability in the SLF empirical equations; specifically a 'mid' SLF in south Greenland and 'late' SLF in north Greenland (boundary at ~73^{o} latitude). We note that small departures from these parametric equations were permitted as consecutive reconstructions were refined. The resulting 10 alternate scenarios based on the LGM extent and SLF analysis (top panel on right-hand-side of diagram) were then used with 10 different HTM climate histories (Section 4.2.2; Figure 6) to produce 100 GrIS reconstructions. These reconstructions were individually amalgamated into the 11 alternate global ice models and used to compute RSL for all 243 viscosity Earth models. The workflow depicted on the right-hand-side of the diagram resulted in a collection of 267,300 sets of model predictions that were compared against the full constraint database. It is from this ensemble that the best fitting GrIS reconstruction and Earth structure were selected.

Figure S3: The distribution of marine limit observations along (a) northeast and (c) northwest Greenland which can indirectly constrain the LGM ice extent by bounding the amplitude of sea-level change. The marine limit is shown by the grey horizontal line in (b) and (d). In addition, the optimal RSL predictions from the Huy2 model (solid curve), the Funder et al. (2011a) LGM extent (dashed curve), and the O'Cofaigh et al. (2012) revised extent (dotted curve) are shown. These results are based on the optimum Earth model for Huy2 (LT120, UMV0.5, LMV2; see Fig. 11).

Figure S4: Predictions of ice sheet volume (top) and area (bottom) for the original Huy2 model with its DDF tuning of minus 30% (solid curves) and with zero scaling (dashed curves) which produces a large volume and extent deficit at present-day. The revised PDD algorithm incorporated in this study (dotted curves) produced the present-day geometry well without tuning of the DDFs.

Figure S5: The sea-level forcing is based on parametric equations to define at what depth ice can remain grounded. In Simpson et al. (2009), a total of three different sea-level forcings were investigated that resulted in early (dashed curve), intermediate (solid curve), and late (dotted curve) retreat histories. In this study we not only vary this parameterization spatially across Greenland but also sample a continuous range of parametric equations (grey envelop) which share the same characteristic quadratic form as those used by Simpson et al. (2009). From the continuous spectrum of SLF parametric equations, a total of 10 parametric equations were found to adequately sample a differentiable range of ice sheet responses.

Figure S6: The Huy3 RSL predictions are shown for the optimal Earth model (LT120, UMV0.5, LMV2) and the light grey envelop around these results represents the range in predictions when a series of alternate NAIC components from a high-variance subset were adopted within the non-Greenland ice

model (Tarasov et al., 2012). The black dashed curve represents the Huy3 model predictions with the original ICE-5G NAIC component in place. Sea-level index points are shown as crosses with both time and height error bars. Lower limiting dates are denoted by grey upward pointing triangles, while upper limiting dates are shown by white downward pointing triangles with both time and height error bars. The black horizontal line highlights present day sea-level. The grey dashed horizontal line represents the marine limit which marks the highest point reached by sea-level during ice-free conditions at each location.

Figure S7: Changes in ice thickness for the Huy3 model: a) 12 ka minus 16 ka, b) 8 ka minus 12 ka, c) 4 ka minus 8 ka, d) present minus 4 ka.

Figure S8: The (a) lower and (b) upper bound in computed present-day uplift rates given uncertainties in Earth viscosity structure generated using the nominal 95% confidence interval of the χ^2 analysis and the Huy3 ice model reconstruction. The (c) lower and (d) upper bound in computed present-day uplift rates given uncertainties in the high-variance subset of NAIC reconstructions.

Figure S9: The ice-equivalent sea-level evolution of the Huy3 reconstruction. As noted in the Introduction, this does not account for the increase in ocean basin volume associated with the retreat of marine-based ice and so overestimates the actual global mean sea level change associated with the addition of melt water to the oceans.

Figure S10: Deglaciation dates for the Huy3 reconstruction. The map indicates the time each grid cell becomes ice free and does not include the influence of any subsequent regrowth of ice.

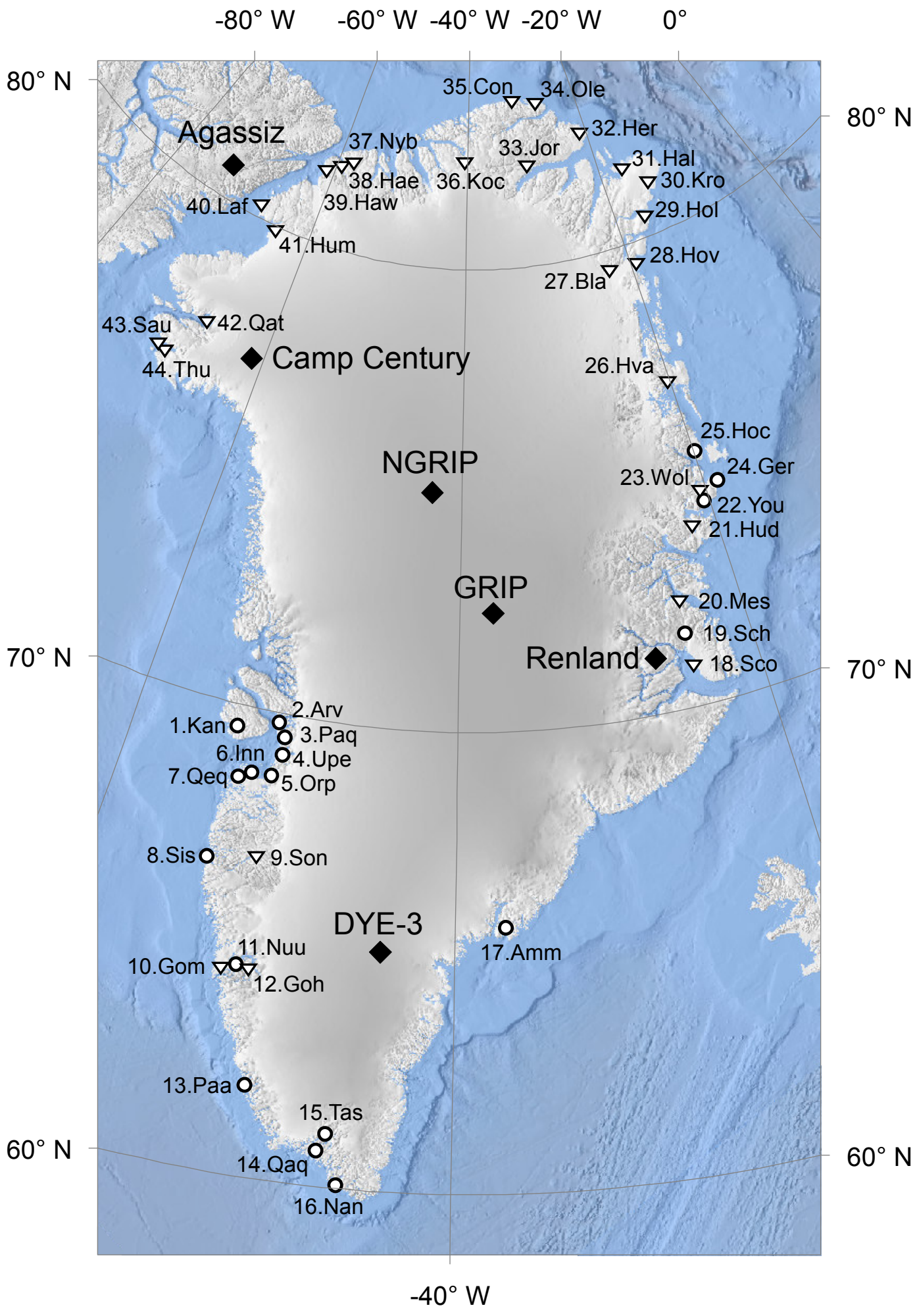
-80° W
-60° W
-40° W
-20° W
0°
80° N
70° N
60° N
-40° W
Agassiz
Camp Century
NGRIP
GRIP
Renland
DYE-3
35.Con
34.Ole
32.Her
37.Nyb
33.Jor
31.Hal
38.Hae
36.Koc
30.Kro
39.Haw
29.Hol
40.Laf
41.Hum
28.Hov
27.Bla
43.Sau
42.Qat
44.Thu
26.Hva
25.Hoc
24.Ger
23.Wol
22.You
21.Hud
20.Mes
19.Sch
18.Sco
2.Arv
1.Kan
3.Paq
6.Inn
4.Upe
7.Qeq
5.Orp
8.Sis
9.Son
17.Amm
11.Nuu
10.Gom
12.Goh
13.Paa
15.Tas
14.Qaq
16.Nan

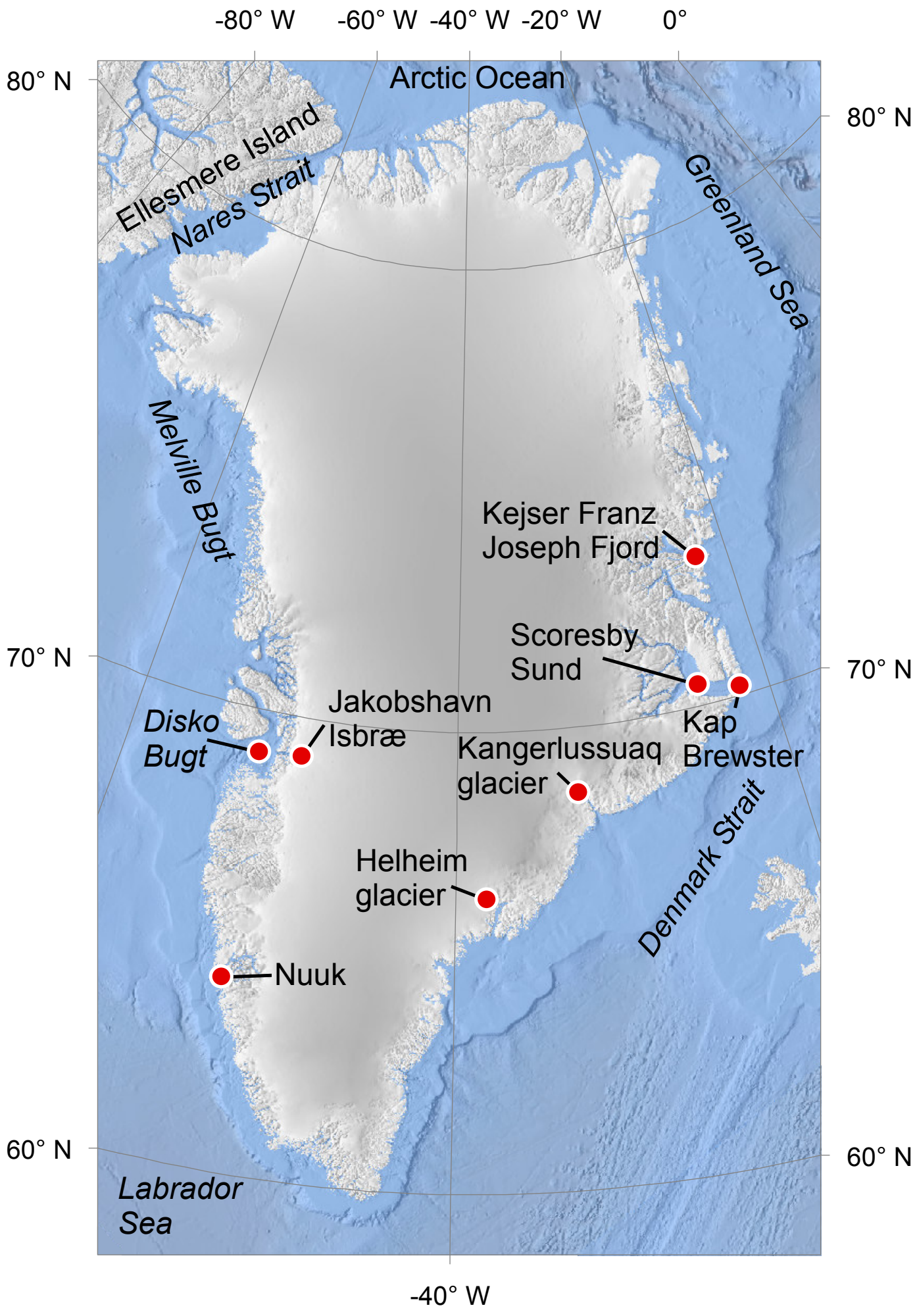
-80° W
-60° W
-40° W
-20° W
0°
80° N
70° N
60° N
Arctic Ocean
Ellesmere Island
Nares Strait
Greenland Sea
Melville Bugt
Kejser Franz
Joseph Fjord
Scoresby
Sund
Kap
Brewster
Jakobshavn
Isbræ
Disko
Bugt
Kangerlussuaq
glacier
Helheim
glacier
Denmark Strait
Nuuk
Labrador
Sea

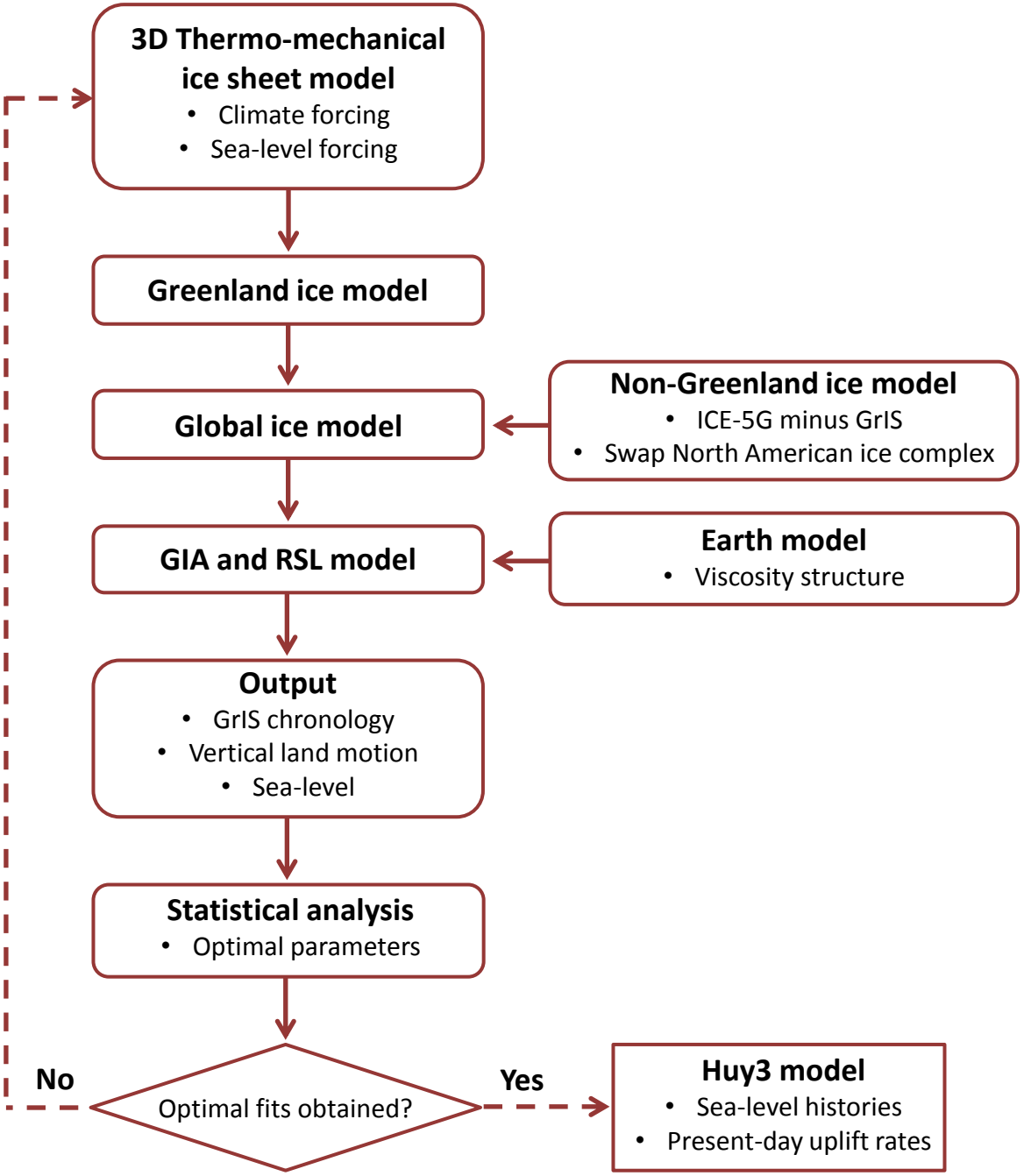
3D Thermo-mechanical ice sheet model
• Climate forcing
• Sea-level forcing
Greenland ice model
Global ice model
Non-Greenland ice model
• ICE-5G minus GrIS
• Swap North American ice complex
GIA and RSL model
Earth model
• Viscosity structure
Output
• GrIS chronology
• Vertical land motion
• Sea-level
Statistical analysis
• Optimal parameters
No
Optimal fits obtained?
Yes
Huy3 model
• Sea-level histories
• Present-day uplift rates

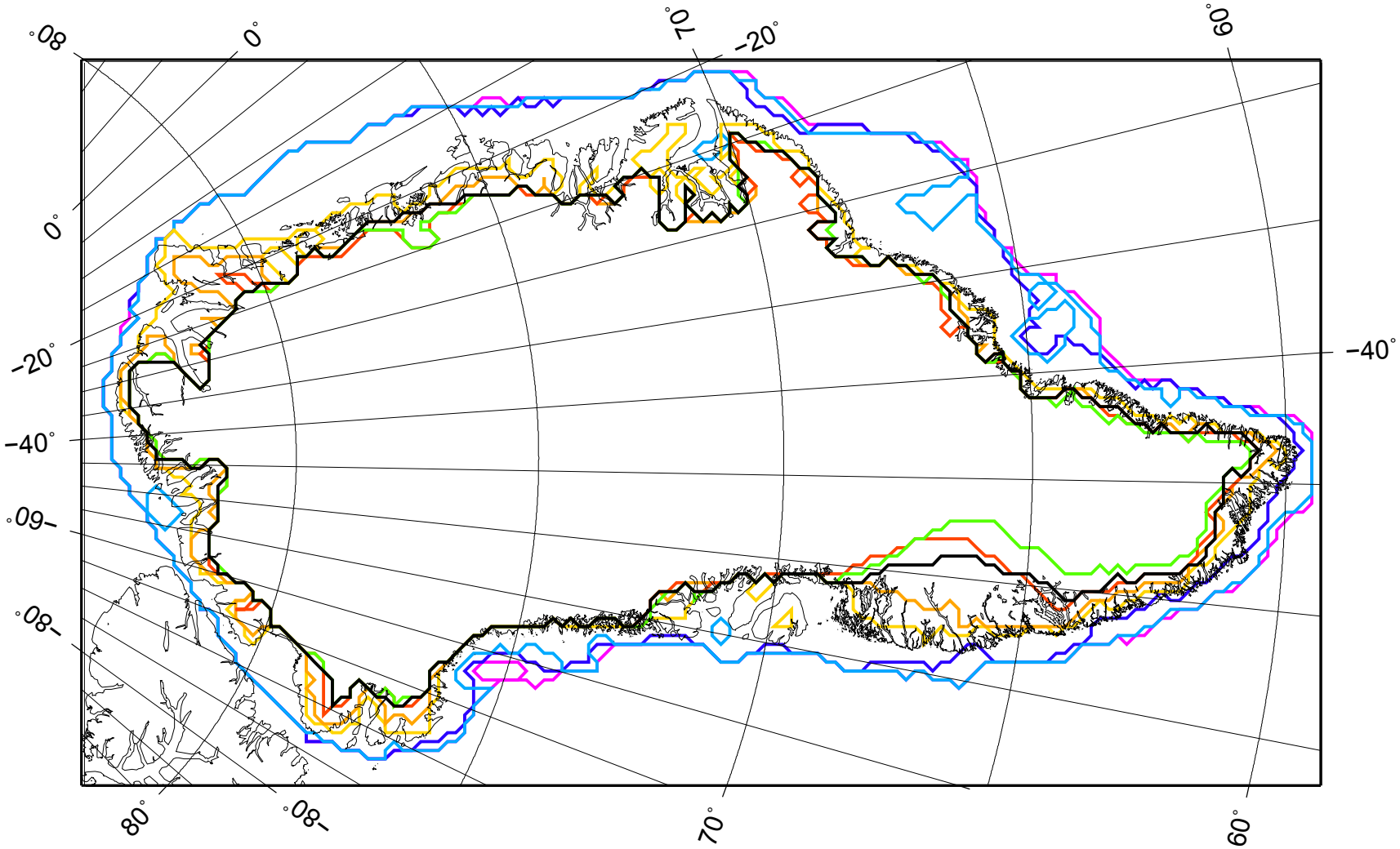
80°
0°
70°
−20°
60°
0°
−20°
−40°
−60°
−80°
−40°
80°
−80°
70°
60°

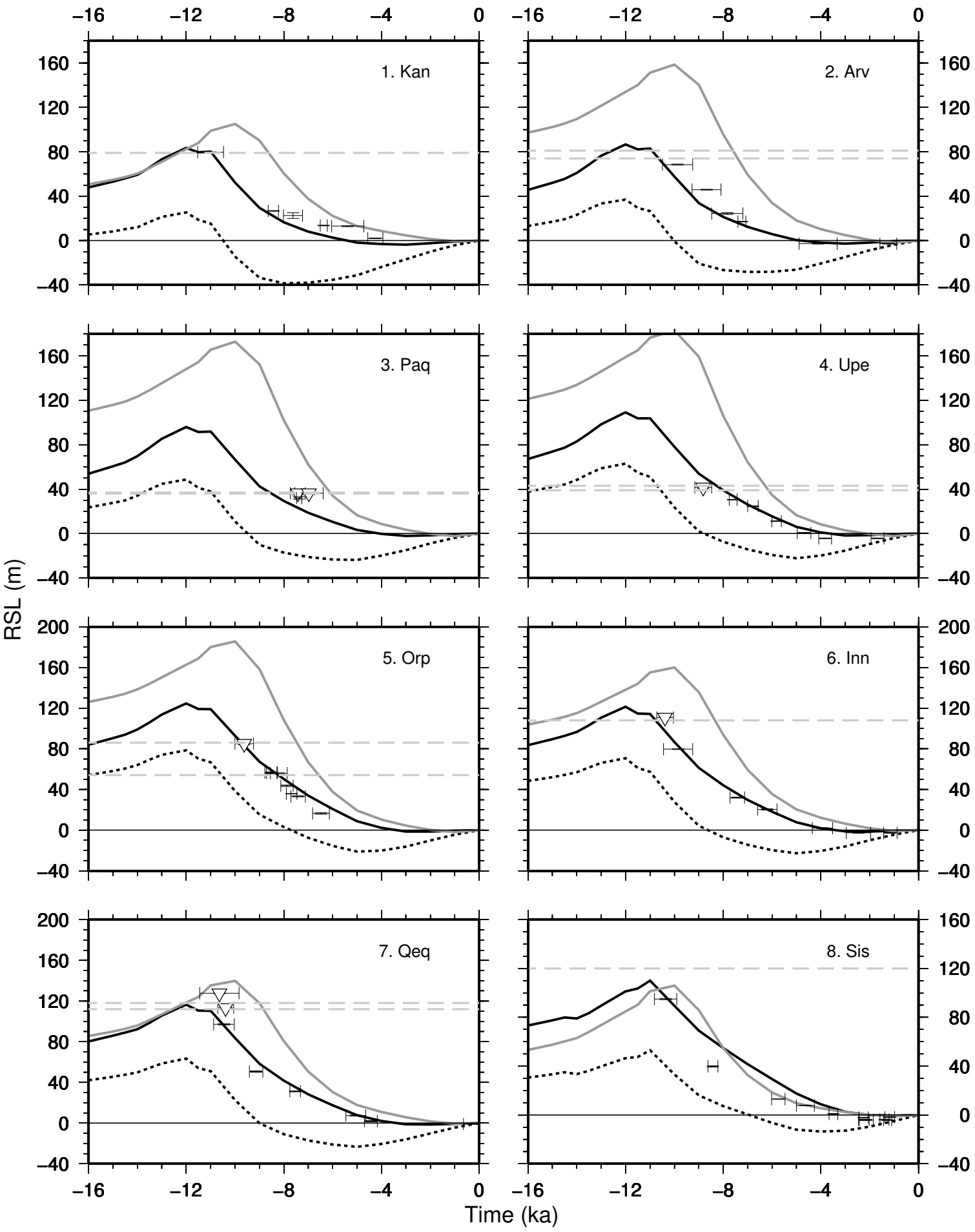
1. Kan
2. Arv
3. Paq
4. Upe
5. Orp
6. Inn
7. Qeq
8. Sis
RSL (m)
Time (ka)
−16
−12
−8
−4
0
160
120
80
40
0
−40
200

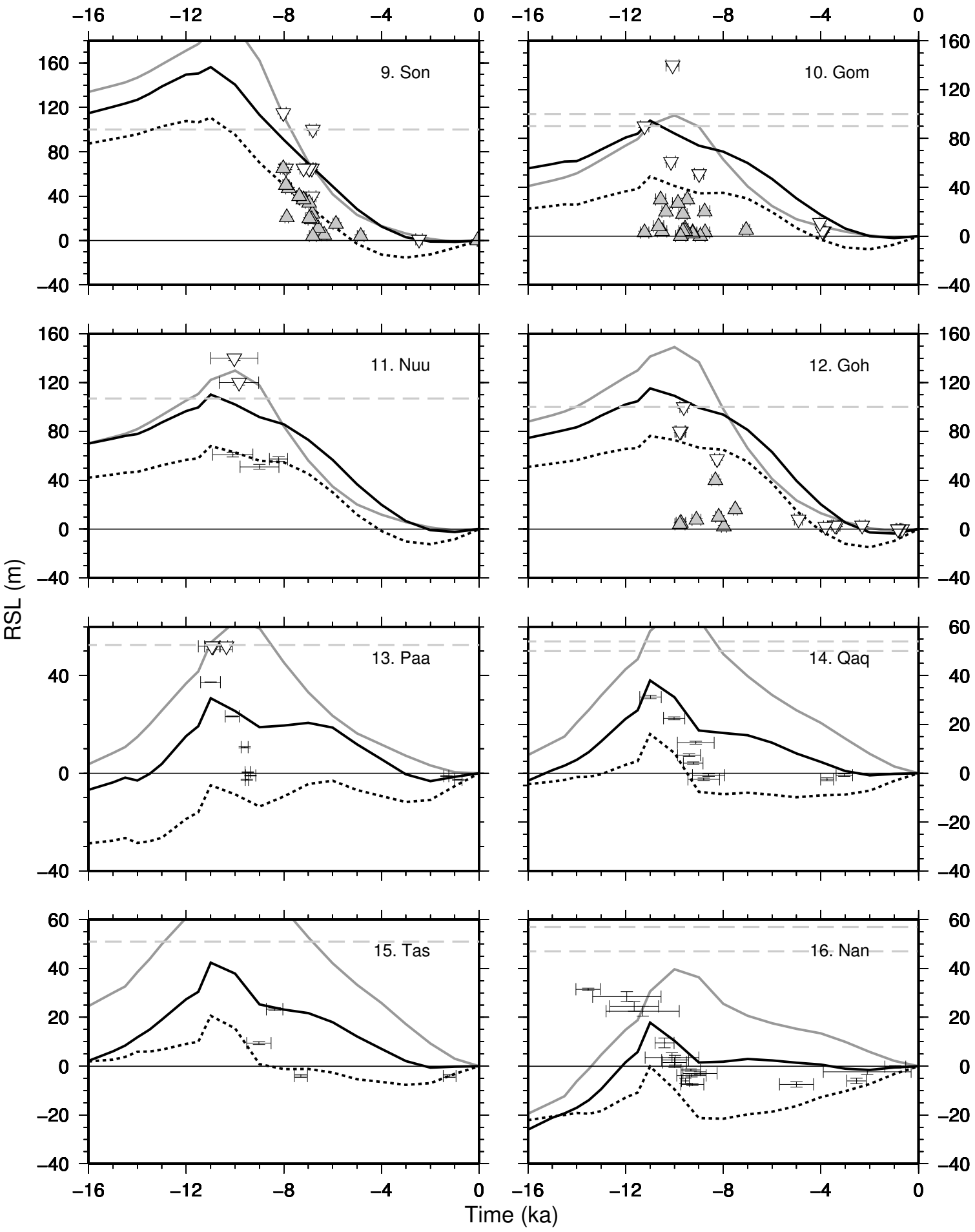
9. Son
10. Gom
11. Nuu
12. Goh
13. Paa
14. Qaq
15. Tas
16. Nan
RSL (m)
Time (ka)
−16
−12
−8
−4
0
160
120
80
40
0
−40
60
20
−20

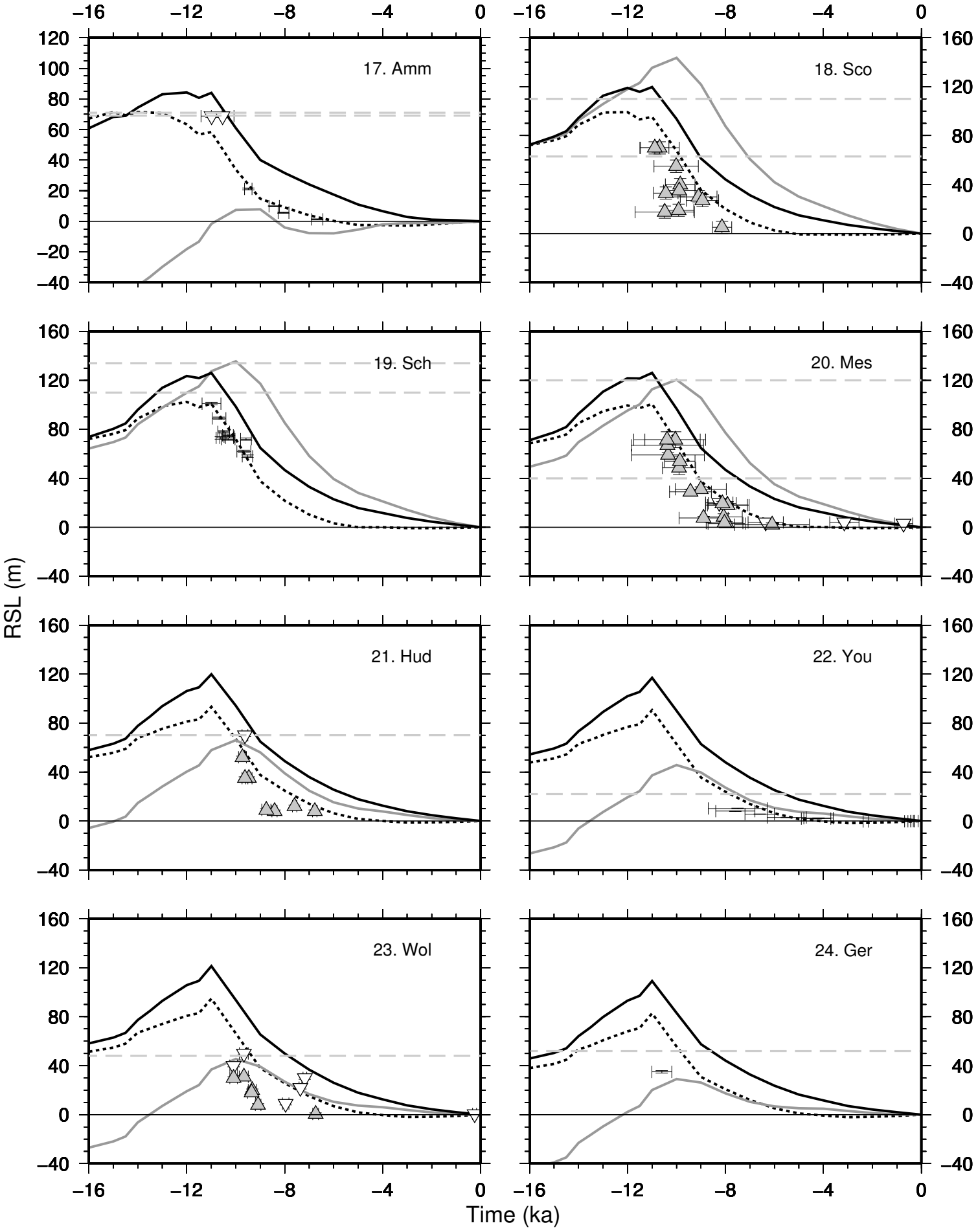
17. Amm
18. Sco
19. Sch
20. Mes
21. Hud
22. You
23. Wol
24. Ger
RSL (m)
Time (ka)
−16
−12
−8
−4
0
120
100
80
60
40
20
0
−20
−40
160

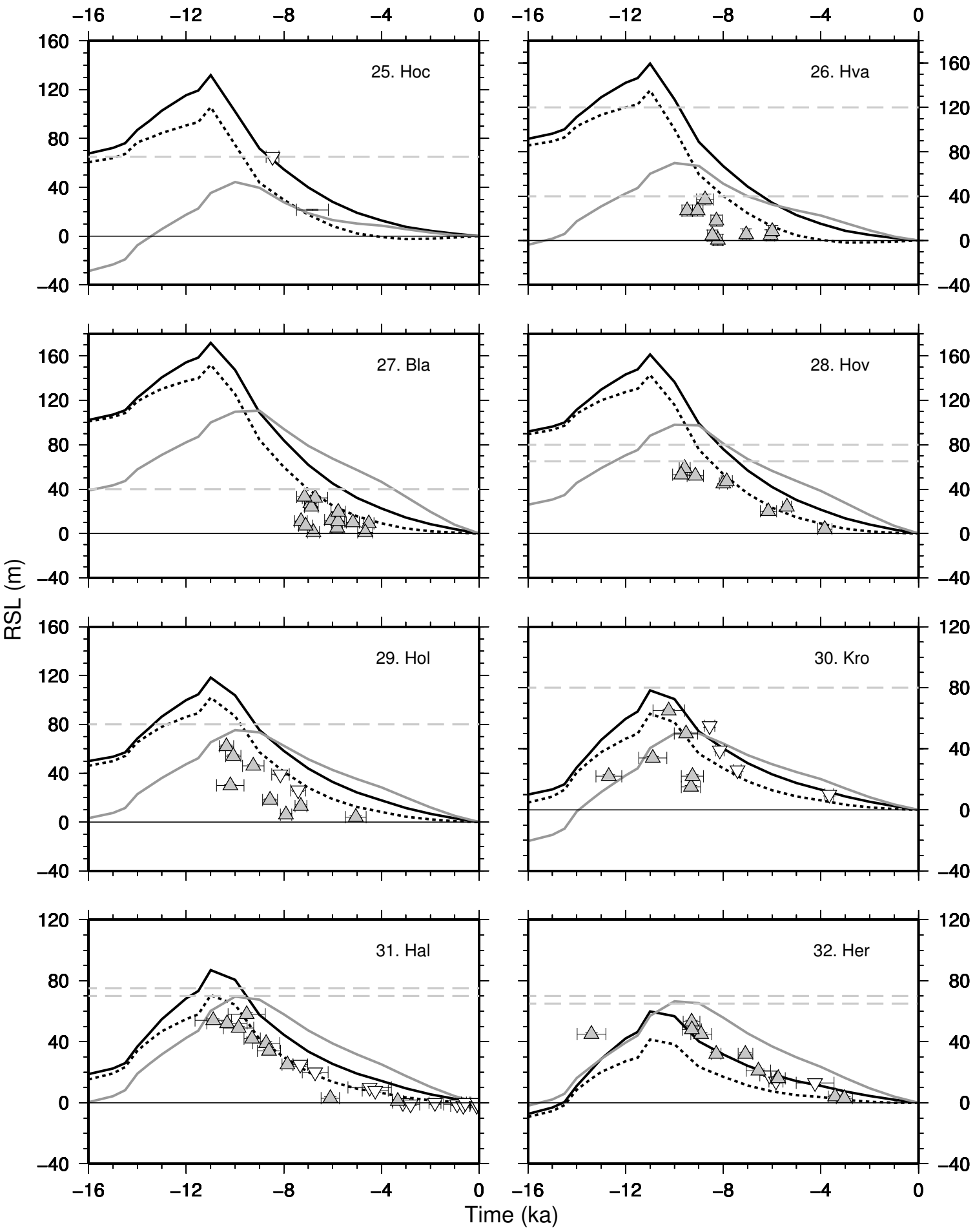
25. Hoc
26. Hva
27. Bla
28. Hov
29. Hol
30. Kro
31. Hal
32. Her
RSL (m)
Time (ka)
−16
−12
−8
−4
0
160
120
80
40
0
−40

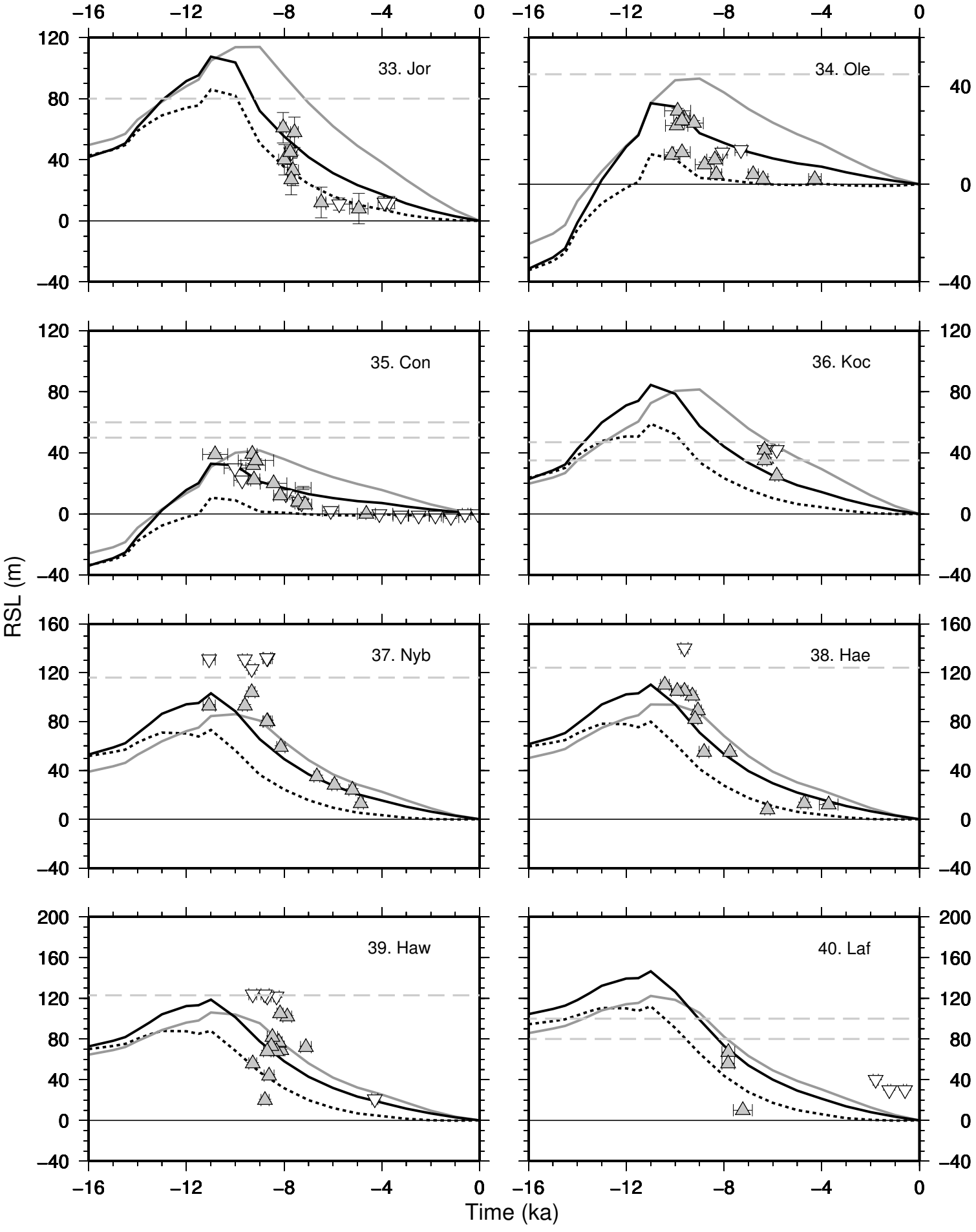
33. Jor
34. Ole
35. Con
36. Koc
37. Nyb
38. Hae
39. Haw
40. Laf
RSL (m)
Time (ka)

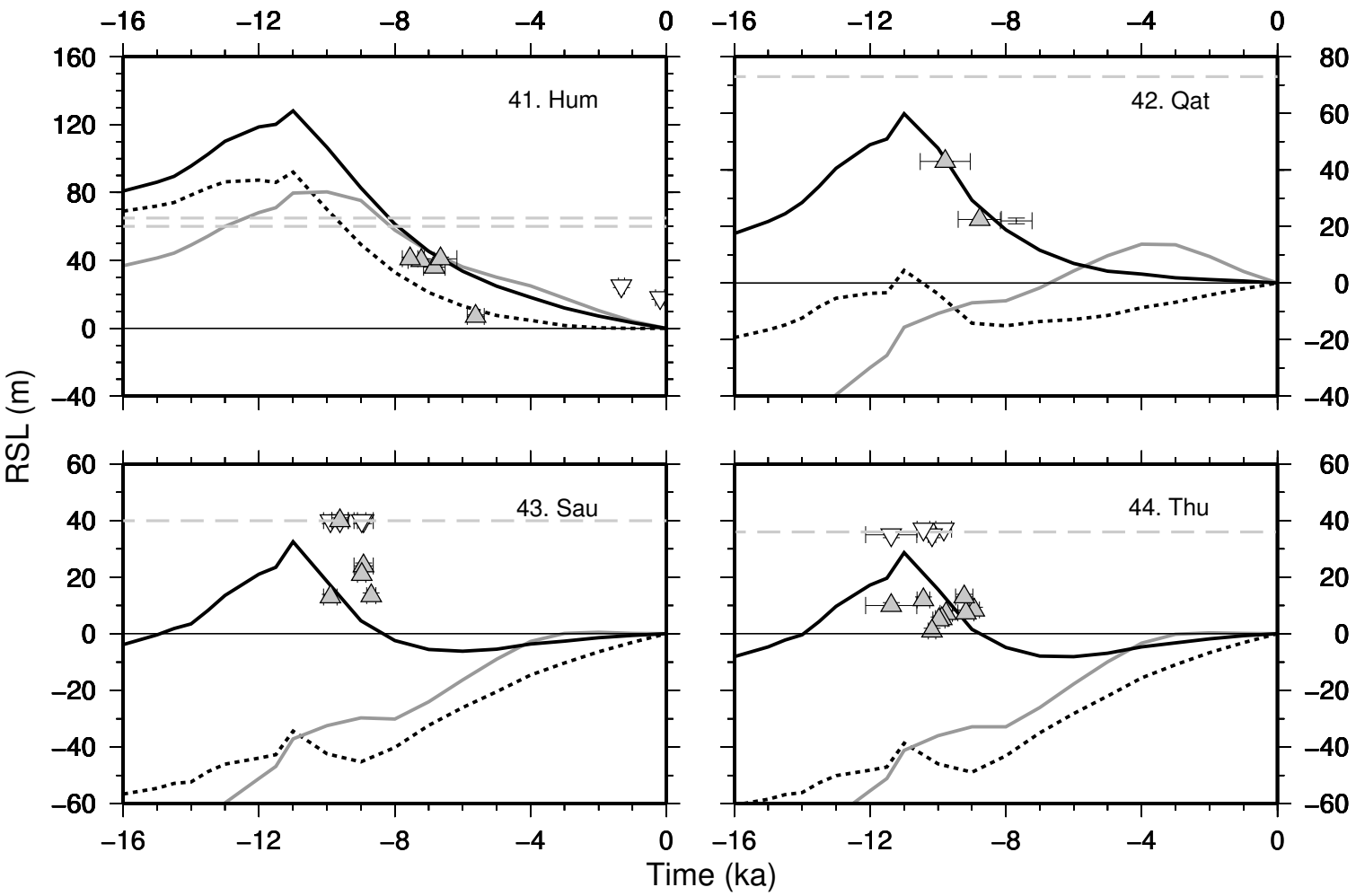
41. Hum
42. Qat
43. Sau
44. Thu
RSL (m)
Time (ka)
−16
−12
−8
−4
0
160
120
80
40
0
−40
60
20
−20
−60

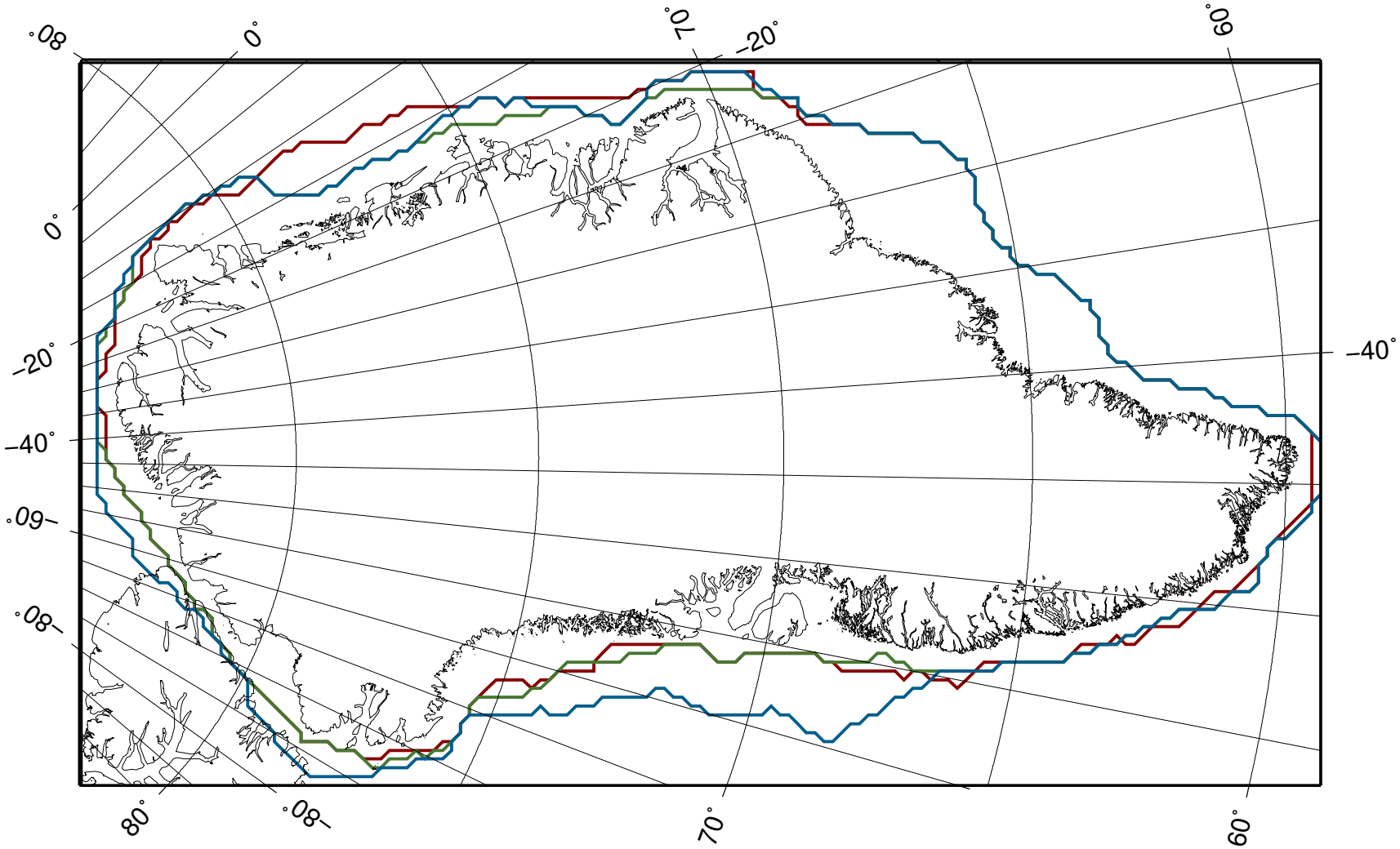
80°
0°
70°
−20°
60°
0°
−20°
−40°
−60°
−80°
−40°
80°
−80°
70°
60°

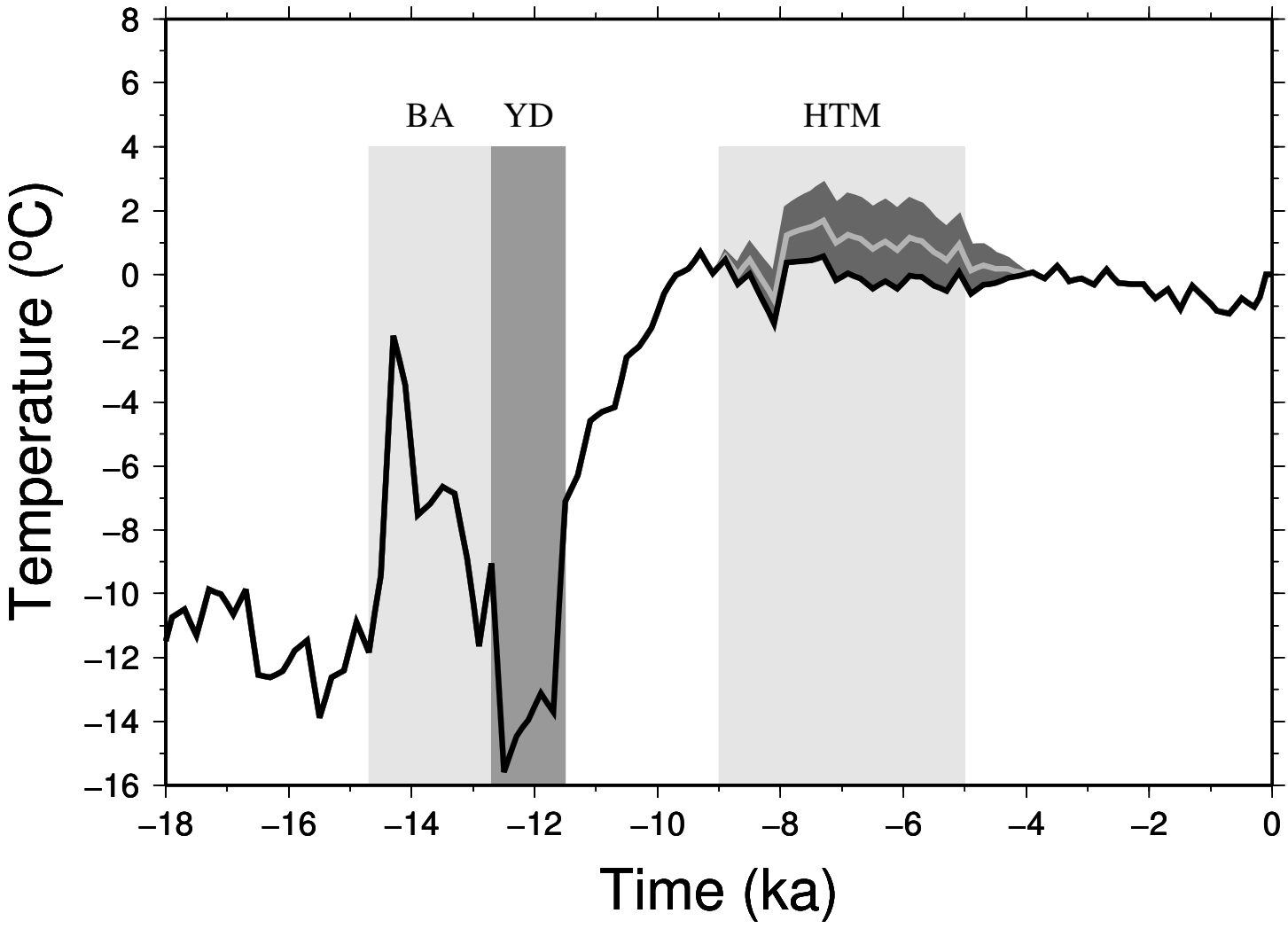
BA
YD
HTM
Temperature (°C)
Time (ka)
8
6
4
2
0
−2
−4
−6
−8
−10
−12
−14
−16
−18
−16
−14
−12
−10
−8
−6
−4
−2
0

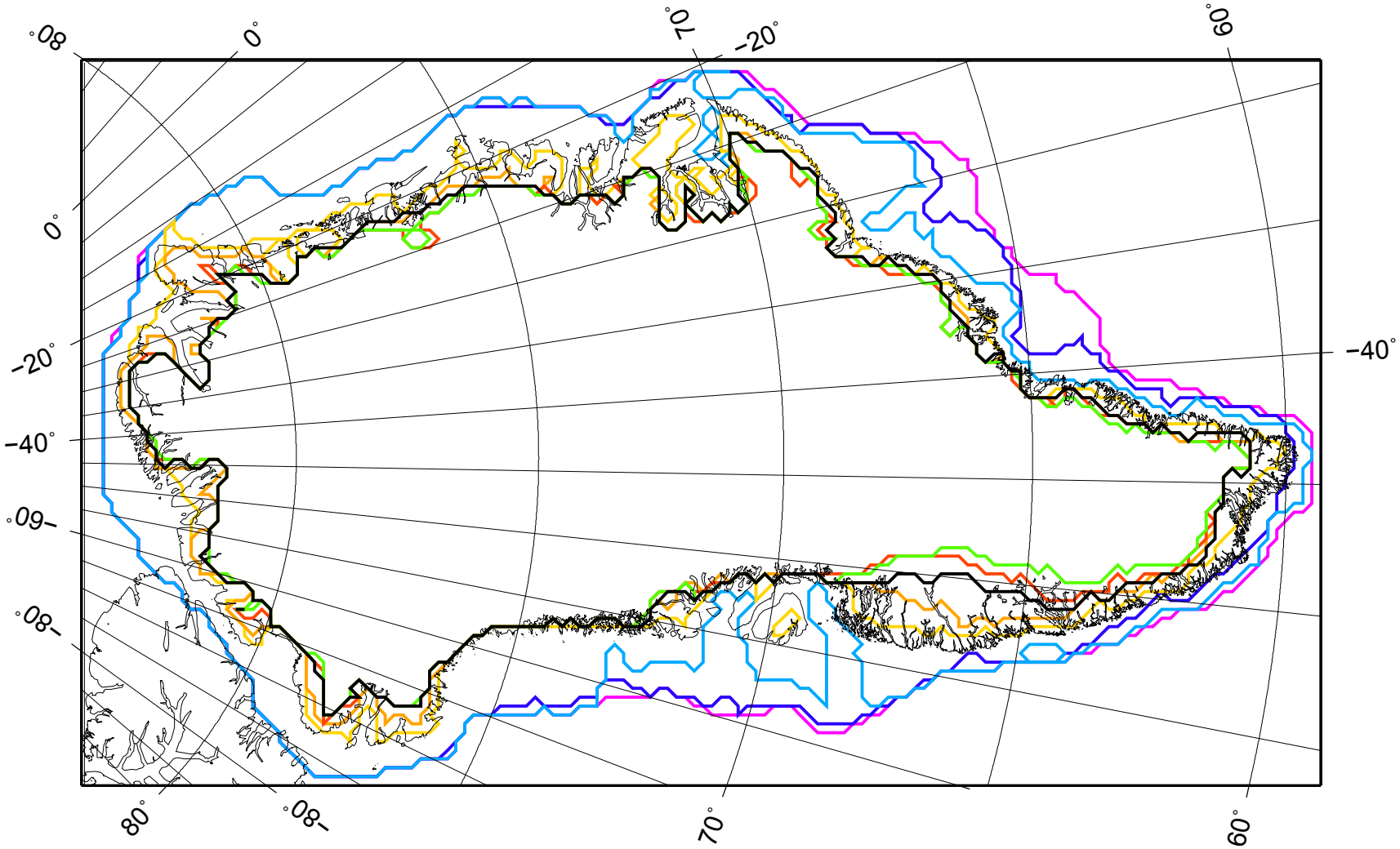
80°
0°
70°
−20°
60°
0°
−20°
−40°
−60°
−80°
−40°
80°
−80°
70°
60°

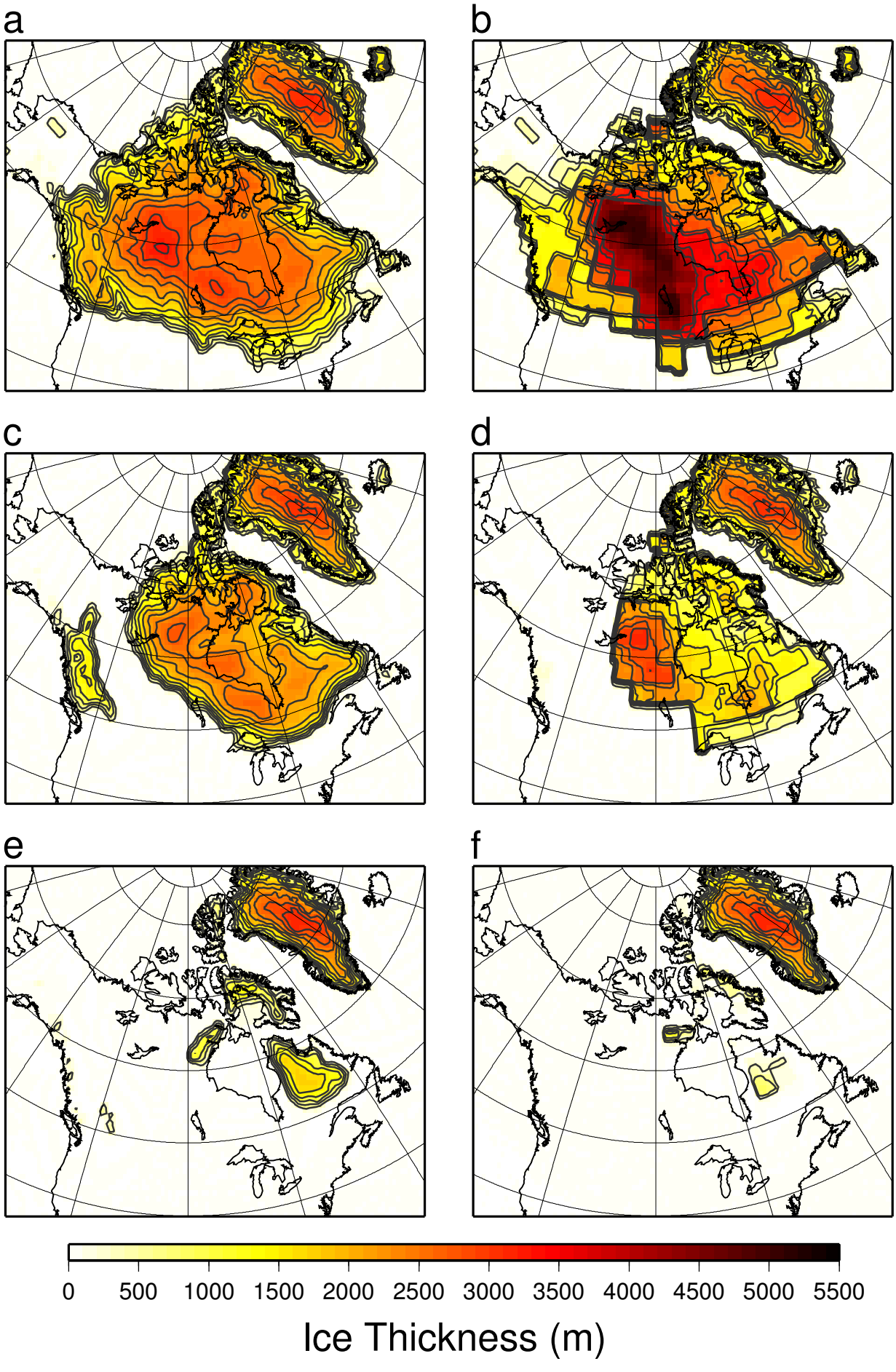
a
b
c
d
e
f
0
500
1000
1500
2000
2500
3000
3500
4000
4500
5000
5500
Ice Thickness (m)

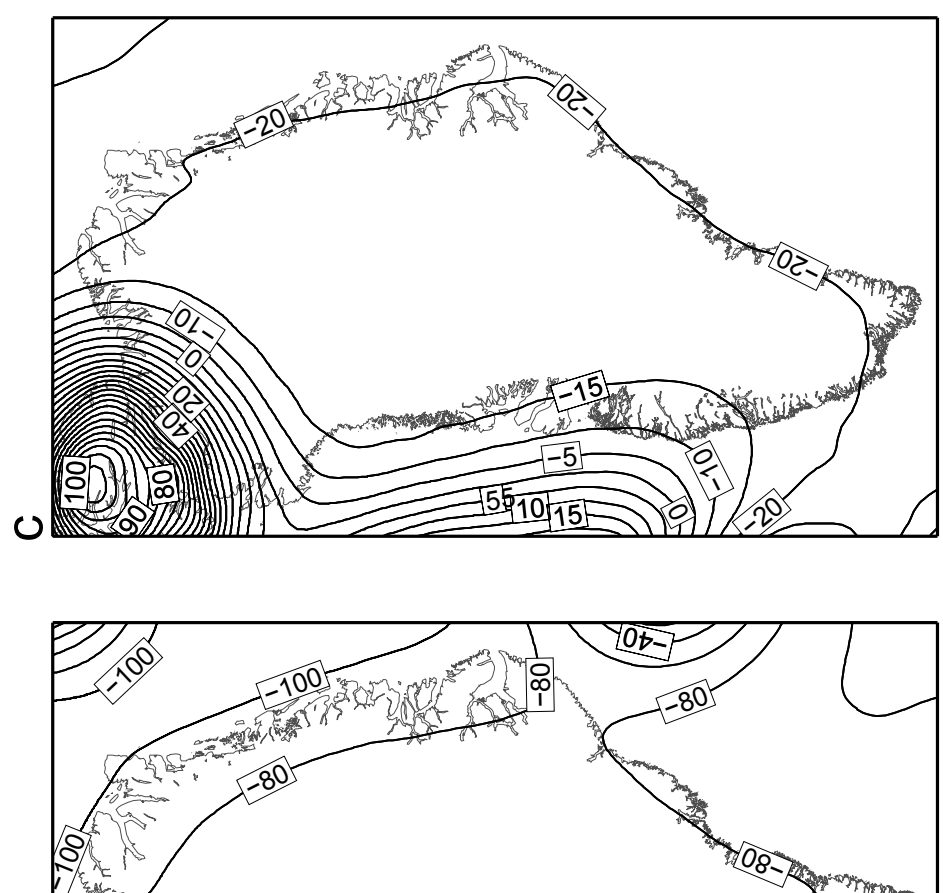
c
−20
−20
−20
−10
0
20
40
100
80
60
−15
−5
5
10
15
0
−10
−20
b
−100
−100
−80
−40
−80
−80
−100
−80
−80
−60
−40
−60
−20
−100
−100
−100
−80
a
−120
−120
−100
−60
−80
−100
−120
−100
−80
−40
−20
40
20
−40
−100
−120
−100
−80

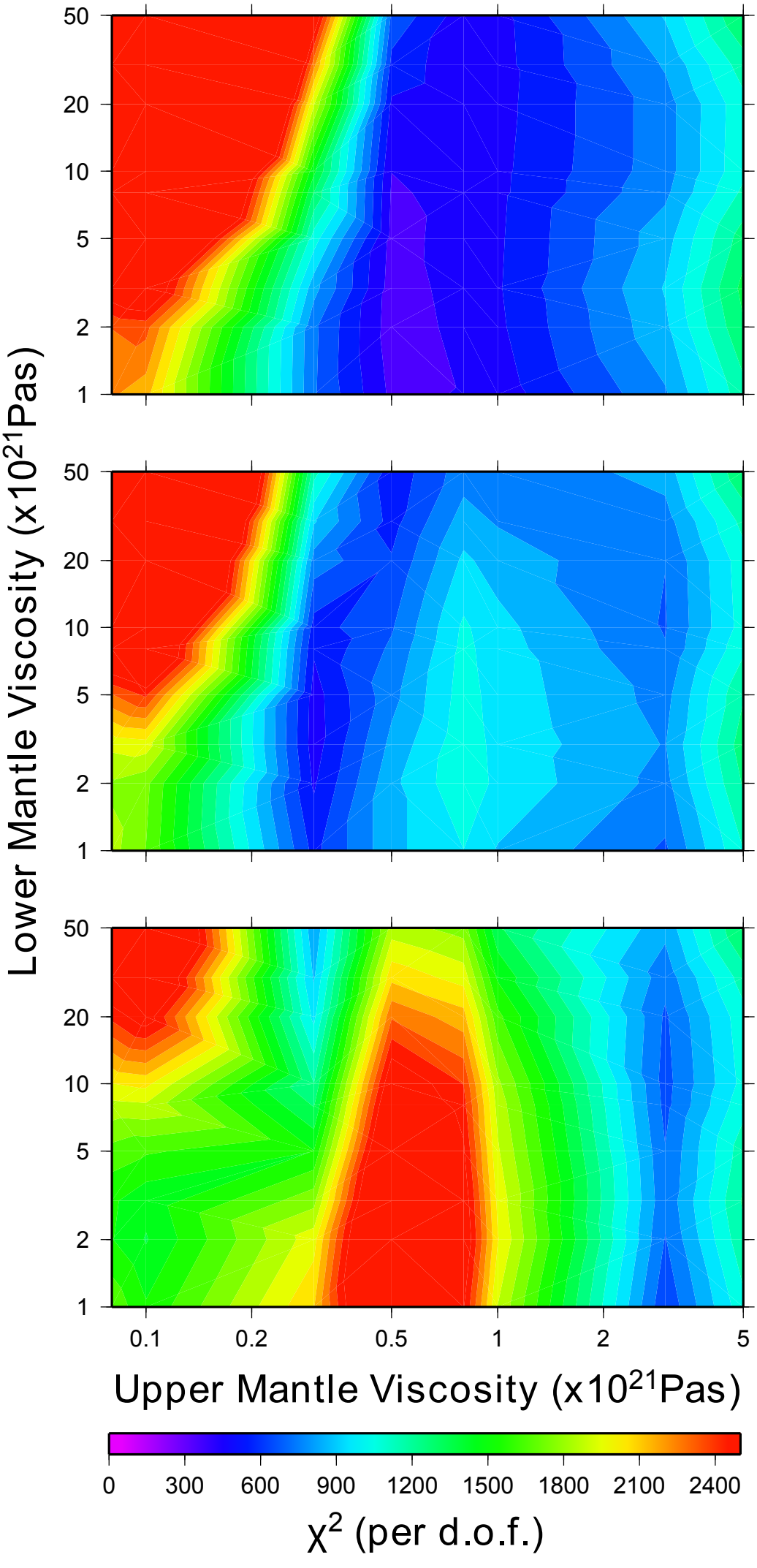
Lower Mantle Viscosity (x10^21Pas)
50
20
10
5
2
1
0.1
0.2
0.5
1
2
5
Upper Mantle Viscosity (x10^21Pas)
0
300
600
900
1200
1500
1800
2100
2400
χ^2 (per d.o.f.)

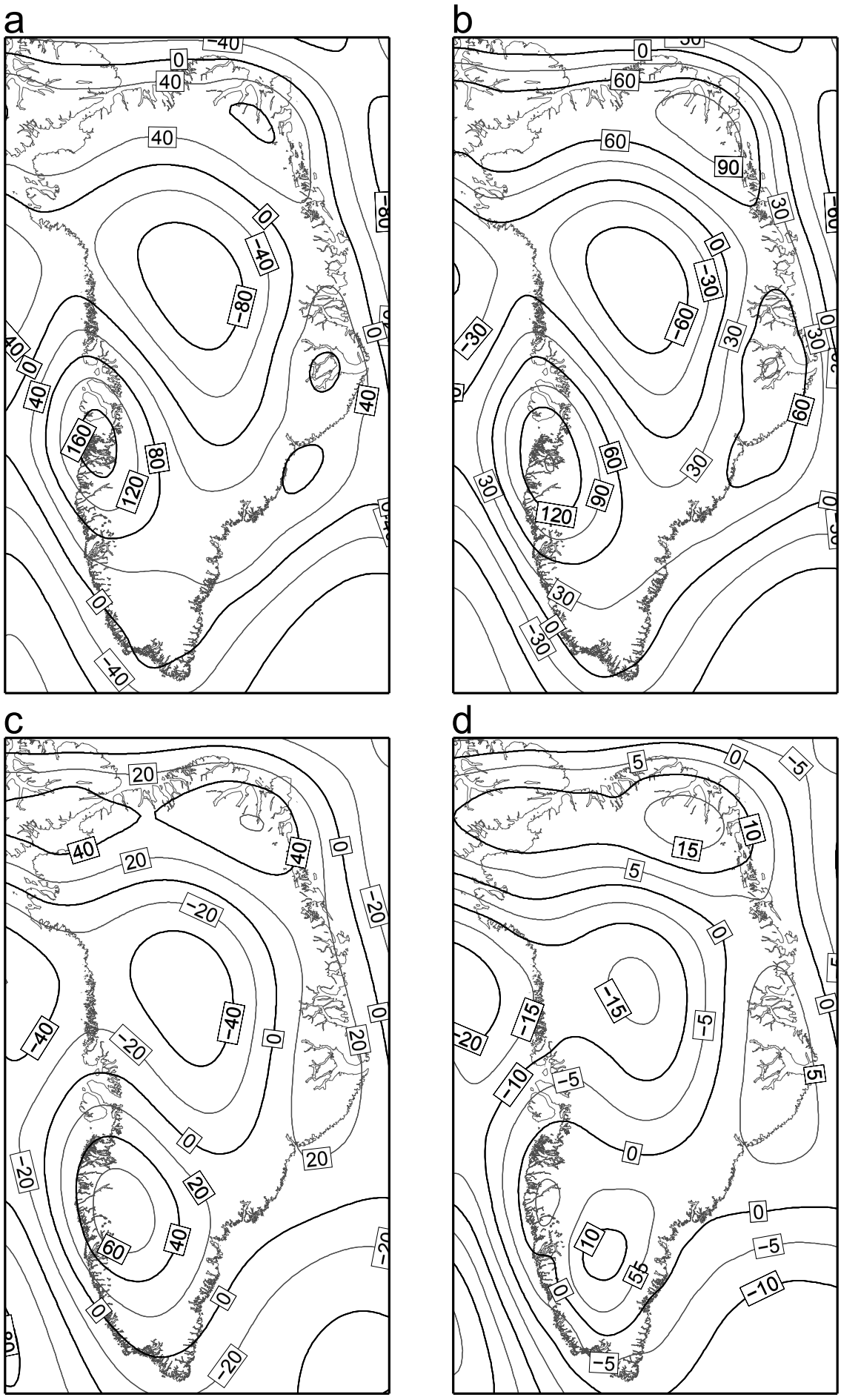
a
b
c
d

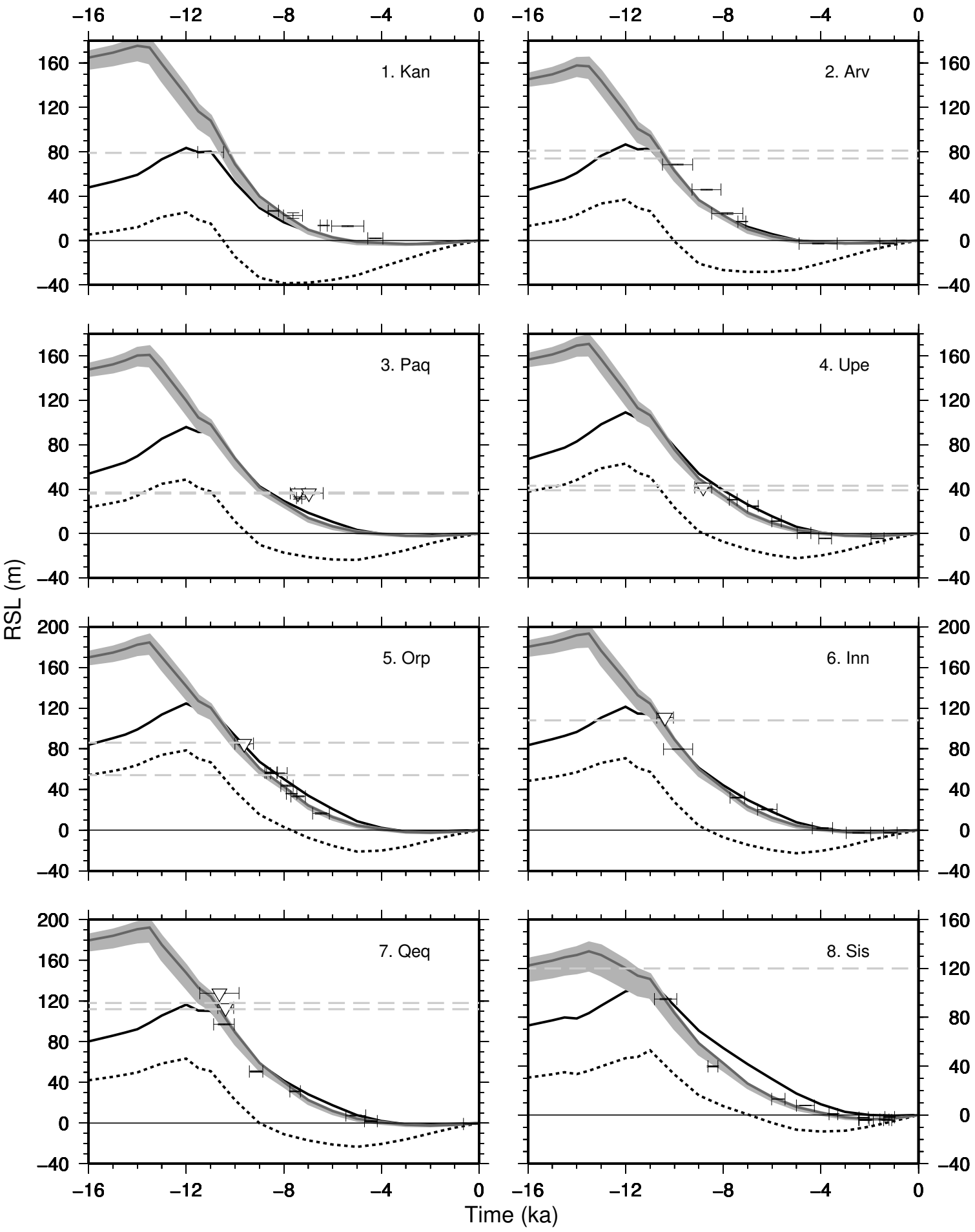
1. Kan
2. Arv
3. Paq
4. Upe
5. Orp
6. Inn
7. Qeq
8. Sis
RSL (m)
Time (ka)
−16
−12
−8
−4
0
160
120
80
40
0
−40
200

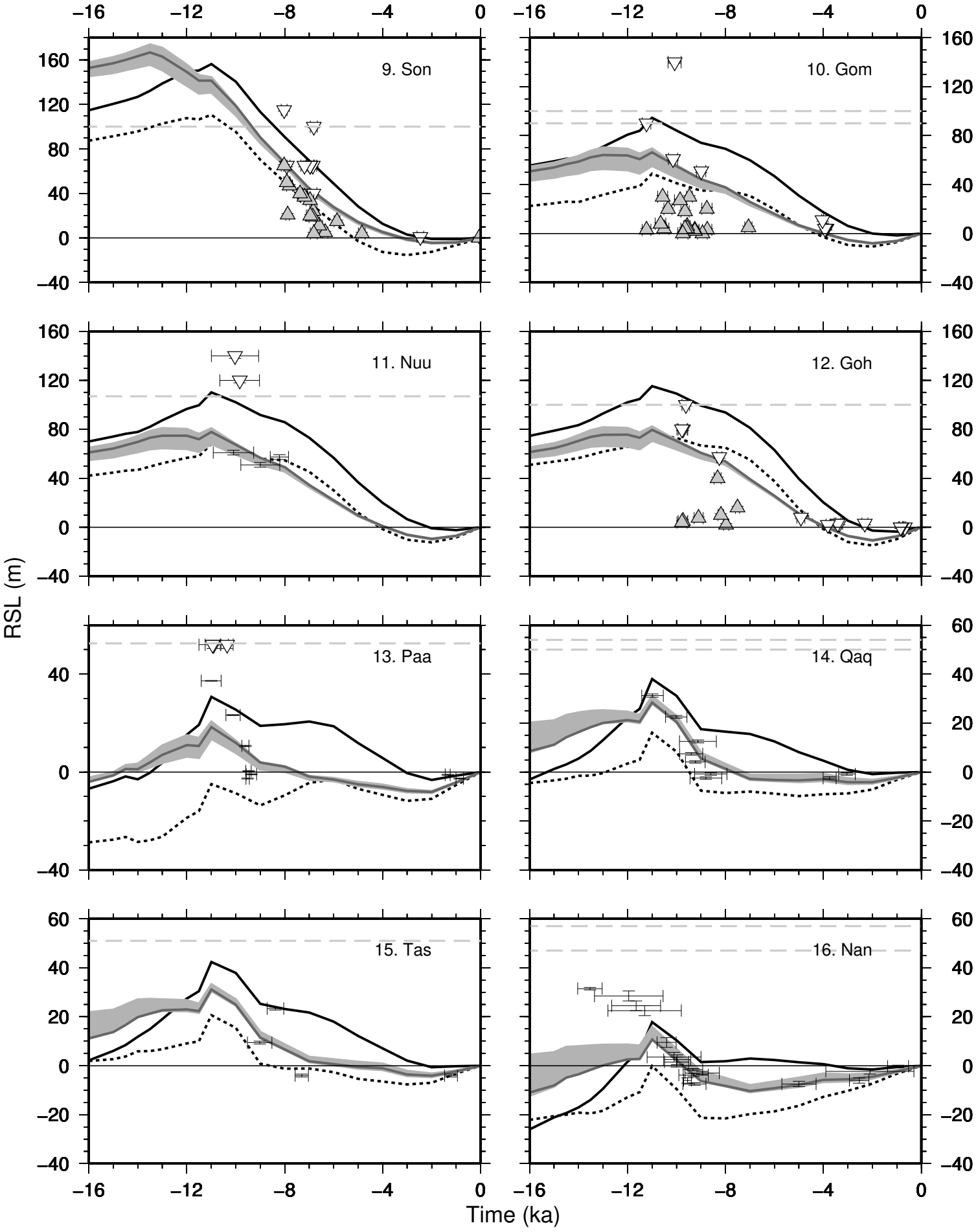
9. Son
10. Gom
11. Nuu
12. Goh
13. Paa
14. Qaq
15. Tas
16. Nan
RSL (m)
Time (ka)
−16
−12
−8
−4
0
160
120
80
40
0
−40
60
20
−20

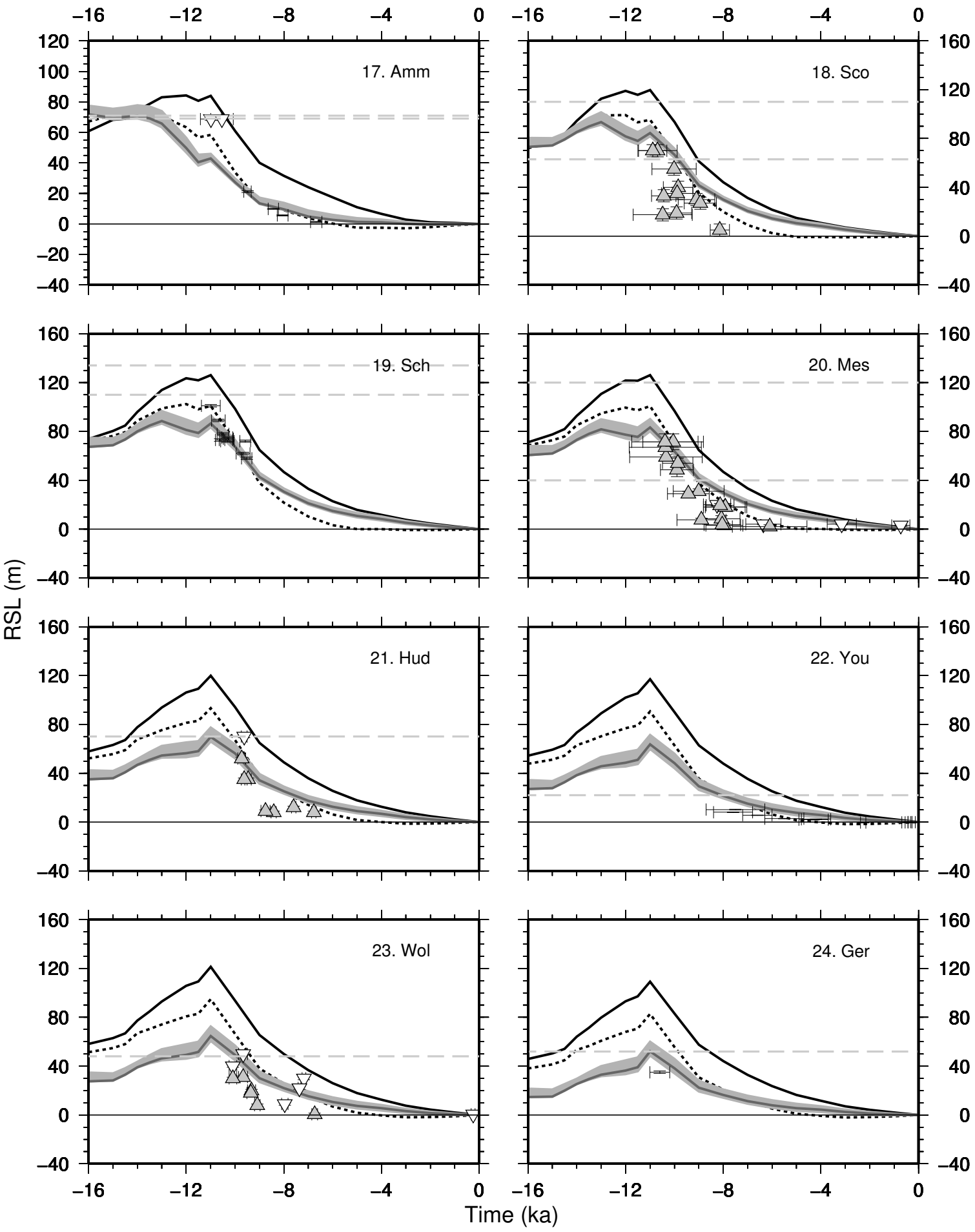
17. Amm
18. Sco
19. Sch
20. Mes
21. Hud
22. You
23. Wol
24. Ger
RSL (m)
Time (ka)
−16
−12
−8
−4
0
120
100
80
60
40
20
0
−20
−40
160

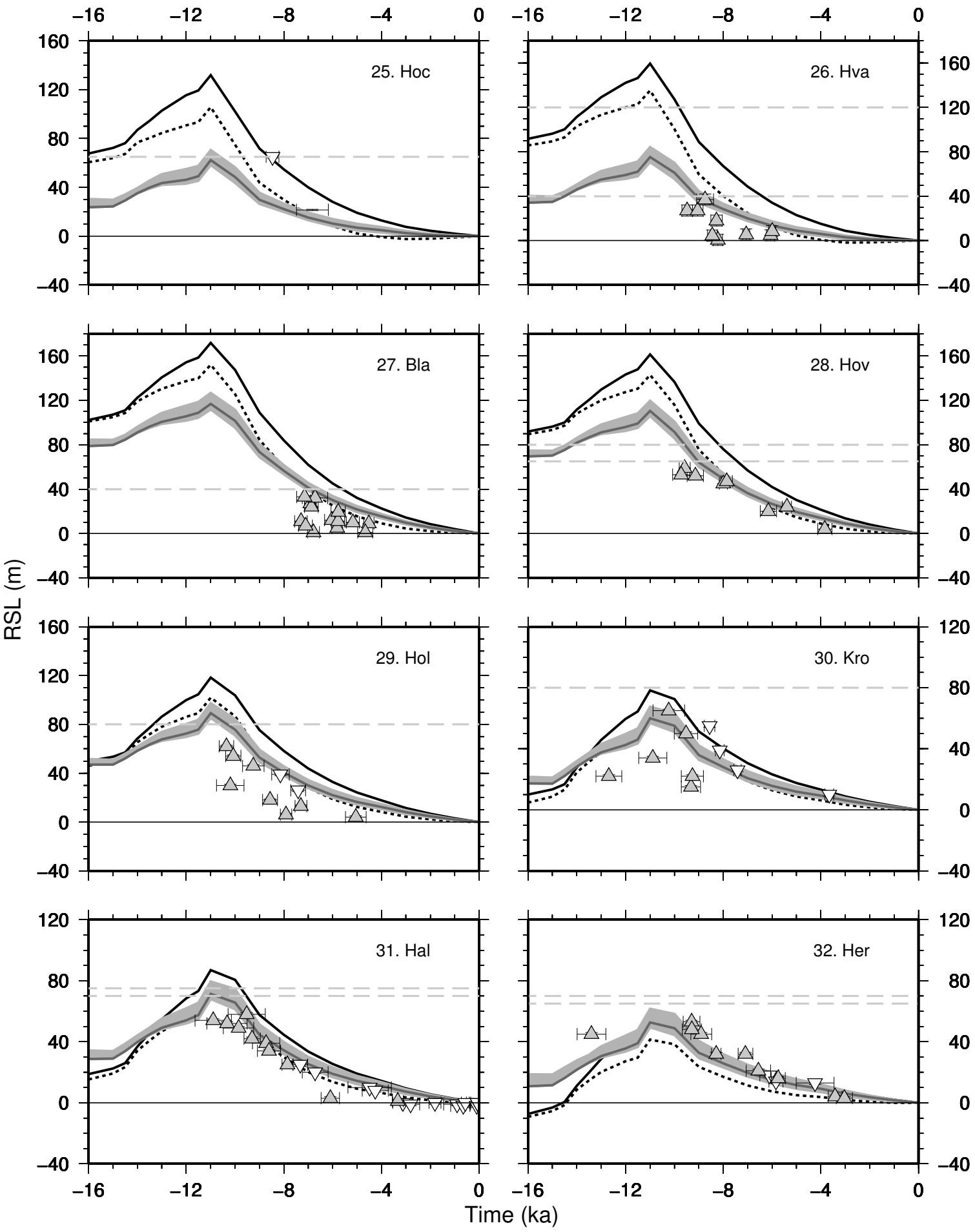
25. Hoc
26. Hva
27. Bla
28. Hov
29. Hol
30. Kro
31. Hal
32. Her
RSL (m)
Time (ka)
−16
−12
−8
−4
0
160
120
80
40
0
−40

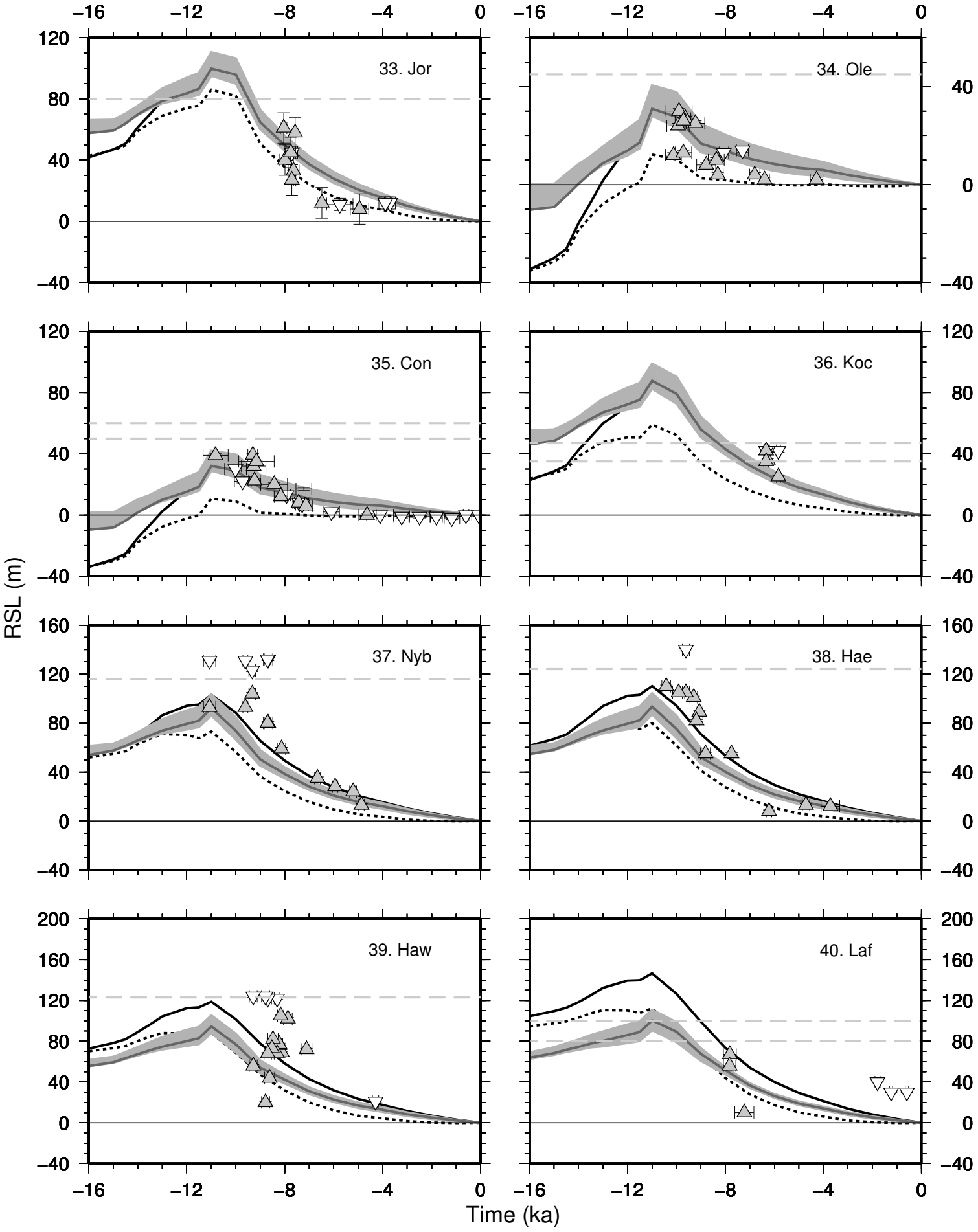
33. Jor
34. Ole
35. Con
36. Koc
37. Nyb
38. Hae
39. Haw
40. Laf
RSL (m)
Time (ka)
−16
−12
−8
−4
0
120
80
40
0
−40
160
200

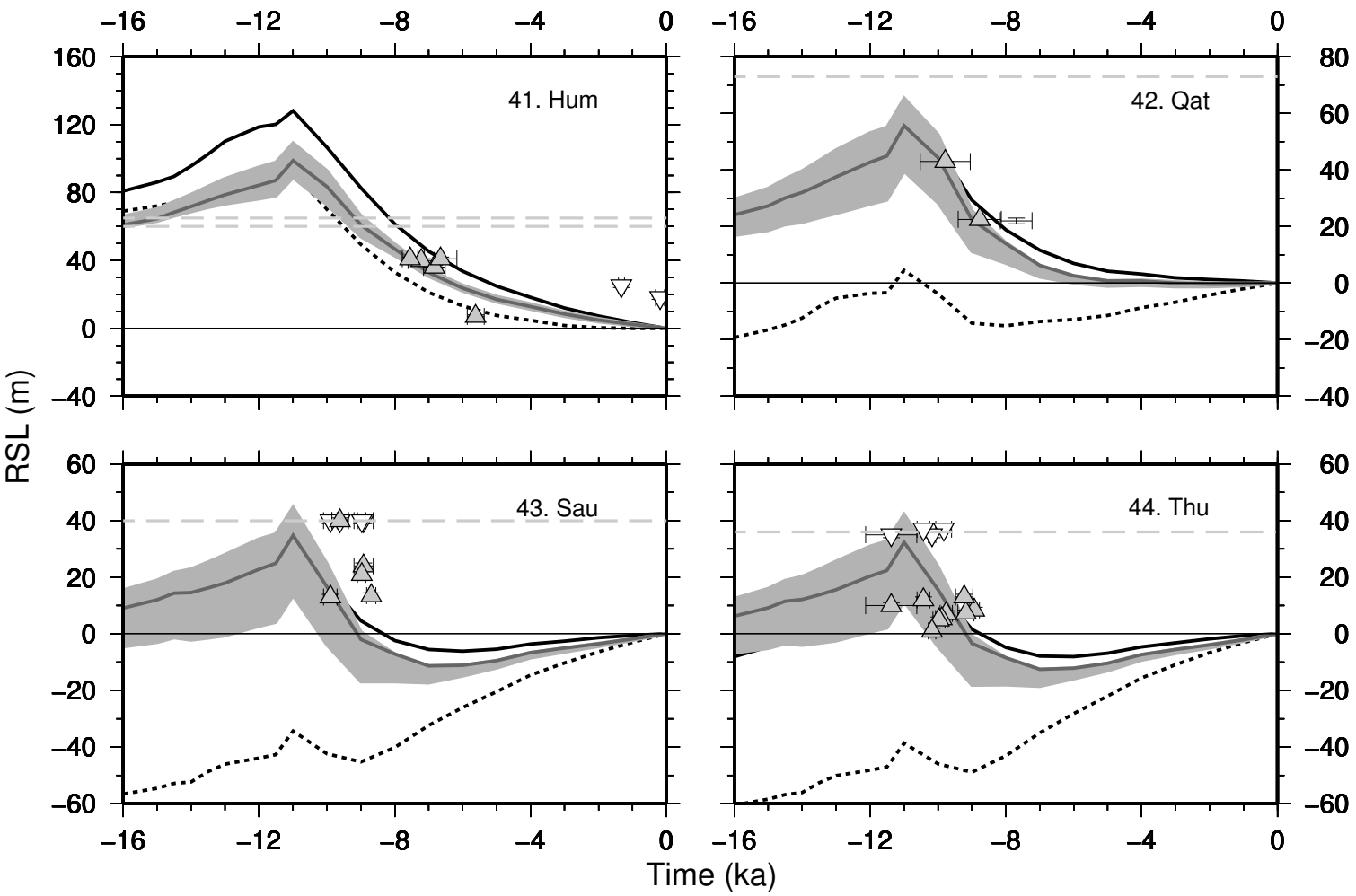
41. Hum
42. Qat
43. Sau
44. Thu
RSL (m)
Time (ka)
−16
−12
−8
−4
0
160
120
80
40
0
−40
60
20
−20
−60

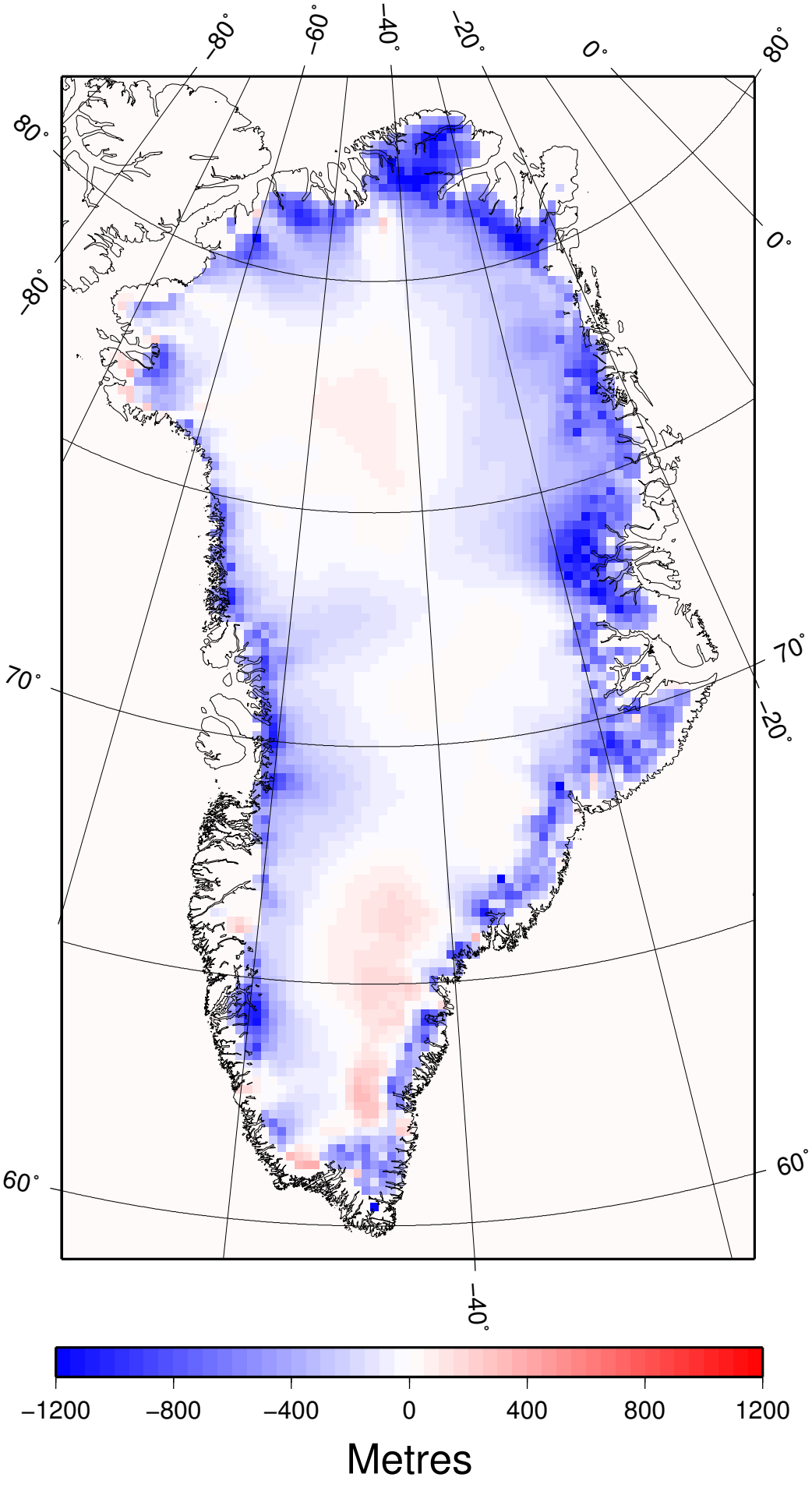
−80°
−60°
−40°
−20°
0°
80°
80°
80°
0°
70°
70°
−20°
60°
60°
−40°
−1200
−800
−400
0
400
800
1200
Metres

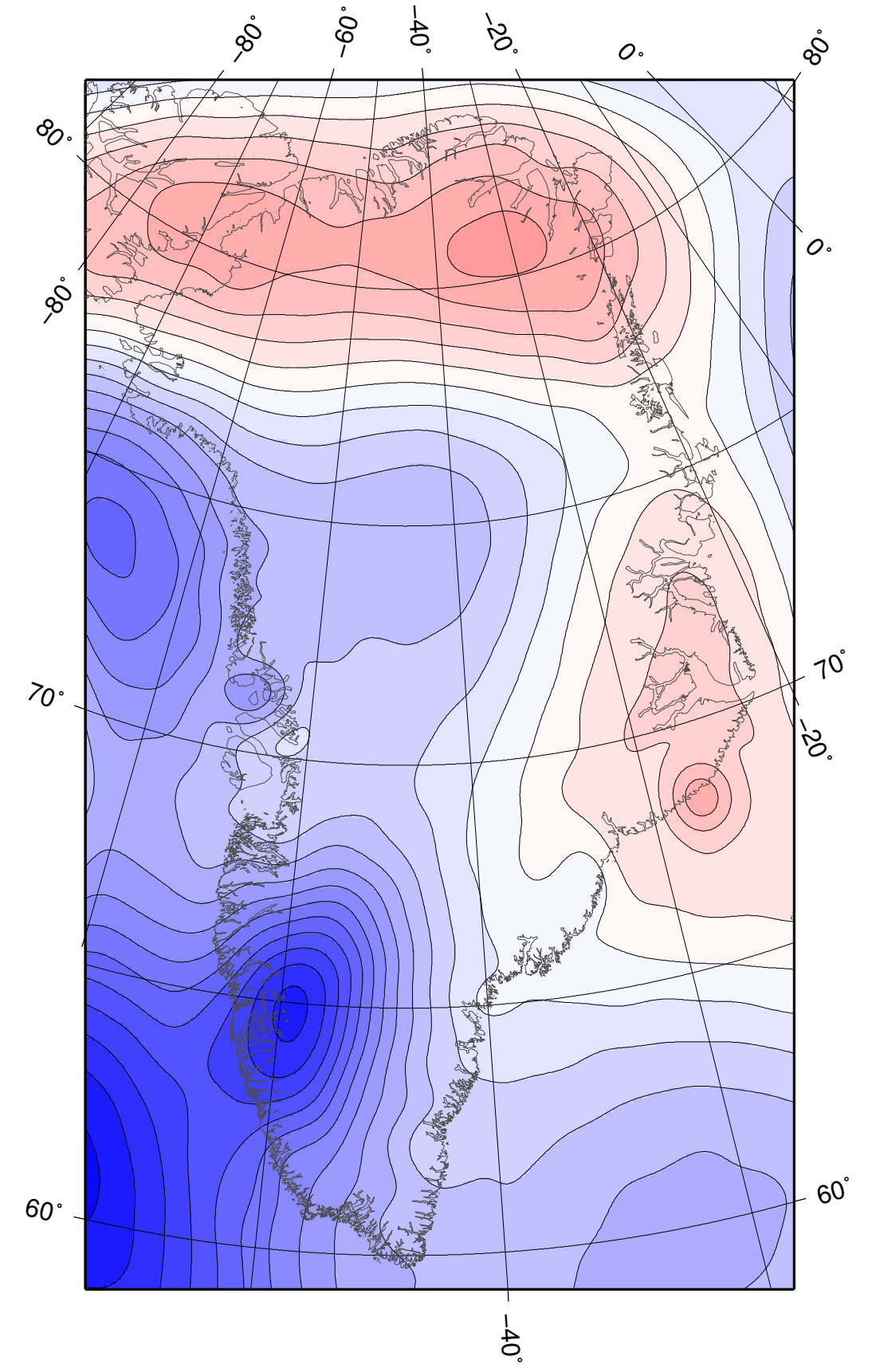
−80°
−60°
−40°
−20°
0°
80°
80°
−80°
0°
70°
70°
−20°
60°
60°
−40°
−7
−6
−5
−4
−3
−2
−1
0
1
2
3
4
5
6
7
Uplift Rate (mm/yr)

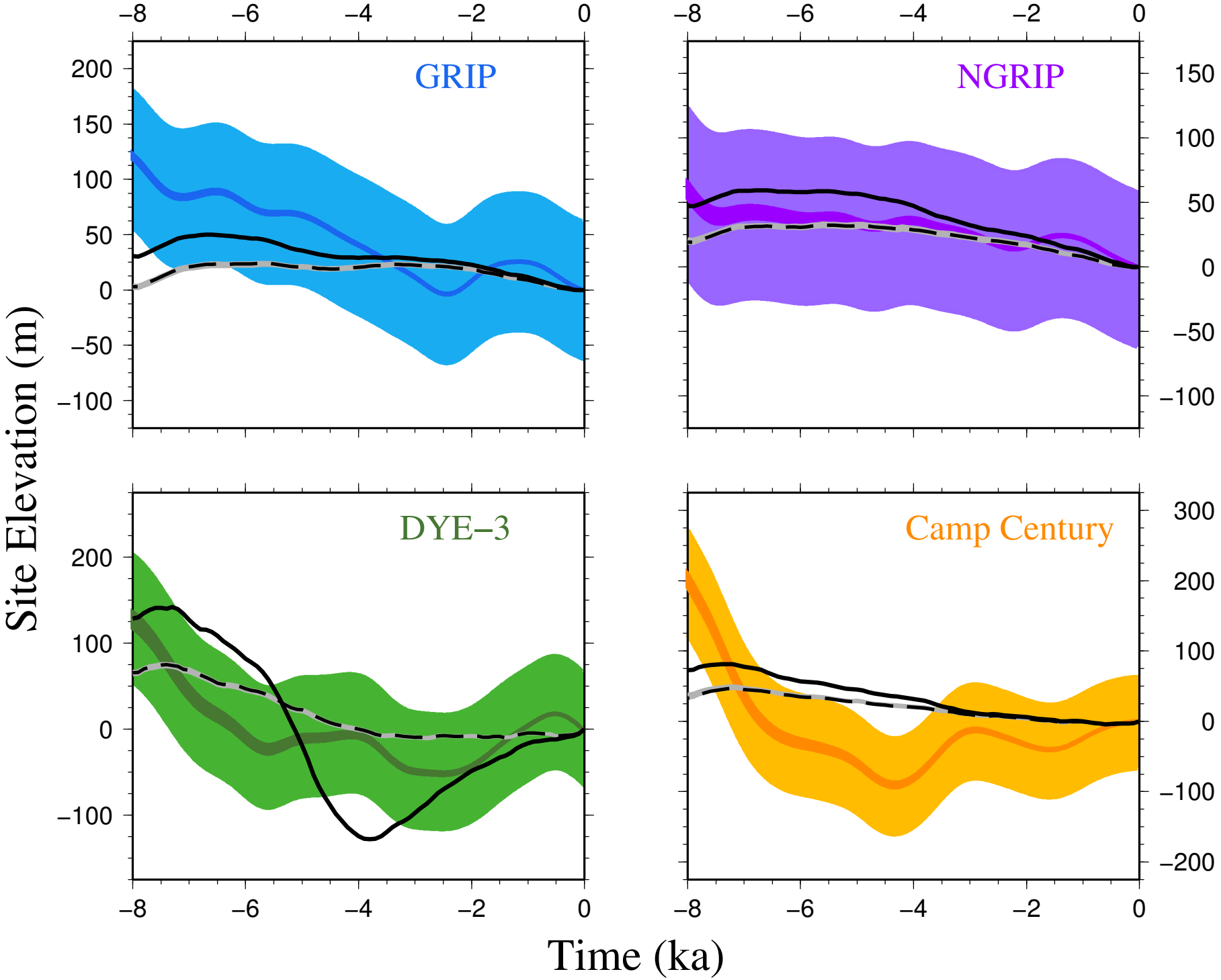
GRIP
NGRIP
DYE–3
Camp Century
Site Elevation (m)
Time (ka)
–8
–6
–4
–2
0
200
150
100
50
0
–50
–100
300
–200

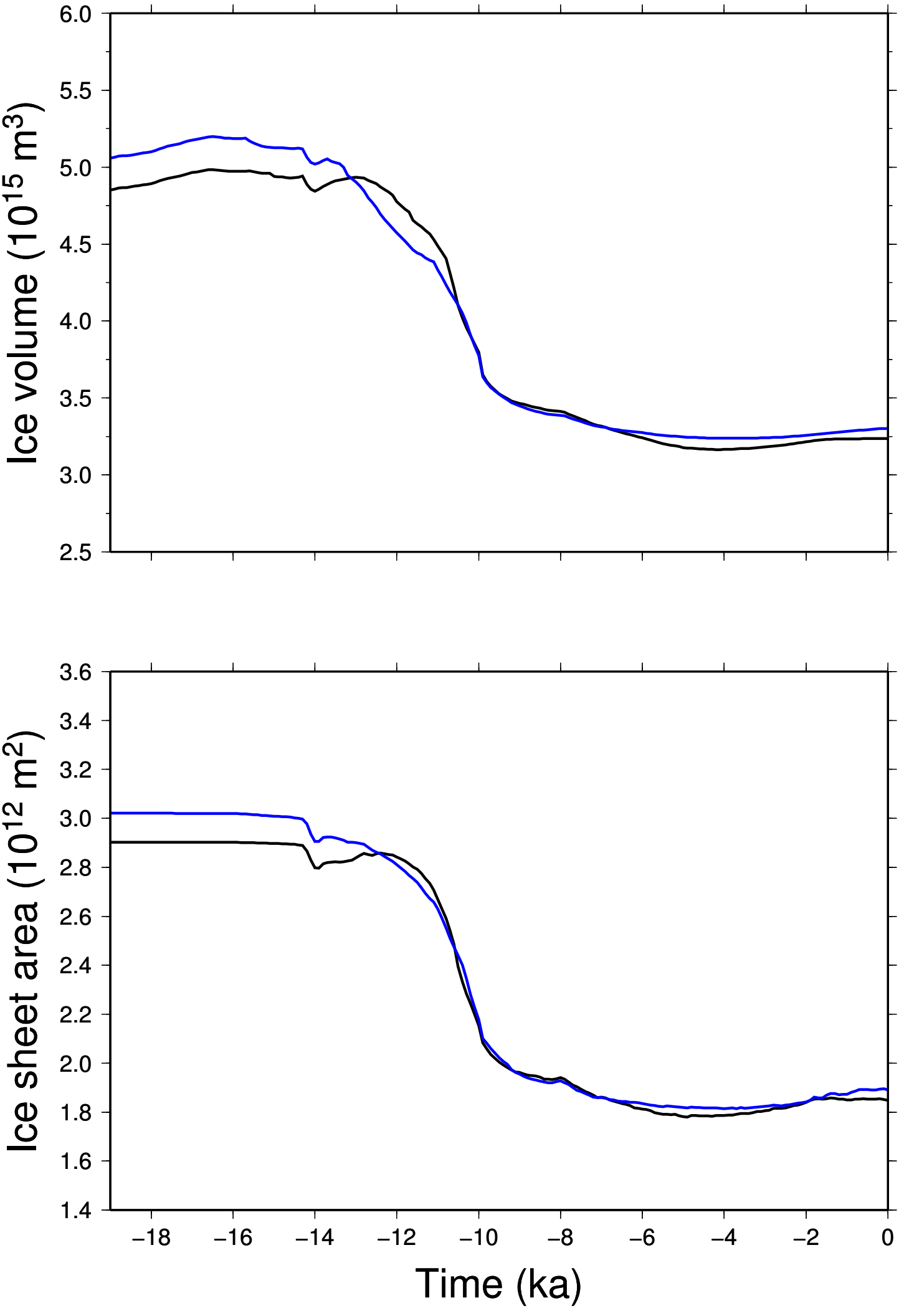
6.0
5.5
5.0
4.5
4.0
3.5
3.0
2.5
Ice volume (10^{15} m^3)
3.6
3.4
3.2
3.0
2.8
2.6
2.4
2.2
2.0
1.8
1.6
1.4
Ice sheet area (10^{12} m^2)
−18
−16
−14
−12
−10
−8
−6
−4
−2
0
Time (ka)

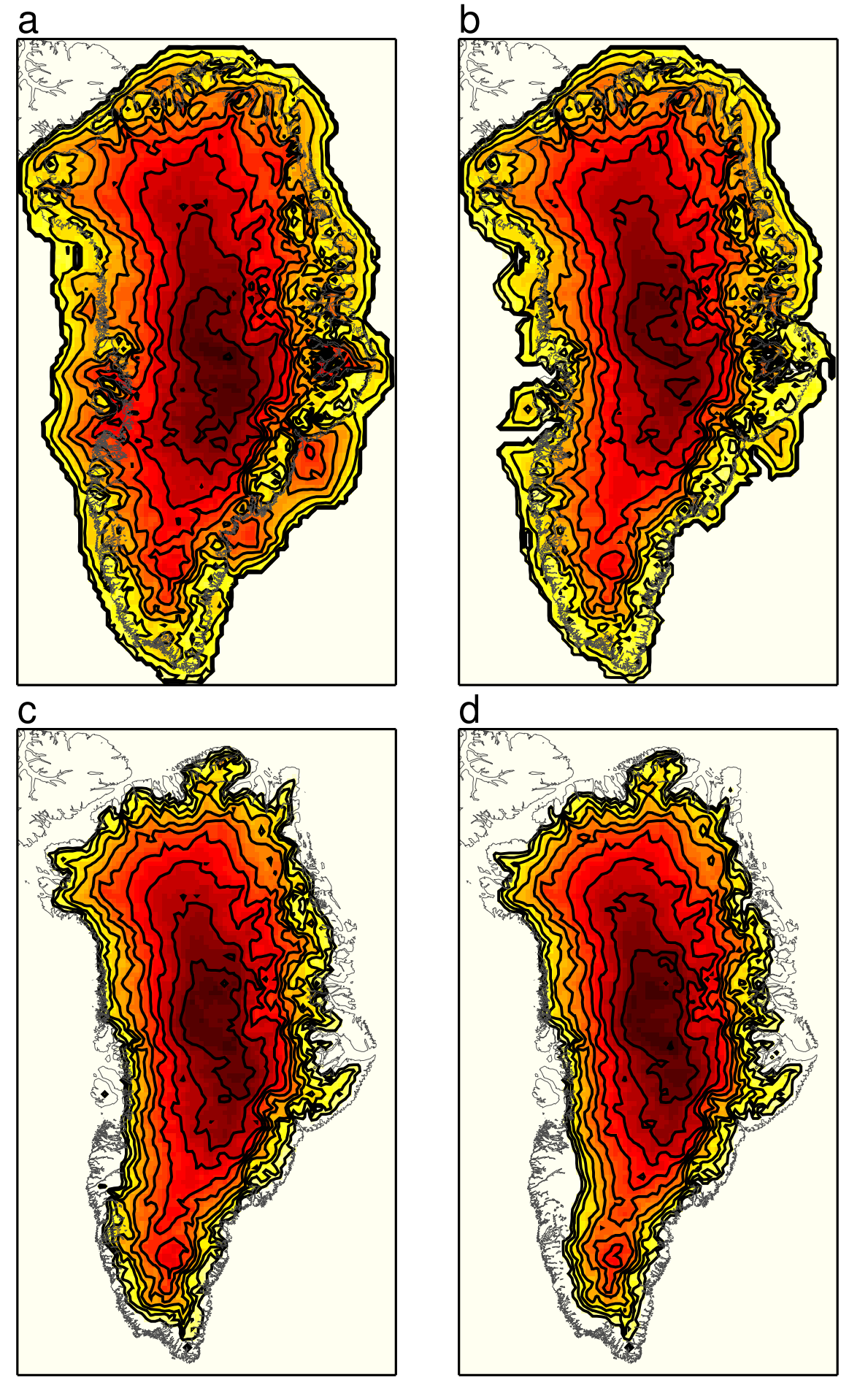
a
b
c
d
0
300
600
900
1200
1500
1800
2100
2400
2700
3000
3300
3600
Ice thickness (m)

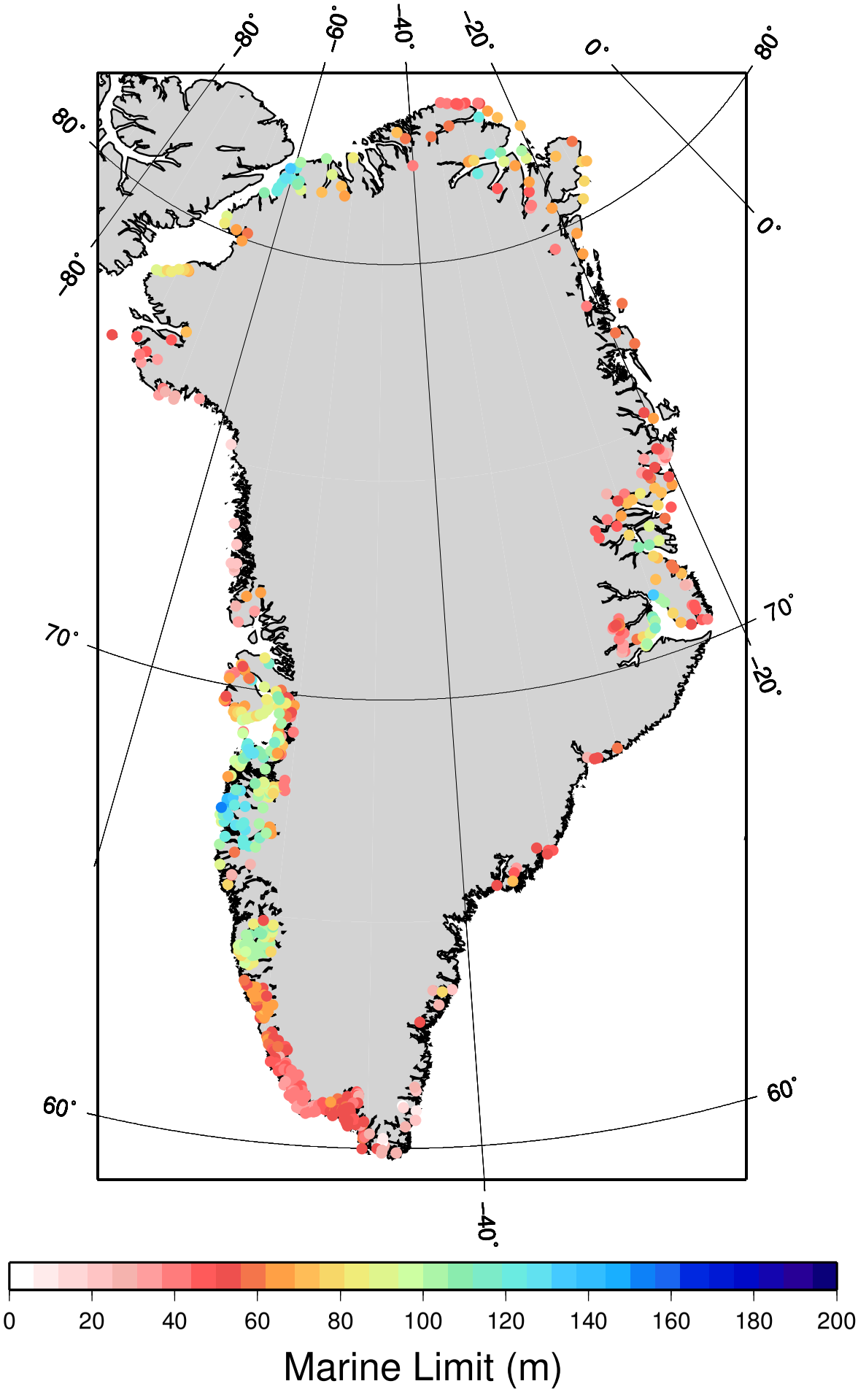
-80°
-60°
-40°
-20°
0°
80°
80°
-80°
70°
70°
-20°
60°
60°
-40°
0
20
40
60
80
100
120
140
160
180
200
Marine Limit (m)

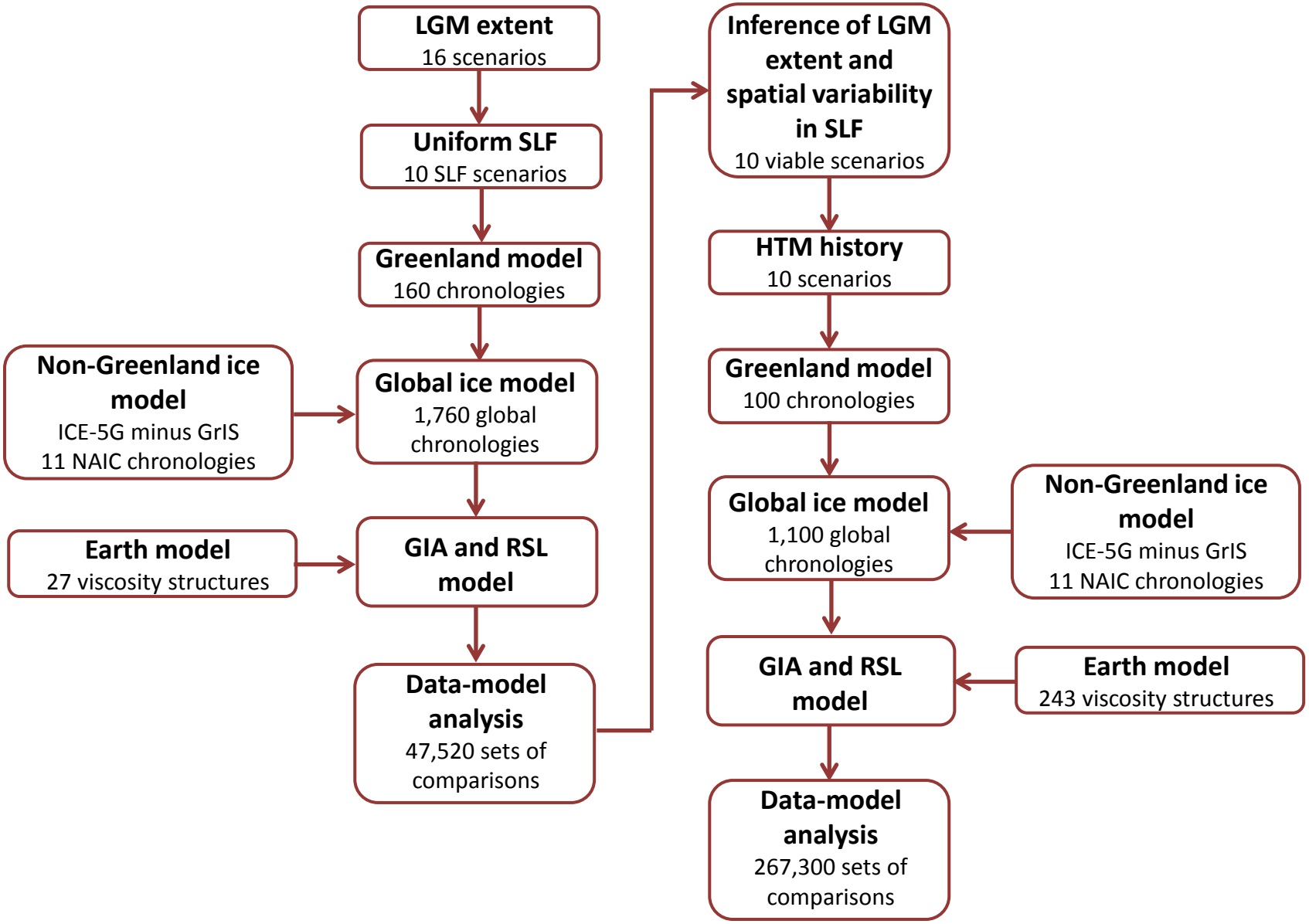
LGM extent
16 scenarios
Uniform SLF
10 SLF scenarios
Greenland model
160 chronologies
Non-Greenland ice model
ICE-5G minus GrIS
11 NAIC chronologies
Global ice model
1,760 global chronologies
Earth model
27 viscosity structures
GIA and RSL model
Data-model analysis
47,520 sets of comparisons
Inference of LGM extent and spatial variability in SLF
10 viable scenarios
HTM history
10 scenarios
Greenland model
100 chronologies
Global ice model
1,100 global chronologies
Non-Greenland ice model
ICE-5G minus GrIS
11 NAIC chronologies
GIA and RSL model
Earth model
243 viscosity structures
Data-model analysis
267,300 sets of comparisons

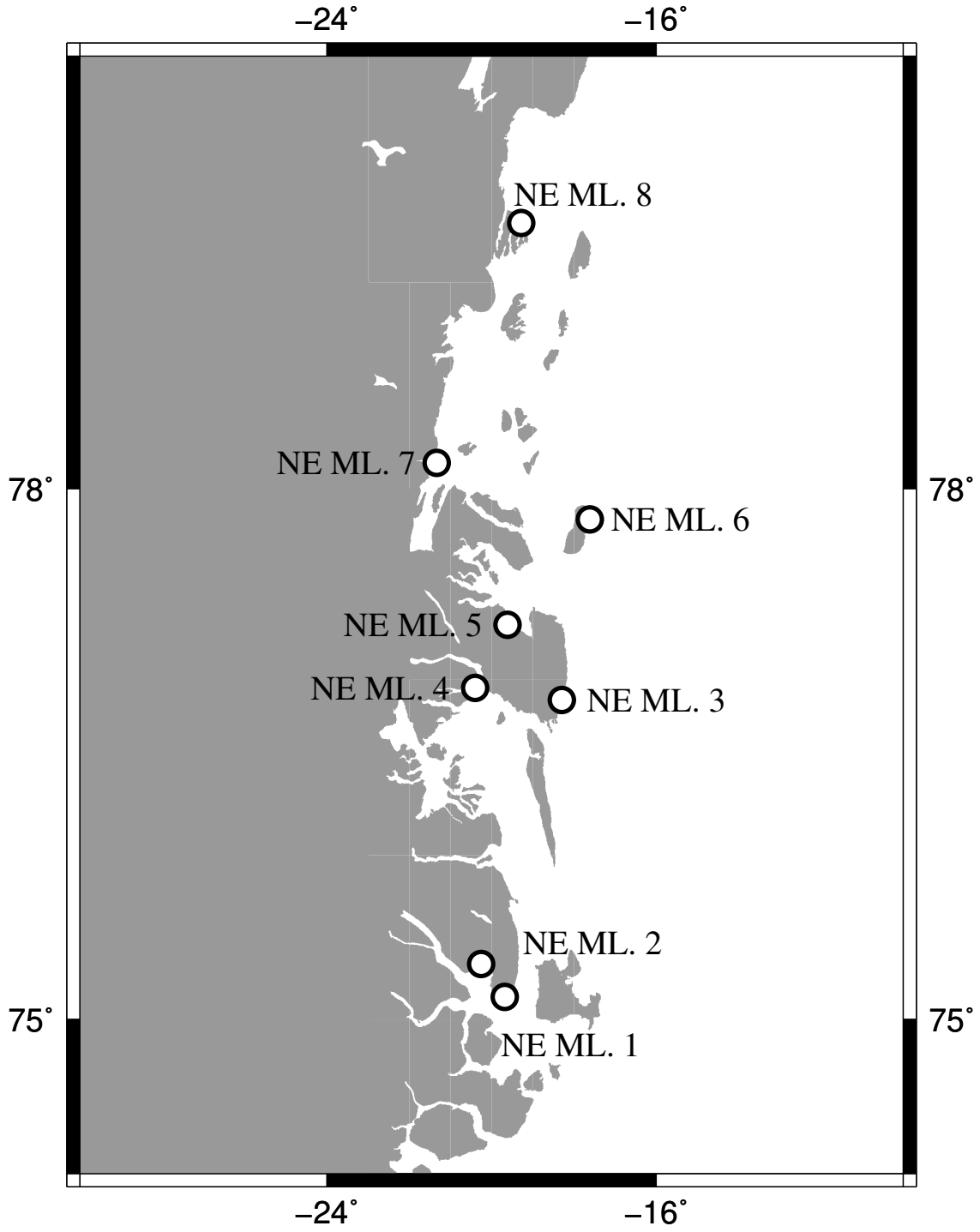
–24˚
–16˚
NE ML. 8
NE ML. 7
78˚
NE ML. 6
NE ML. 5
NE ML. 4
NE ML. 3
NE ML. 2
75˚
NE ML. 1

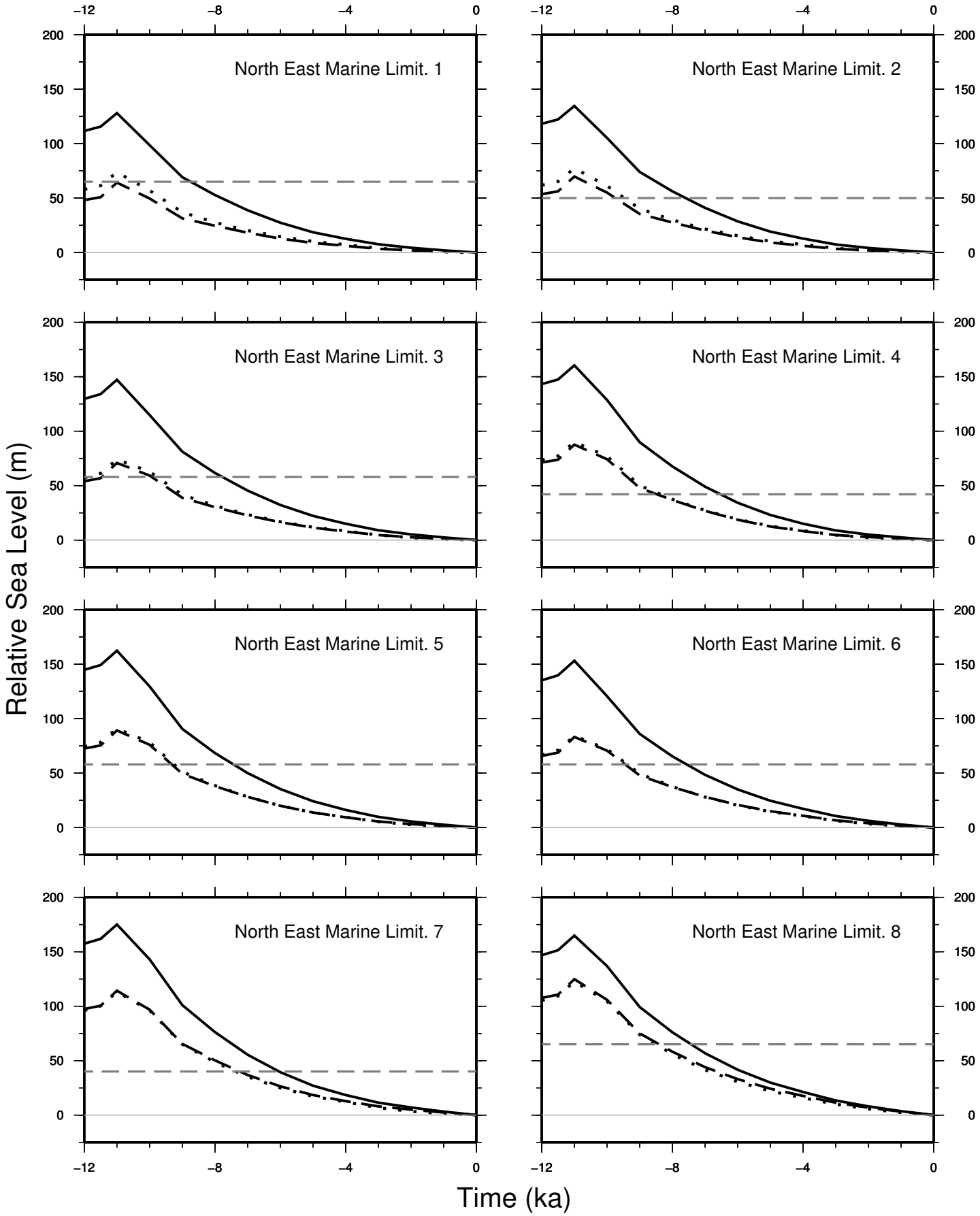
North East Marine Limit. 1
North East Marine Limit. 2
North East Marine Limit. 3
North East Marine Limit. 4
North East Marine Limit. 5
North East Marine Limit. 6
North East Marine Limit. 7
North East Marine Limit. 8
Relative Sea Level (m)
Time (ka)
−12
−8
−4
0
200
150
100
50
0

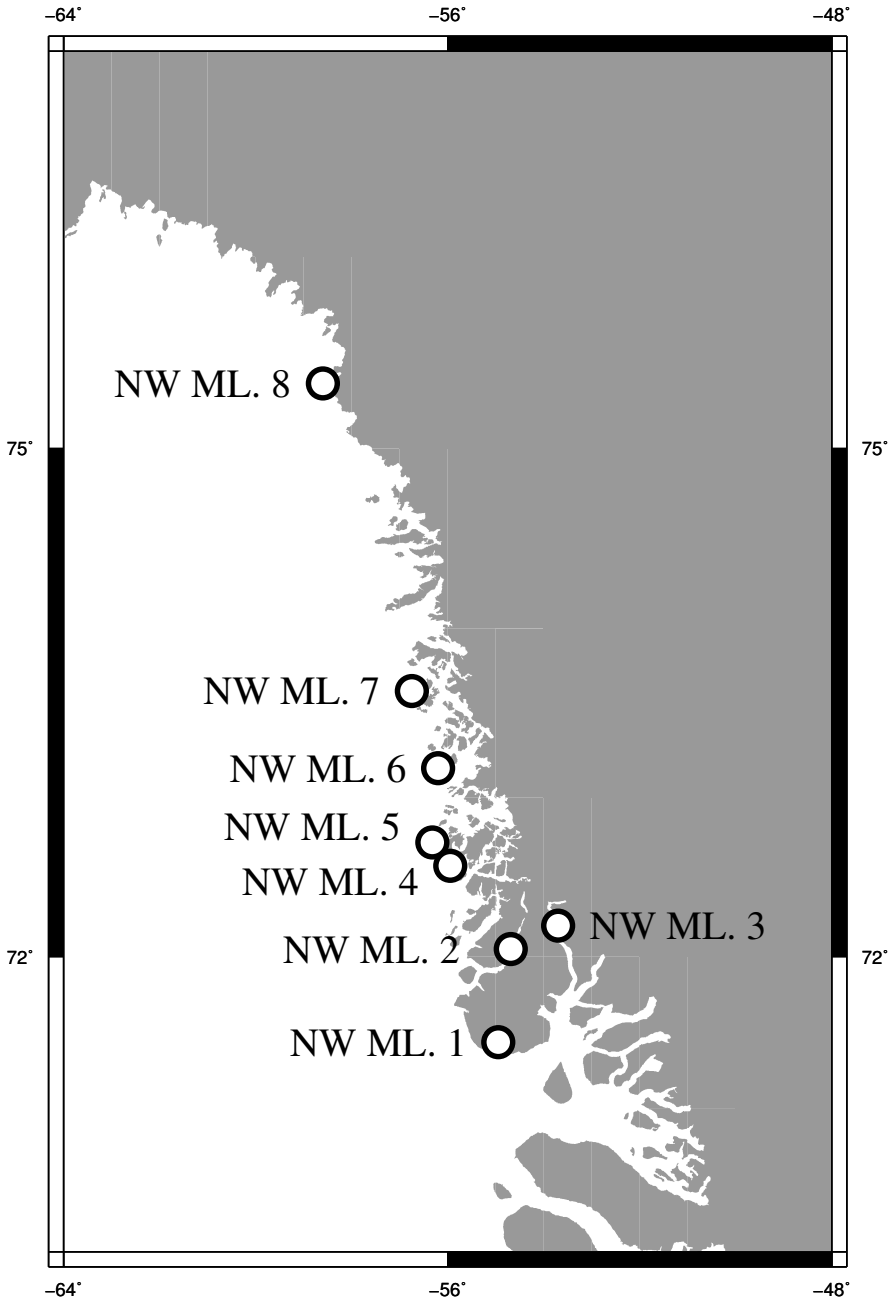
–64˚
–56˚
–48˚
75˚
72˚
NW ML. 8
NW ML. 7
NW ML. 6
NW ML. 5
NW ML. 4
NW ML. 3
NW ML. 2
NW ML. 1

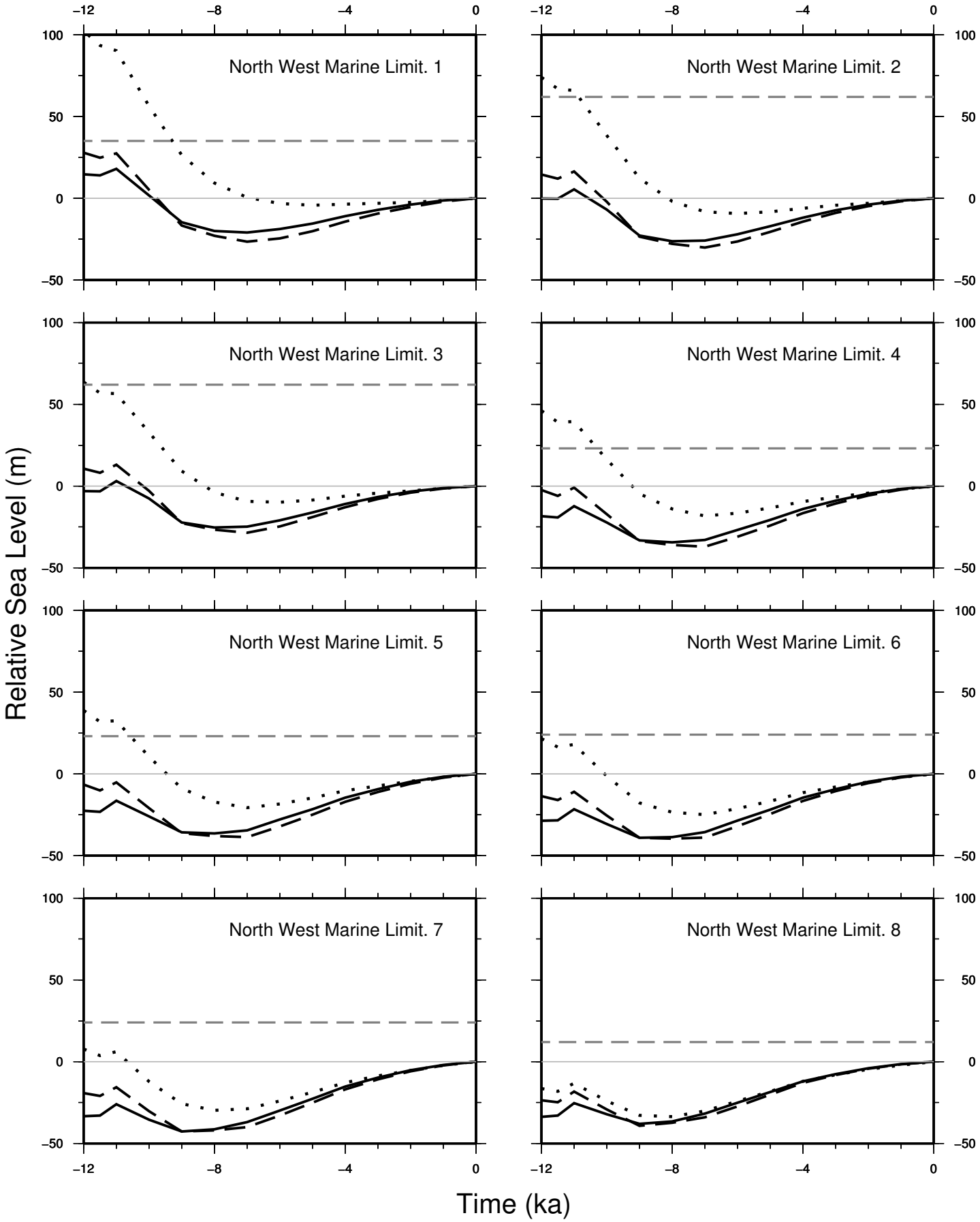
North West Marine Limit. 1
North West Marine Limit. 2
North West Marine Limit. 3
North West Marine Limit. 4
North West Marine Limit. 5
North West Marine Limit. 6
North West Marine Limit. 7
North West Marine Limit. 8
Relative Sea Level (m)
Time (ka)
−12
−8
−4
0
100
50
0
−50

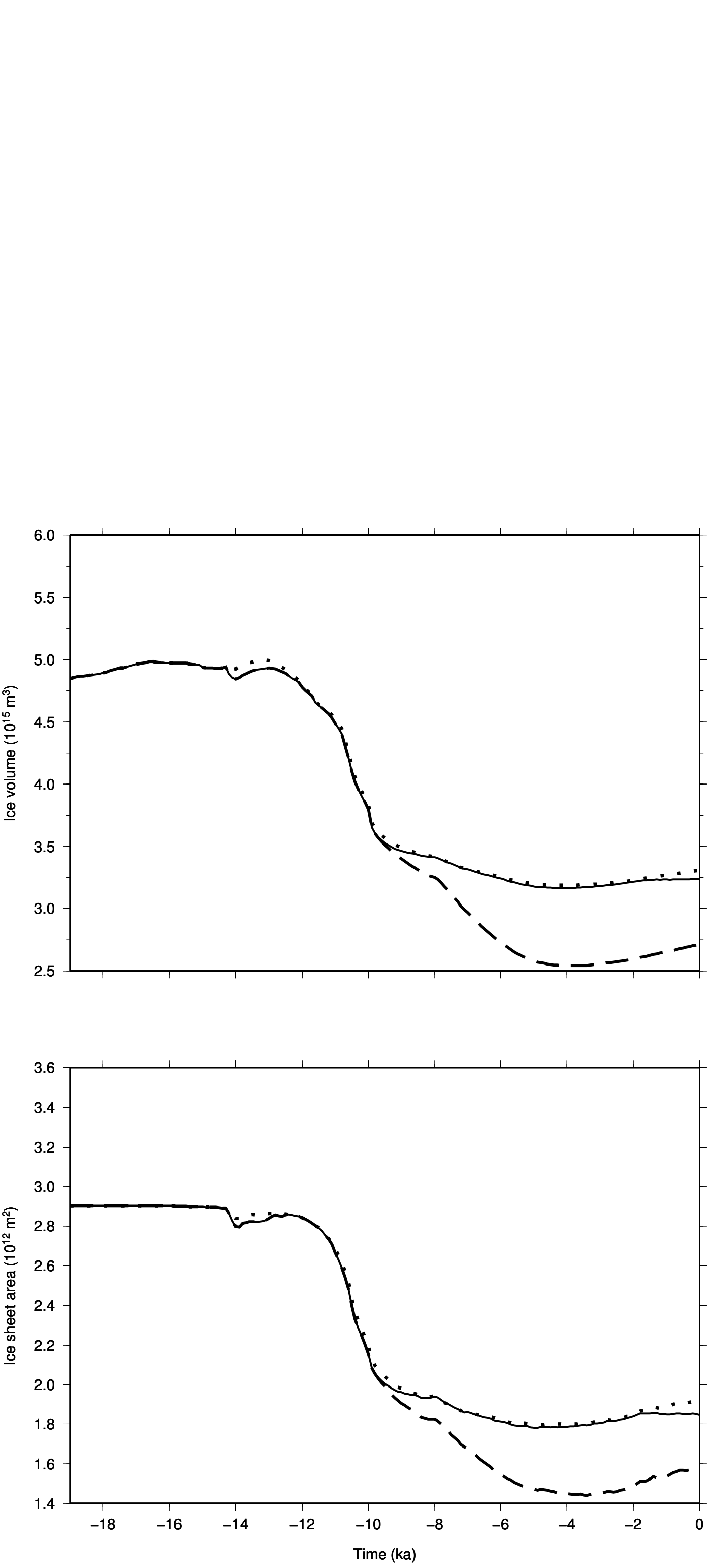
Ice volume (10^{15} m^3)
6.0
5.5
5.0
4.5
4.0
3.5
3.0
2.5
Ice sheet area (10^{12} m^2)
3.6
3.4
3.2
3.0
2.8
2.6
2.4
2.2
2.0
1.8
1.6
1.4
−18
−16
−14
−12
−10
−8
−6
−4
−2
0
Time (ka)

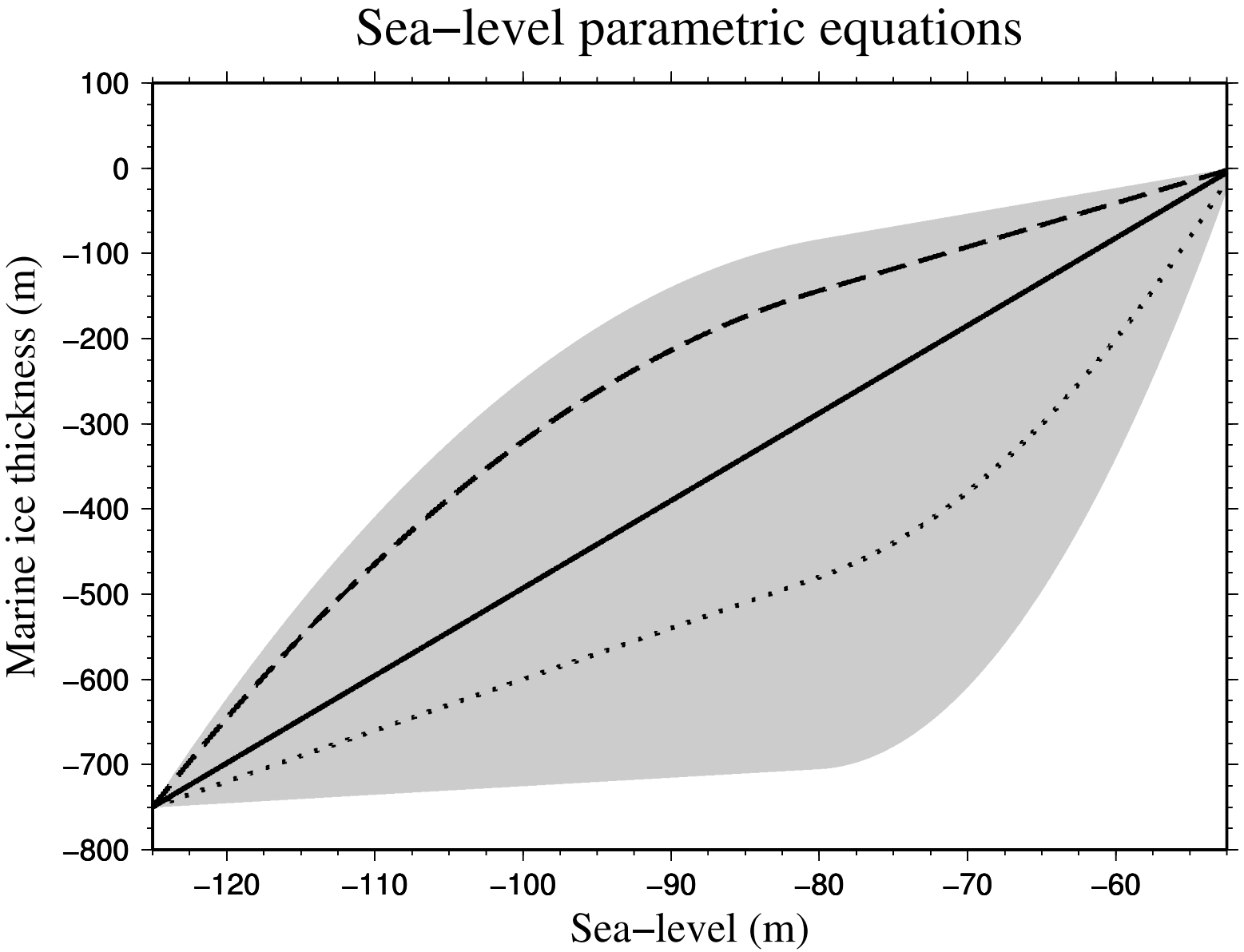
Sea–level parametric equations
Marine ice thickness (m)
100
0
–100
–200
–300
–400
–500
–600
–700
–800
–120
–110
–100
–90
–80
–70
–60
Sea–level (m)

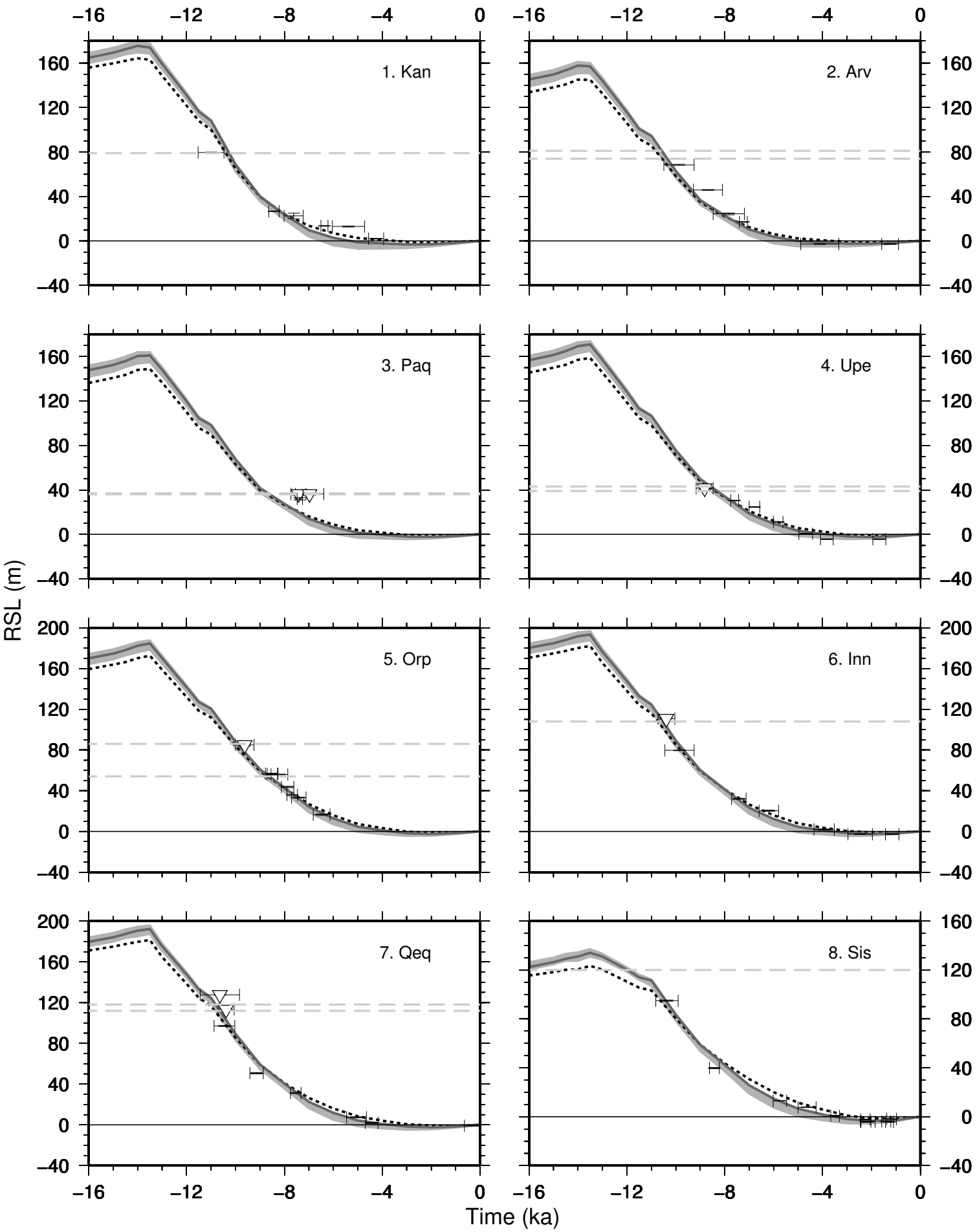
1. Kan
2. Arv
3. Paq
4. Upe
5. Orp
6. Inn
7. Qeq
8. Sis
RSL (m)
Time (ka)
−16
−12
−8
−4
0
160
120
80
40
0
−40
200

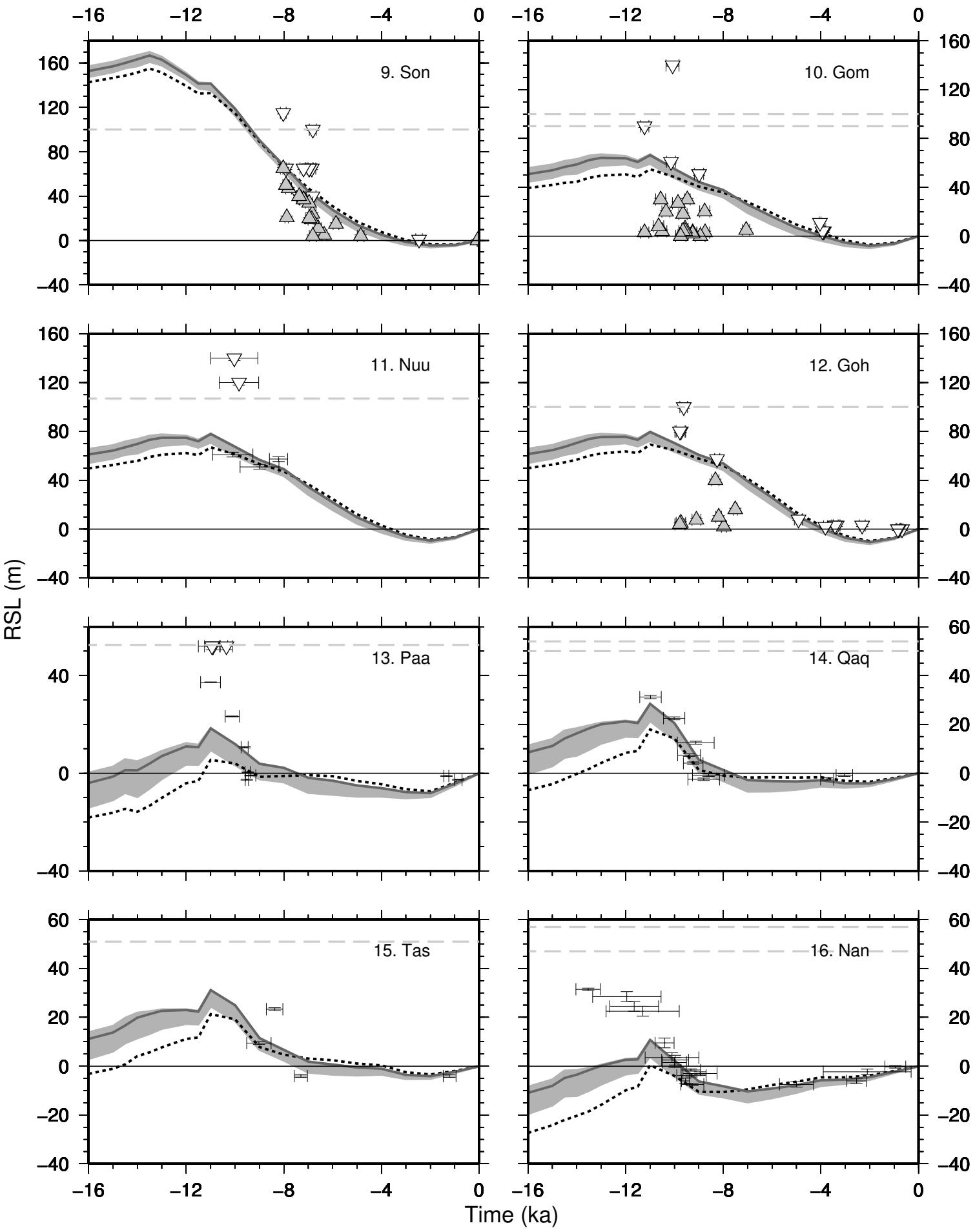
9. Son
10. Gom
11. Nuu
12. Goh
13. Paa
14. Qaq
15. Tas
16. Nan
RSL (m)
Time (ka)
−16
−12
−8
−4
0
160
120
80
40
0
−40
60
20
−20

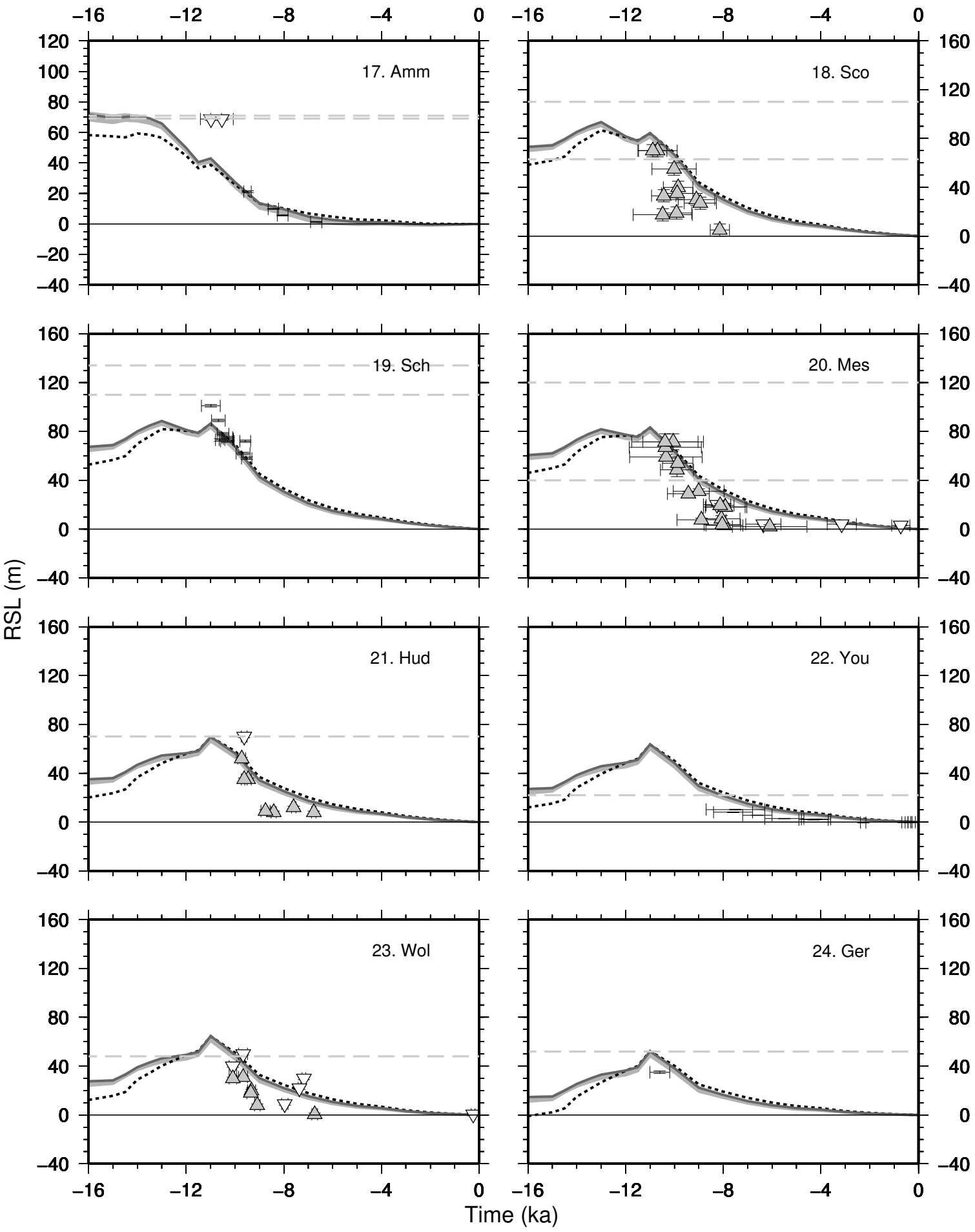
17. Amm
18. Sco
19. Sch
20. Mes
21. Hud
22. You
23. Wol
24. Ger
RSL (m)
Time (ka)
−16
−12
−8
−4
0
120
100
80
60
40
20
0
−20
−40
160

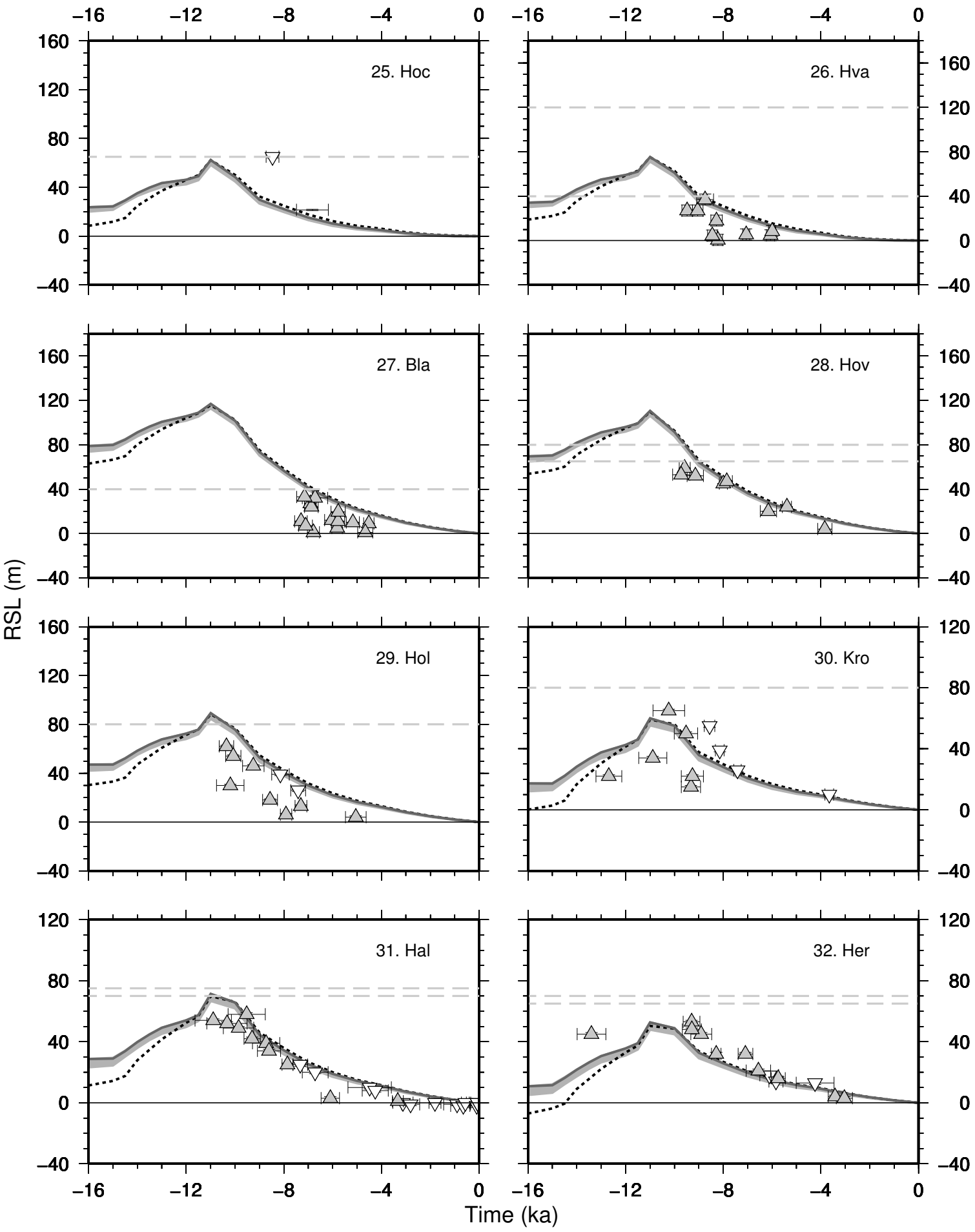
25. Hoc
26. Hva
27. Bla
28. Hov
29. Hol
30. Kro
31. Hal
32. Her
RSL (m)
Time (ka)
−16
−12
−8
−4
0
160
120
80
40
0
−40

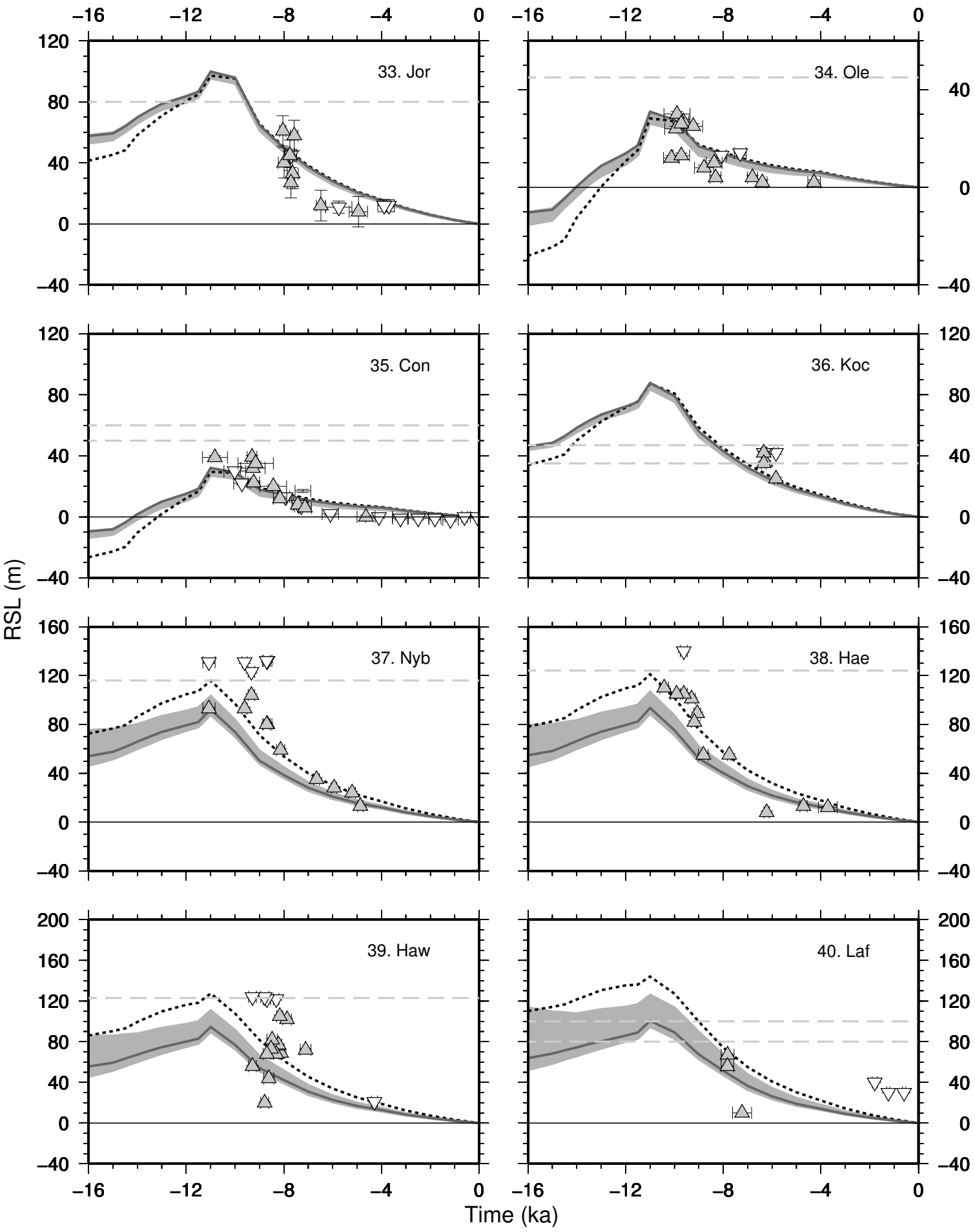
33. Jor
34. Ole
35. Con
36. Koc
37. Nyb
38. Hae
39. Haw
40. Laf
RSL (m)
Time (ka)

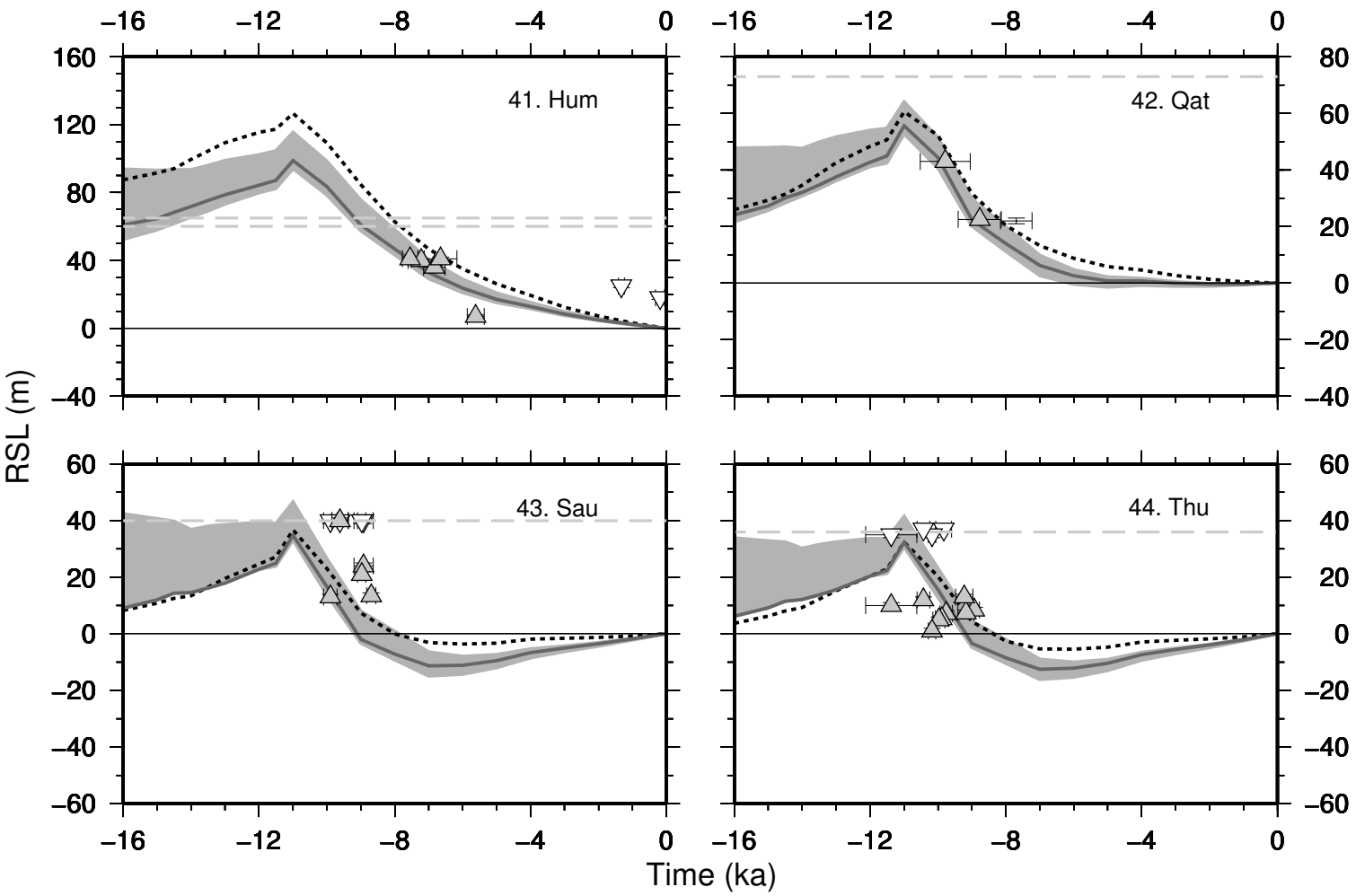
41. Hum
42. Qat
43. Sau
44. Thu
RSL (m)
Time (ka)
−16
−12
−8
−4
0
160
120
80
40
0
−40
60
20
−20
−60

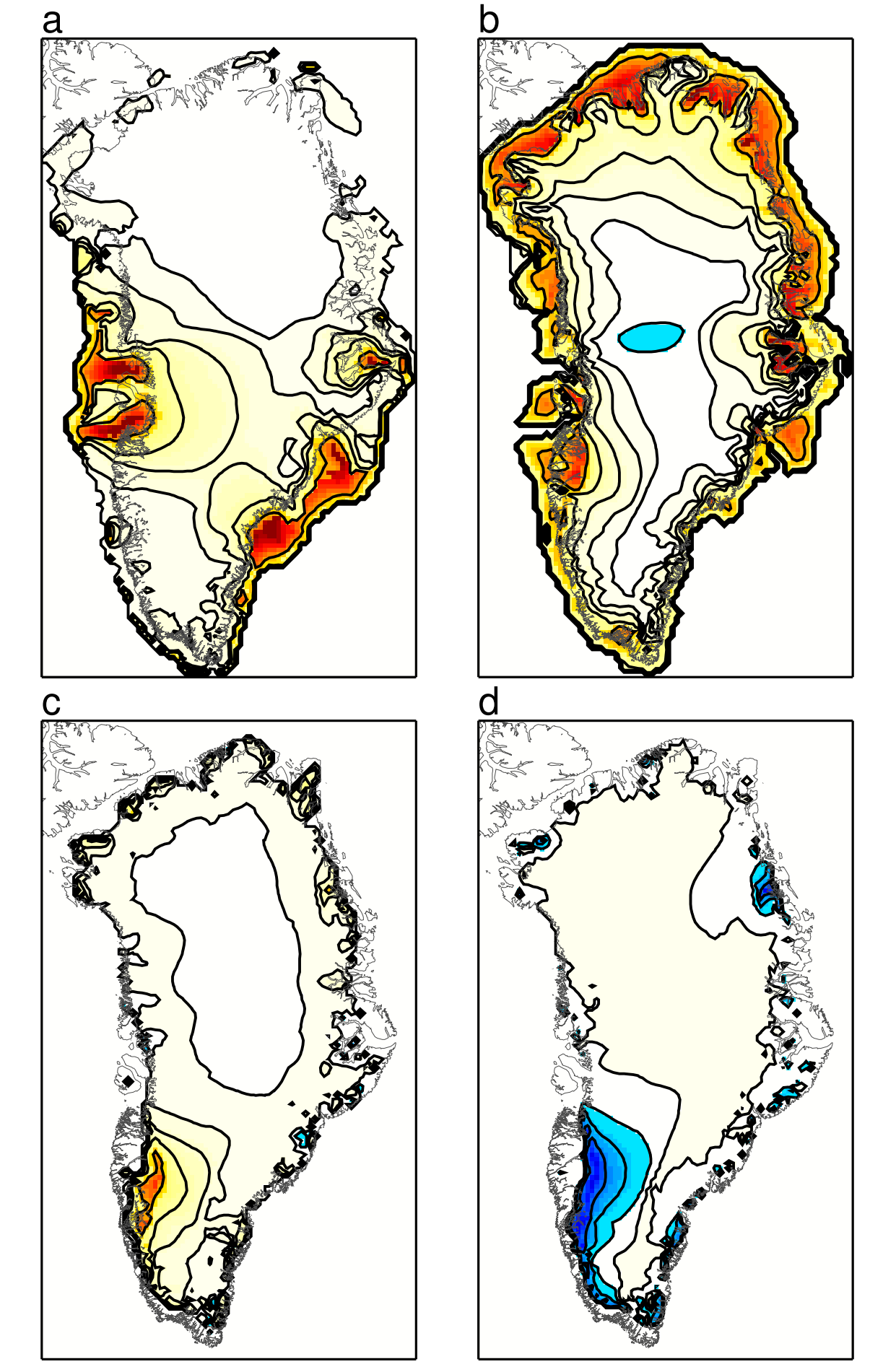
a
b
c
d
−2000 −1750 −1500 −1250 −1000 −750 −500 −250 0 250 500 750 1000
Changes in ice thickness (m)

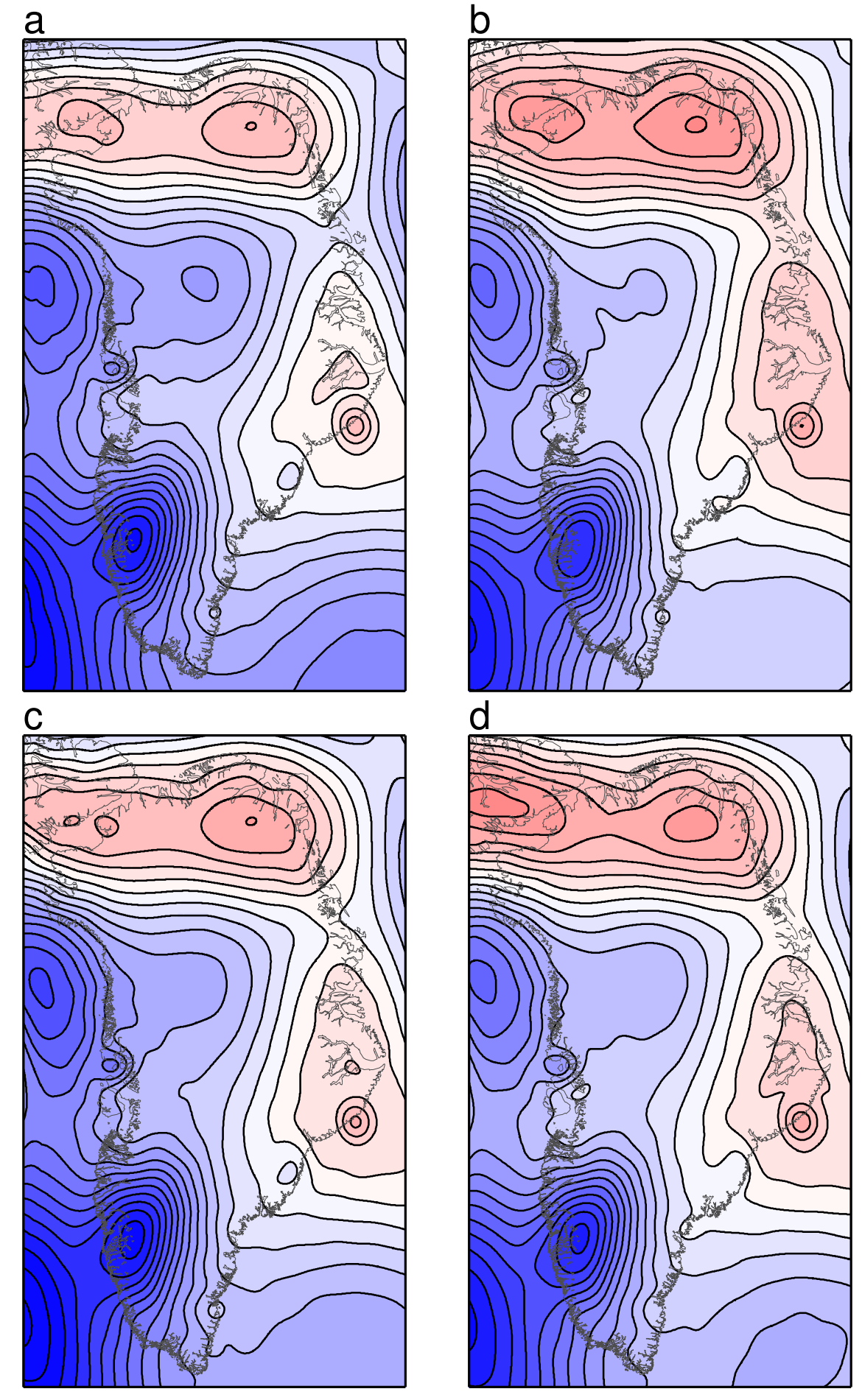
a
b
c
d
−7
−6
−5
−4
−3
−2
−1
0
1
2
3
4
5
6
7
Uplift Rate (mm/yr)

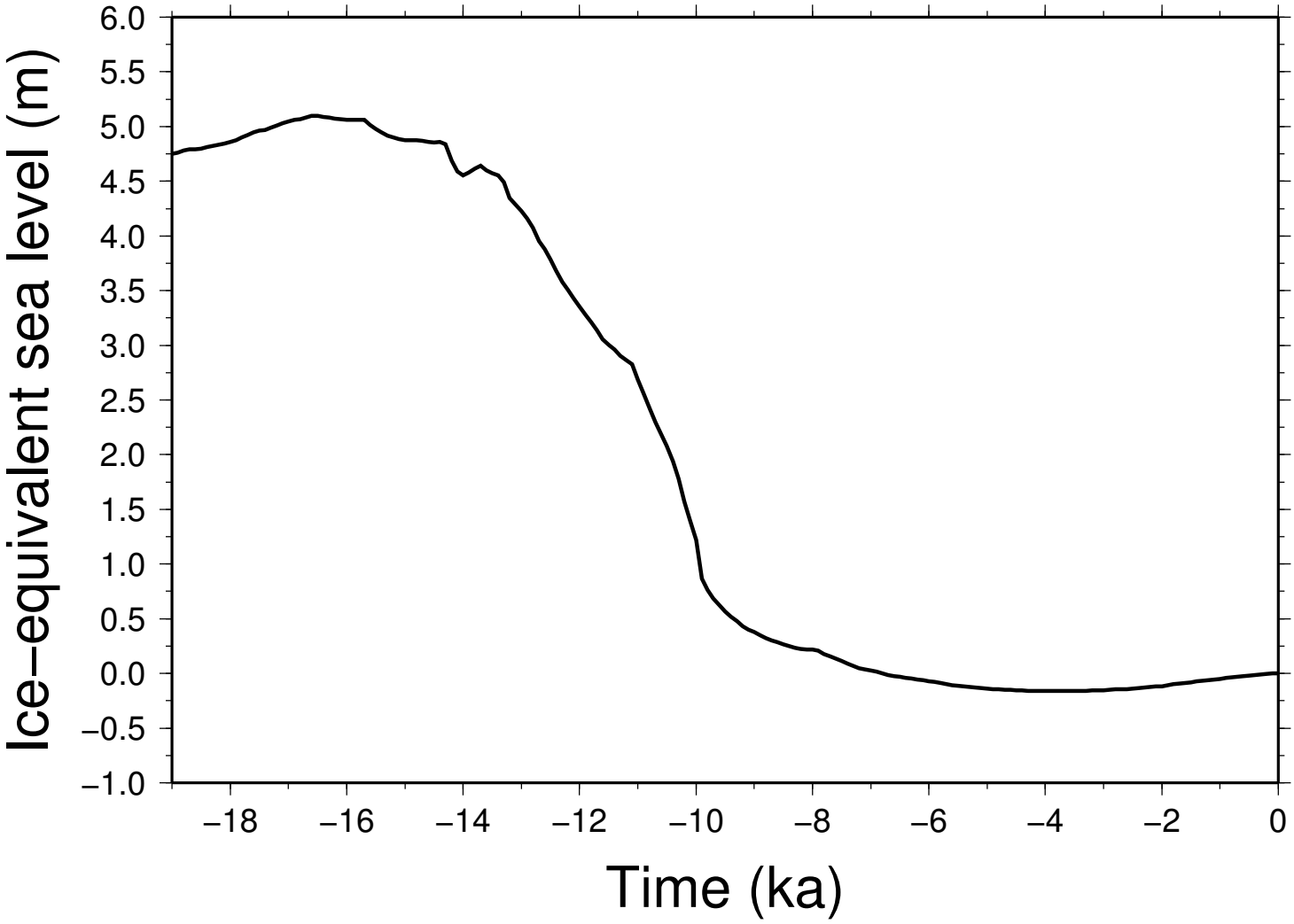
Ice–equivalent sea level (m)
6.0
5.5
5.0
4.5
4.0
3.5
3.0
2.5
2.0
1.5
1.0
0.5
0.0
–0.5
–1.0
–18
–16
–14
–12
–10
–8
–6
–4
–2
0
Time (ka)

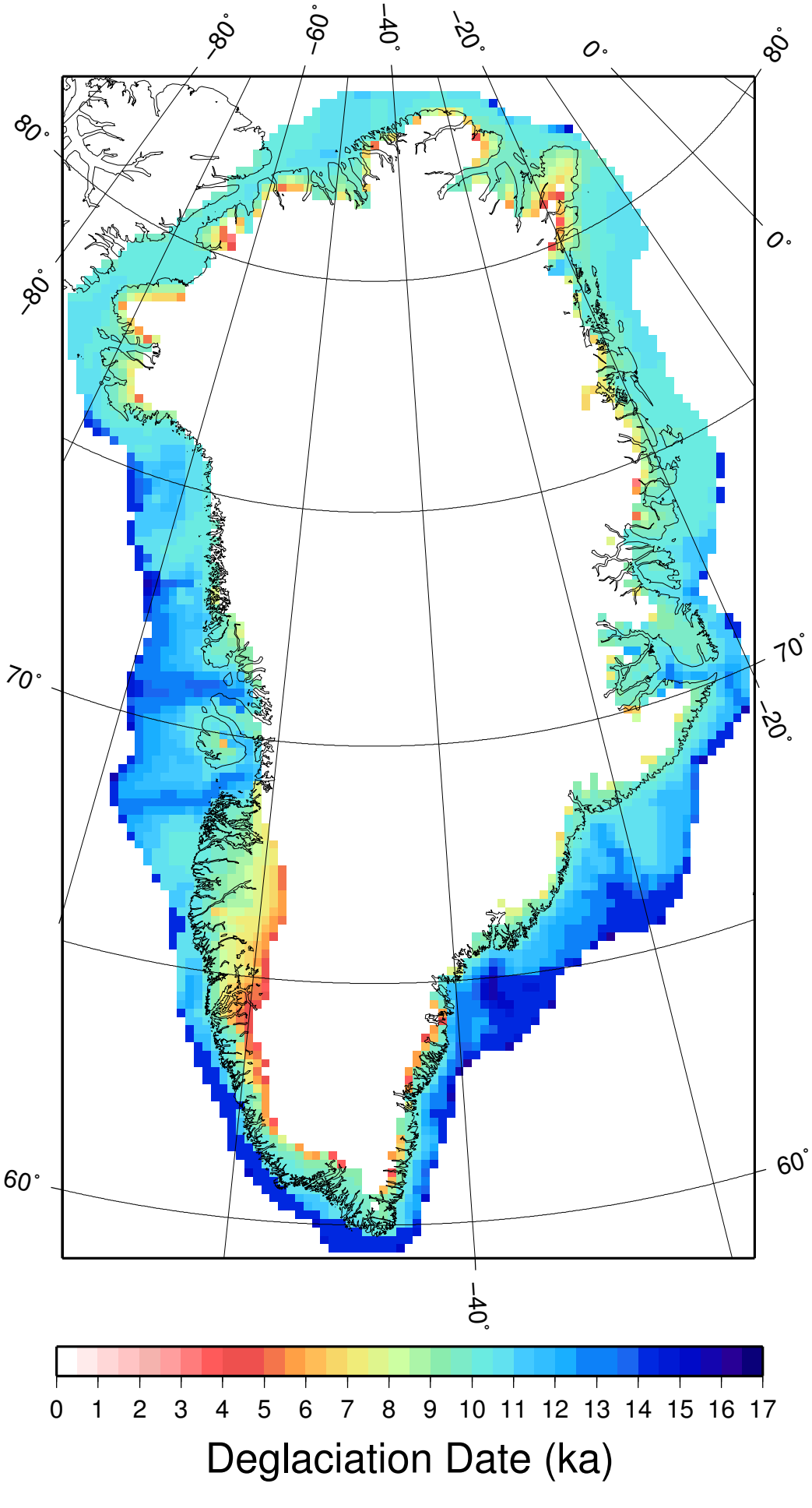
-80°
-60°
-40°
-20°
0°
80°
80°
-80°
0°
70°
70°
-20°
60°
60°
-40°
0 1 2 3 4 5 6 7 8 9 10 11 12 13 14 15 16 17
Deglaciation Date (ka)